Computational Modeling of Organic Structure, Spectra, and Reactivity

A DISSERTATION
SUBMITTED TO THE FACULTY OF
UNIVERSITY OF MINNESOTA
BY

Ashley Nicole Garr

IN PARTIAL FULFILLMENT OF THE REQUIREMENTS
FOR THE DEGREE OF
DOCTOR OF PHILOSOPHY

Christopher J. Cramer

January 2013

© Ashley Garr 2013

Abstract

Theoretical modeling of organic molecules and reactions is a powerful tool and can lead to further insight into these chemical systems. Modeling allows portions of the potential energy surface that cannot be examined experimentally, such as transition states. These transition states can lend themselves to better understanding of the system's reactivity. Modeling can also be used to perform analysis that would time-consuming and tedious experimentally or clarify ambiguous experimental results. In this thesis, the use of theoretical modeling to examine the structure, spectra, and reactivity of organic systems will be explored. In this thesis modeling is used to examine the regioselectivity of indole aryne cycloadditions and kinetic isotope effects of substituted anilines. The use of proton nucleomers to calculate linear free energy relationships to reduce both experimental and computational time is examined. A significant portion of this thesis is dedicated to the use of calculated nuclear magnetic resonance chemical shifts and coupling constants to differentiate between stereo- and structural isomers; something that can be very difficult to do using experimental spectra.

Table of Contents

List of Tables

List of Figures and Schemes

List of Abbreviations

ABTS—2,2’-azino-bis(3-ethylbenzothiazoline)-6-sulphonic acid

AKIE—Apparent kinetic isotope effects

An—Aniline

Bu—Butyl

Calc—Calculated

Comp—Computed

COSY—Correlation spectroscopy

CSGT—Continuous set of gauge transformations

CSIA—Compound-specific isotope analysis

DEPT—Distortionless enhancement by polarization transfer

DFT—Density functional theory

EA—Elemental analyzer

EIE—Equilibrium isotope effect

Eq—Equation

Et—Ethyl

ET—Electron transfer

Exp—Experimental

Fig—Figure

GB-SA—Generalized Born-surface areas

GC—Glassy carbon

GC/IRMS—Gas chromatography/isotope ratio mass spectrometry

GC/MS—Gas chromatography/mass spectrometry

GIAO—Gauge-independent atomic orbital

HAT—Hydrogen-atom transfer

HF—Hartree-Fock

HMBC—Heteronuclear multiple bond correlation

HPLC—High-performance liquid chromatography

HSQC—Heteronuclear single quantum coherence

IEFPCM—Integral equation formalism polarizable continuum model

IEP—Isoelectric point

iPr—Isopropyl

KIE—Kinetic isotope effect

LC-MS/MS—Liquid chromatograpy-mass spectroscopy/mass spectroscopy

Me—Methyl

MES—2-morpholinoethanesulfonic acid

MUE—Mean unsigned error

NMR—Nuclear magnetic resonance

NOESY—Nuclear overhauser effect spectroscopy

NOM—Natural organic matter

PA—Polyacrylate

PCM—Polarizable continuum model

PDMS/DVB—Polydimethylsiloxane/divinyl benzene

PPM—Parts per million

PTFE—Polytetrafluoroethylene SHE—Standard hydrogen electrode

RC—Regenerated cellulose

SPE—Solid phase extraction

SPME—Solid-phase microextraction

t-Bu—*tert*-Butyl

TMS-Tetramethylsilane

TS—Transition state

UE—Unsigned error

UV-vis—Ultraviolet-visible

XANES—X-ray absorption near edge structure

XRD—X-ray diffraction

Preface

Citations from previously published work in this thesis are as follows:

Chapter 5
Reprinted with permission from:
La Macchia, G.; Gagliardi, L.; Carlson, G. S.; Jay, A. N.; Davis, E.; Cramer, C. J. *J. Phys. Org. Chem.* **2008**, *21*, 136-145.
Link: http://onlinelibrary.wiley.com/doi/10.1002/poc.1297/abstract
Copyright 2007 John Wiley & Sons Ltd.

Chapter 6
Reprinted with permission from:
Garr, A. N.; Luo, D.; Brown, N.; Cramer, C. J.; Buszek, K. R.; VanderVelde, D. *Org. Lett.* **2010**, *12*, 96-99.
Link: http://pubs.acs.org/doi/full/10.1021/ol902415s
Copyright 2010 American Chemical Society

Chapter 7
Reprinted with permission from:
Skarpeli-Liati, M.; Turgeon, A.; Garr, A. N.; Arnold, W. A.; Cramer, C. J.; Hofstetter, T. B. *Anal. Chem.* **2011**, *83*, 1641-1648.
Link: http://pubs.acs.org/doi/full/10.1021/ac102667y
Copyright 2011 American Chemical Society

Chapter 8
Reprinted with permission from:
Skarpeli-Liati, M.; Jiskra, M.; Turgeon, A.; Garr, A. N.; Arnold, W. A.; Cramer, C. J.; Schwarzenbach, R. P.; Hofstetter, T. B. *Environ. Sci. Technol.* **2011**, *45*, 5596-5604.
Link: http://pubs.acs.org/doi/full/10.1021/es200743t
Copyright 2011 American Chemical Society

Chapter 1. Introduction[1]

1.1 General Overview

Computational chemistry is a growing field that is becoming an indispensable tool to the experimental chemist. Computational chemistry can examine parts of mechanisms that cannot be seen experimentally such as transition state (TS) structures. It can also be used to predict properties and spectra and calculate accurately quantities that could be time-consuming to determine experimentally.[1] This thesis uses computational chemistry to examine the structure, spectra (specifically NMR), and reactivity of different organic molecules.

1.2 Computational Methods

1.2.1 Density Functionals

Working towards a solution to the fundamental equation of quantum mechanics, the Schrödinger equation:

$$H\Psi = E\Psi \tag{1}$$

where H is the Hamiltonian operator, E is the energy eigenvalue, and Ψ is the wave function, is one model for computational chemistry. This work makes use of an alternative model, density functional theory (DFT), developed initially by Hohenberg, Kohn, and Sham in the 1960s[2-4], where the energy and molecular properties are determined not from the wave function but instead from the electron density.[1] The density functionals used are PBE,[5] mPWPW91,[6-8] and the hybrid functionals B3LYP[9-12] and M06-2X.[13] Hybrid functional refers to the mixing of nonlocal Hartree-Fock (HF)

[1] I'd like to thank the University of Minnesota and the Minnesota Supercomputing Institute for supporting the calculations performed in this thesis.

exchange with local density functional exchange, which often leads to improved reaction barrier heights because local DFT tends to underestimate them and HF theory overestimates them.[14] B3LYP contains 20% HF exchange[11] and M06-2X contains 54% HF exchange.[13]

1.2.2 Basis Sets

Selection of a basis set (mathematical functions used to express wave functions and electron densities[1]) is an important choice, with the goal of balancing efficiency with accuracy. Local DFT scales as N^3 where N is the number of basis functions while hybrid DFT scales formally as N^4.[1] A variety of basis sets are used in this work: MIDI!,[15] the Pople basis sets 6-31+G(d,p), 6-311+G(d), 6-311+G(2d,p), 6-311+G(2df,p), and 6-311+G(2df,2p);[16-20] and the Dunning basis set aug-cc-pVDZ.[21,22] These basis sets employ a variety of diffuse and polarization functions to take into account the various needs of the molecules in question.

1.2.3 Solvation Models

In general, computations take place in the gas-phase, but most of the chemistry examined here takes place in solution. In chapters 5, 7, and 8, solvation effects are not expected to influence the outcome and are therefore ignored. In chapters 2—4 and chapter 6, implicit solvation models are employed. Implicit solvation models form a cavity around the molecule of interest and represent the surrounding solution as a continuum.[1] Integral equation formalism polarizable continuum model (IEFPCM)[23-27] is used in chapters 2—4 modeling chloroform solvation for NMR calculations where it is applied during the optimization process. The SMD solvation model[28,29] is used in chapter

6 to examine solvation effects on the regioselectivity of indole aryne cycloadditions and is included as single-point calculations.

1.2.4 Nuclear Magnetic Resonance (NMR) Chemical Shift Calculations

NMR chemical shift calculations comprise a significant portion of this thesis. For the most part, there are two methods for calculating chemical shifts, the continuous set of gauge transformations (CSGT) method[30] and the gauge-independent atomic orbital or GIAO-method.[31,32] While both methods give comparable results, the CSGT method requires a larger basis set to arrive at the same values.[33] The GIAO-method, which places a gauge origin in the center of all atomic orbitals leading to gauge independence,[32] is used here to calculate and compare chemical shifts of isomers.

1.3 Organization of Thesis

This thesis covers a plethora of topics all centering around organic molecules and their structure, reactivity, and spectra. Chapters 2—4 are dedicated to the examination of calculated NMR chemical shifts to aid experimentalists in the assignment of their spectra. Nuclear magnetic resonance (NMR) is one of the most powerful tools at an organic chemist's disposal for structure elucidation.[1,34,35,36] However, there are many cases in the literature where misassignment has occurred.[37] Computational NMR calculations have the benefit of allowing a chemist to know precisely which chemical shifts correspond to which nuclei. Comparing the computed shifts with the experimentally determined shifts can help assign structures. Level of theory, basis set, solvation, and error analysis are examined to develop an easy-to-use method for chemical shift calculations. The method

was used on structural and stereoisomers and the calculated shifts were compared to experimental shifts.

The rest of the chapters depart from the NMR theme to examine different aspects of structure and reactivity. Chapter 5 examines the use of hydrogen nucleomers to examine linear free-energy relationships. Linear free-energy relationships can be used to predict the reactivity of substituted aryl compounds.[38] Determining linear free-energy relationships experimentally would be time-consuming because it would involve reacting (and possibly synthesizing) several substituted compounds. Determining the relationship computationally is relatively straightforward, if somewhat laborious, essentially exchanging one substituent for another.

Because computational chemistry also allows the structure of points along the potential energy surface to be examined and the possible mechanisms of a reaction to be modeled, it can be a useful tool to more closely examine and validate experimental results. Chapter 6 discusses the regioselectivity of 4,5-, 5,6-, and 6,7-indole aryne cycloadditions. Chapters 7 and 8 examine equilibrium and kinetic isotope effects of substituted anilines.

Chapter 2. Validation of NMR Protocol[2]

2.1 Introduction

Structure assignment by NMR spectroscopy is a vital tool for organic chemists. But as illustrated in a review by Nicolaou and Snyder, there are many examples in the literature where NMR was used as the primary spectroscopic tool to assign the structure of a molecule, only to have the structure corrected and reassigned later.[37] A similar review by Maier continues to illustrate the errors that can arise from ambiguous experimental data. Many of the incorrect structures discussed in the review are isomers of the reassigned structure, usually determined by total synthesis.[39]

Computational chemical shift calculations are gaining more attention as a useful tool in assigning structures from experimental spectra. Bifulco *et al.* wrote a review discussing the use of computed chemical shifts to assign structure.[40] Many papers seem to concentrate solely on the use of ^{13}C chemical shifts at a variety of levels of theory, including molecular mechanics, HF, and DFT for the assignment of structures.[41-47] However, there are examples of also using ^{1}H or even ^{15}N chemical shifts or coupling constants to examine molecular structure.[35,48-55]

New methods for calculating chemical shifts and methods for analyzing the fit of the computed shifts compared to experimentally determined shifts have also been developed. In particular, Wiitala and coworkers developed functionals specifically optimized to predict ^{1}H and ^{13}C chemical shifts. WC04 was optimized to predict ^{13}C chemical shifts and WP04 was optimized to predict ^{1}H chemical shifts.[34] Goodman and

---

[2] I would like to acknowledge the work of Patrick H. Willoughby in the Hoye Group at the University of Minnesota. His scripts for converting MacroModel files to Gaussian input files and for parsing data from output files greatly streamlined this work.

coworkers developed two new methods to analyze the fit of data, the CP3 and DP4 methods. The CP3 method is used when there are two sets of experimental data to compare[56,57] and the DP4 method is used when there is only one set of experimental data.[58]

Because isomers can be especially challenging to assign based solely on experimental spectra and total synthesis can be an extremely time-consuming endeavor, a consistent and user-friendly computational protocol was desired for the assignment of small organic molecules from both proton and carbon chemical shifts. This chapter uses a simple set of isomers (methylcyclohexanols) to develop and demonstrate a protocol that will be used to examine more complex cases.

2.2 Developing Protocol

To obtain the set of conformers for each isomer, a conformational search was done utilizing the Schrodinger software program Macromodel.[59] In general, default settings were used, including the 5.02 kcal/mol energy difference cutoff. The MMFFs force field[60,61] was used for torsional sampling in continuum (GB-SA) chloroform solvation.

For the further optimization of each conformer, the M06-2X functional was chosen because it was designed specifically for main group compounds.[13] The 6-31+G(d,p) basis set was used for the optimizations.[16,17] It includes diffuse and polarization functions so the conformers would be optimized at, most likely, an acceptable level of theory for the molecule without the basis set becoming excessively large. NMR experiments generally take place in deuterated chloroform, therefore

IEFPCM[23-27] chloroform solvation was employed and the solvation cavity was developed using Bondi's atomic radii,[62] which as implemented in Gaussian09, includes explicit hydrogens. An ultrafine integration grid was also used.

WC04 and WP04 functionals were developed by use of a training set of forty-three molecules.[34] These functionals were then tested against the ability of the B3LYP,[9-12] PBE1,[5,63] and mPW1PW91[8,64,65] functionals. While WC04 and WP04 did outperform the other functionals, by including a simple linear correction the other functionals produced results similar to WC04 and WP04.[34] WC04 and WP04 are implemented in the Gaussian09 suite of programs[66] through the use of IOps.[34] A new or infrequent user of the software could find the use of IOps prohibitive, so B3LYP, arguably the most popular density functional currently available, was chosen as the level of theory for the NMR calculations described here.

The NMR calculations were done using the GIAO method,[31,32] which is the default method implemented in Gaussian09, as opposed to the CGST method,[30] which requires larger basis sets to achieve accurate results.[33] The NMR calculations also included IEFPCM chloroform solvation to mimic experimental conditions with the solvation cavity described by Bondi's radii. An ultrafine integration was again used. A slightly larger basis set, 6-311+G(2d,p),[17,19,20] was used for the NMR calculations than for the optimizations. The chemical shifts calculated for the conformers were taken relative to the standard tetramethylsilane and the computed δ values were Boltzmann-weighted according to the equation:[34,45]

$$\delta_{\text{calc}} = \sum_i \left(\delta_{\text{comp},i} \times e^{-E_i/RT} / \sum_i e^{-E_i/RT} \right) \qquad (2)$$

where E is the electronic energy of the conformer, R is the gas constant, and T is the temperature (298.15 K). Finally, the linear correction from Wiitala *et al*. was applied to the calculated δ to improve the accuracy of the B3LYP NMR calculation. For ^{13}C chemical shifts:[34]

$$\delta_{corr} = (0.9488 \times \delta_{calc}) - 2.1134 \quad (3)$$

For ^{1}H chemical shifts:[34]

$$\delta_{corr} = (0.9333 \times \delta_{calc}) + 0.1203 \quad (4)$$

After applying the corrections, the corrected chemical shifts were compared to the experimental shifts through mean unsigned error.

2.3 Methylcyclohexanols

The chemical shifts of six isomers of methylcyclohexanols shown in **Figure 1** were calculated by the method described above and compared to experimental data from Wiitala *et al.*[34] Wiitala *et al*. performed calculations on the methylcyclohexanol isomers to test the effectiveness of the functionals WP04 and WC04, which were specifically designed to predict chemical shift data. This work looked to develop a more user-friendly method that produced similarly accurate results.

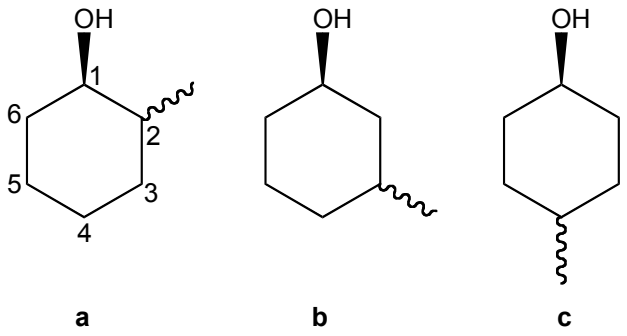

Figure 1. Set of methylcyclohexanol isomers.

The conformers of the methylcyclohexanols involved both chairs and OH rotomers. The *cis* and *trans* isomers of **1a** and **1b** consisted of six conformers each, while the *cis* and *trans* isomers of **1c** of four conformers each. Tables 1 and 2 contain the linearly corrected proton and carbon-13 chemical shifts for **1a**-**1c** respectively. The *cis* and *trans* isomers are noted in the table by a "-c" or a "-t" following the designation of the isomer.

Table 1. Linearly Corrected ^{1}H NMR Chemical Shifts in ppm for Isomers **1a-c**.

	1a-c[a]	**1a**-t[a]		**1b**-c[a]	**1b**-t[a]		**1c**-c[a]	**1c**-t[a]
1	3.71	3.05	1	3.48	3.98	1	3.80	3.41
2	1.59	1.25	2a	0.84	1.25	2a	1.56	1.21
3a	1.48	1.04	2e	1.89	1.69	2e	1.76	1.88
3e	1.41	1.68	3	1.42	1.84	3a	1.39	1.03
4a	1.31	1.27	4a	0.83	1.01	3e	1.46	1.70
4e	1.65	1.63	4e	1.59	1.65	4	1.44	1.32
5a	1.66	1.35	5a	1.34	1.73	5a	1.40	1.02
5e	1.38	1.75	5e	1.75	1.50	5e	1.47	1.71
6a	1.53	1.22	6a	1.08	1.51	6a	1.61	1.18
6e	1.75	1.87	6e	1.89	1.63	6e	1.65	1.96
Me	0.98[b]	1.04[b]	Me	0.96[b]	0.92[b]	Me	0.96[b]	0.92[b]

[a]Computed δ_H at the B3LYP/6-311+G(2d,p)//M06-2X/6-31+G(d,p) level of theory with a linear correction applied

[b]Average δ_H over the three methyl protons

Table 2. Linearly Corrected ^{13}C NMR Chemical Shifts in ppm for Isomers **1a-c**.

	1a-c[a]	1a-t[a]	1b-c[a]	1b-t[a]	1c-c[a]	1c-t[a]
1	71.4	76.4	71.3	67.6	67.9	71.5
2	38.0	42.2	45.0	42.0	32.1	37.9
3	29.9	34.5	34.0	29.2	30.1	34.3
4	26.3	27.4	35.2	35.4	34.0	34.5
5	22.4	26.8	25.7	21.6	30.0	34.4
6	33.7	36.4	36.5	34.1	34.3	35.8
Me	15.8	17.2	21.3	21.0	20.4	20.8

[a]Computed δ_C at the B3LYP/6-311+G(2d,p)//M06-2X/6-31+G(d,p) level of theory with a linear correction applied

Table 3 shows a comparison of the mean unsigned errors calculated between the linearly corrected computed ^{1}H chemical shifts and experimental ^{1}H chemical shifts from Wiitala *et al.*[34] In the case of each set of *cis*/*trans* isomers, the correct assignment between the computed shifts and the experimentally determined shifts leads to a dramatically smaller MUE than the incorrect assignment. The MUEs presented here are comparable to MUEs calculated by Wiitala *et al*. using the WP04 functional for the chemical shift calculation.[67] Wiitala found the WP04 functional gave an average MUE of 0.052 for the methylcyclohexanol isomers will the proposed method here gives an average MUE of 0.05.

Table 3. Mean Unsigned Errors Between Computed and Experimental δ_H for **1a-1c**.

		Exp[a]							
		1a-c	**1a**-t		**1b**-c	**1b**-t		**1c**-c	**1c**-t
Comp[b]	**1a**-c	0.06	0.30	**1b**-c	0.06	0.27	**1c**-c	0.05	0.26
	1a-t	0.26	0.05	**1b**-t	0.30	0.03	**1c**-t	0.27	0.05

[a]From experimental δ_H from Wiitala *et al.*[34]
[b]From computed δ_H at the B3LYP/6-311+G(2d,p)//M06-2X/6-31+G(d,p) level of theory with a linear correction applied

Table 4 gives a comparison of the MUE for the computed and experimental ^{13}C chemical shifts. Once again, the experimental shifts were from Wiitala *et al.*[34] As seen

with the ^{1}H comparisons, the correct assignment for each set of *cis*/*trans* isomers has a smaller MUE than the incorrect assignment. The MUEs presented are once again comparable to MUEs found using the WC04 functional to calculate the chemical shifts. The average MUE for WC04 from Wiitala was 1.30, the proposed method average MUE is 1.4.

Table 4. Mean Unsigned Errors Between Computed and Experimental δ_C for **1a-1c**.

		Exp[a]							
		1a-c	**1a**-t		**1b**-c	**1b**-t		**1c**-c	**1c**-t
Comp[b]	**1a**-c	1.2	4.3	**1b**-c	1.1	3.6	**1c**-c	1.3	2.7
	1a-t	4.1	2.6	**1b**-t	2.2	1.1	**1c**-t	4.0	1.2

[a]From experimental δ_C from Wiitala *et al.*[34]

[b]From computed δ_C at the B3LYP/6-311+G(2d,p)//M06-2X/6-31+G(d,p) level of theory with a linear correction applied

The ^{13}C shifts' MUE are slightly less sensitive for differentiating between isomers. In fact, as seen in Tables 5 and 6, without the linear correction the MUE between computed and experimental ^{13}C shifts are not sufficient to differentiate between isomers. Carbon's decreased sensitivity and the inability of ^{13}C shifts—without the linear correction—to differentiate these isomers is consistent with results from Wiitala *et al.*[67]

Table 5. Raw Calculated ^{13}C NMR Chemical Shifts in ppm for Isomers **1a-c**.

	1a-c[a]	1a-t[a]	1b-c[a]	1b-t[a]	1c-c[a]	1c-t[a]
1	77.5	82.8	77.4	73.4	73.8	77.6
2	42.3	46.7	49.7	46.5	36.1	42.2
3	33.7	38.5	38.1	33.0	33.9	38.4
4	29.9	31.1	39.4	39.5	38.1	38.6
5	25.8	30.4	29.4	25.0	33.8	38.5
6	37.8	40.6	40.7	38.2	38.4	40.0
Me	18.9	20.4	24.7	24.3	23.7	24.1

[a]Computed δ_C at the B3LYP/6-311+G(2d,p)//M06-2X/6-31+G(d,p) level of theory

MUE is not the only method of comparing chemical shift data. Goodman and coworkers developed two protocols to assign data.[56-58] The CP3 method was designed to assign

confidence levels to calculated shifts based on two experimental sets of data. CP3 confidence levels can be determined by following the procedure in reference 43 or from an applet designed by the Goodman group, which can be accessed at www-jmg.ch.cam.ac.uk/tools/nmr.[68]

Table 6. Mean Unsigned Errors Between Raw Computed and Experimental δ_C for **1a-1c**.

		Exp[a]							
		1a-c	**1a**-t		**1b**-c	**1b**-t		**1c**-c	**1c**-t
Comp[b]	**1a**-c	4.8	2.1	**1b**-c	5.1	7.7	**1c**-c	4.9	2.1
	1a-t	8.4	4.8	**1b**-t	2.3	4.9	**1c**-t	8.0	5.1

[a]From experimental δ_C from Wiitala *et al.*[34]
[b]From computed δ_C at the B3LYP/6-311+G(2d,p)//M06-2X/6-31+G(d,p) level of theory

Using the applet, confidence levels were calculated between the experimental shifts and computed shifts, both with and without the linear correction. As can be seen in Table 7, the CP3 method easily differentiates between the *cis* and *trans* isomers using proton chemical shifts regardless of the use of the linear correction. This is consistent with results found using MUE.

Table 7. CP3 Confidence Intervals for Correct and Incorrect Assignment of δ_H for **1a-1c**.

	1a[a]	**1a**[b]	**1b**[a]	**1b**[b]	**1c**[a]	**1c**[b]
Correct[c]	99.9%	99.9%	99.9%	99.9%	100.0%	99.9%
Incorrect[d]	0.1%	0.1%	0.1%	0.1%	0.0%	0.1%

[a]Comparison between experimental δ_H from Wiitala *et al.*[34] and computed δ_H at the B3LYP/6-311+G(2d,p)//M06-2X/6-31+G(d,p) level of theory
[b]Comparison between experimental δ_H from Wiitala *et al.*[34] and computed δ_H at the B3LYP/6-311+G(2d,p)//M06-2X/6-31+G(d,p) level of theory with a linear correction applied
[c]Correct comparison (cis and cis; trans and trans)
[d]Incorrect comparison (cis and trans)

When confidence levels were calculated using the carbon-13 shift data, the CP3 method once again easily differentiated between the *cis* and *trans* isomer whether or not the linear correction was included. The differentiation is very strong and is correct even

without the linear correction, which is an improvement over using the MUE as a comparison.

Table 8. CP3 Confidence Intervals for Correct and Incorrect Assignment of δ_C for **1a-1c**.

	1a[a]	**1a**[b]	**1b**[a]	**1b**[b]	**1c**[a]	**1c**[b]
Correct[c]	100.0%	100.0%	100.0%	100.0%	100.0%	100.0%
Incorrect[d]	0.0%	0.0%	0.0%	0.0%	0.0%	0.0%

[a]Comparison between experimental δ_C from Wiitala *et al.*[34] and computed δ_C at the B3LYP/6-311+G(2d,p)//M06-2X/6-31+G(d,p) level of theory
[b]Comparison between experimental δ_C from Wiitala *et al.*[34] and computed δ_C at the B3LYP/6-311+G(2d,p)//M06-2X/6-31+G(d,p) level of theory with a linear correction applied
[c]Correct comparison (cis and cis; trans and trans)
[d]Incorrect comparison (cis and trans)

2.4 Conclusions

The protocol described matches the accuracy of the methods designed specifically to calculate chemical shift data without the use of Gaussian IOps. The proton data MUE did a better job of differentiating between the isomers than the carbon-13 data did, because a linear correction was necessary to get a correct assignment with the carbon data. The CP3 and DP4 methods are also extremely useful comparisons, but in most cases the MUE is adequate and easy to use. The protocol described in this chapter will be used in following chapters to examine different sets of isomers.

Chapter 3. Proof of Concept, Examination of Menthols and the Case of Drymaritin

3.1 Introduction

The chemical shift protocol described in the previous chapter was tested against several isomeric systems, including the stereoisomers of menthol and the structural isomers of drymaritin. The protocol proved useful in assigning structures for both stereo- and structural isomers.

3.2 Computational Methods

The protocol described in the previous chapter was used. Each molecule underwent a conformational search using the MMFFs force field[60,61] as implemented in Macromodel from the Schrodinger software package.[59] Torsional sampling, continuum chloroform solvation and a 5.02 kcal/mol energy difference cutoff were used during the conformational search.

Each conformer was then optimized using the M06-2X density functional[13] and 6-31+G(d,p) basis set[16,17] as implemented in the Gaussian09 suite of programs.[53] Optimizations used the integral equation formalism polarized continuum model (IEFPCM)[23-27] for chloroform solvation and Bondi's atomic radii[62] for solute cavity construction. An ultrafine integration grid was also used. Frequency calculations were done to ensure each conformer was a minimum.

Gauge-Independent Atomic Orbital (GIAO)[31,32] NMR calculations were done on each geometry-optimized conformer at the B3LYP/6-311+G(2d,p) level of theory,[9-12,17,19,20] including continuum solvation effects in the same manner already described above. The chemical shifts were taken relative to tetramethylsilane computed at the same

level of theory. The chemical shifts of individual nuclei were then averaged using Boltzmann weighting.[34,45] These weighted chemical shifts were treated with the linear correction developed by Wiitala *et al.*[34] and then compared to experimental chemical shifts.

3.3 Drymaritin

3.3.1 Background

In the case of drymaritin, a canthinone, ambiguity in the interpretation of the NMR data led to a misassignment of its structure, which was eventually discovered through total synthesis.[69]

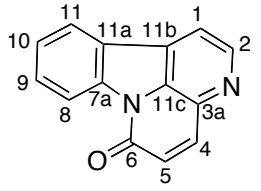

Figure 2. Structure of canthin-6-one.

Canthin-6-one (Figure 2) was first isolated in 1952 by Haynes and coworkers[70] and some of its derivatives have been shown to have antimicrobial, antifungal, and cytotoxic activity.[71-75] In 2004 Hsieh and coworkers isolated a related compound to which they assigned the structure 5-methoxycanthin-4-one (Figure 3) from *Drymaria diandra*. They named the yellow powder drymaritin and assigned its structure on the basis of NMR experiments. Their isolated compound was found to possess anti-HIV activity, something that had only been found in canthin-6-ones previously.[76]

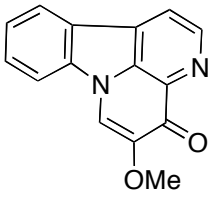

Figure 3. Structure of 5-methoxycanthin-4-one proposed by Hsieh *et al.* as the structure for drymaritin.[76]

In 2009, Wetzel and coworkers undertook the first total synthesis of drymaritin.[69] Starting from 1-(methoxyacetyl)-β-carboline and using a synthetic approach previously published by Puzik et al.,[77] the compound in Figure 3 was synthesized, and its structure confirmed by ^{1}H, ^{13}C, DEPT, HSQC, and HMBC analyses.[69] Wetzel and coworkers found that their spectroscopic data did not match that of the natural product as reported by Hsieh *et al*. They determined that if the molecular formula was correct, the compound assumed to be drymaritin most likely had the structure of **4a** or **4b**.[69]

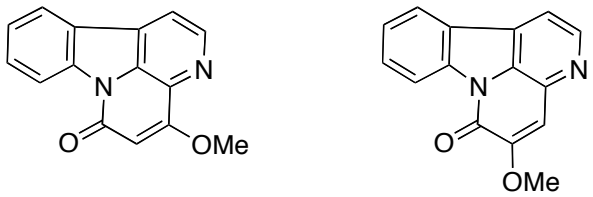

4a **4b**

Figure 4. Possible structures for drymaritin proposed by Wetzel *et al.*

By comparing the spectral data in the literature, particularly that of Wen-sen,[78] Wetzel and coworkers determined that the compound isolated by Hsieh *et al.* was in fact **4a**, a previously known compound.[69] They hypothesized that some ambiguity in HMBC correlations may have caused the misassignment.[69] This chapter asks the question of whether computational chemistry could have been used to resolve the ambiguity from experiment and led to the correct assignment of these structures initially.

3.3.2 Results

Chemical shifts were computed for structures **3**, **4a**, **4b**, and the structure in Figure 5 for completeness.

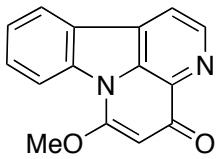

Figure 5. Structure of 6-methoxycanthin-4-one.

Conformational searches yielded two conformers each for structures **3** and **5**, and three conformers each for structures **4a** and **4b**. These conformers differed only in the dihedral angle of the methoxy group (Table 9). Conformers **4a-2** and **4a-3** and conformers **4b-2** and **4b-3** are almost perfect mirror images of each other and therefore have very similar energies. Conformers **5-1** and **5-2** also have very similar dihedral angles.

Table 9. Relative Energies and Dihedral Angles of Conformers for Structues **3**-**5**.

Conformer	Relative E[a]	Dihedral[b]
3-1	0.0	-0.005
3-2	1.0	111.579
4a-1	0.0	-0.005
4a-2	4.7	-154.644
4a-3	4.7	154.730
4b-1	0.0	0.011
4b-2	3.6	110.933
4b-3	3.6	-110.936
5-1	0.0	0.002
5-2	0.0	0.022

[a]Relative electronic energies calculated at the B3LYP/6-311+G(2d,p)//M06-2X/6-31+G(d,p) level of theory (kcal/mol)
[b]Dihedral angle CH_3-O-C-CH

3.3.2.1 Proton Chemical Shifts

The proton chemical shifts were compared to experimental shifts from Hsieh *et al.,*[76] Wetzel *et al.,*[69] and Wen-sen[78] (Table 10). Hsieh and Wetzel both have chemical shifts for structure **3**. Wen-sen gives chemical shifts for structures **4a** and **4b**.

Table 10. Computed and Experimental ^{1}H NMR Chemical Shifts for Structures **3**-**5**.

	3[a]	**3**[b]	**3**[c]	**4a**[a]	**4a**[d]	**4b**[a]	**4b**[d]	**5**[a]
1	8.04	8.75	8.13	7.93	7.95	7.74	8.14	7.96
2	8.87	7.90	9.05	8.66	8.80	8.62	8.78	8.79
4						7.08	7.40	
5				6.07	6.15			5.90
6	7.81	6.11	7.94					
8	7.69	8.53	7.73	8.59	8.59	8.66	8.55	8.11
9	7.68	7.63	7.74	7.67	7.69	7.68	7.58-7.80	7.63
10	7.42	7.43	7.49	7.46	7.50	7.51	7.58-7.80	7.44
11	8.17	7.99	8.17	8.11	8.10	8.11	8.40	8.14
OMe	3.89[e]	4.08	4.03	4.01[e]	4.02	3.97[e]	4.00	4.09[e]

[a]Computed δ_H in ppm at the B3LYP/6-311+G(2d,p)//M06-2X/6-31+G(d,p) level of theory with a linear correction applied
[b]Experimental δ_H in ppm from Hsieh *et al.* for proposed structure **3**[76]
[c]Experiemental δ_H in ppm from Wetzel *et al*. for proposed structure **3**[69]
[d]Experiemntal δ_H in ppm from Wen-sen for proposed structures **4a** and **4b**[78]
[e]Average δ_H over the three methyl protons

Mean unsigned errors (MUE) were computed between the experimental shifts and the calculated shifts (Table 11). The lowest MUE indicates the best fit between the experimental and computed chemical shifts. Hsieh's structure **3** shifts best line up with the computed shifts from structure **4a** (MUE of 0.24), while the MUE when compared to the computed **3** is over twice as large (MUE of 0.58). The other experimental data sets fit best with the computed data sets of the same structures.

Table 11. Mean Unsigned Errors Between Computed and Experimental ^{1}H NMR Chemical Shifts for **3-5**.

	3[b]	**3**[c]	**4a**[d]	**4b**[d,e]
3[a]	0.58	0.09	0.38	0.30
4a[a]	0.24	0.44	0.04	0.33
4b[a]	0.40	0.35	0.18	0.22
5[a]	0.31	0.39	0.12	0.41

[a]Computed δ_H in ppm at the B3LYP/6-311+G(2d,p)//M06-2X/6-31+G(d,p) level of theory with a linear correction applied
[b]Experimental δ_H in ppm from Hsieh *et al.* for proposed structure **3**[76]
[c]Experiemental δ_H in ppm from Wetzel *et al*. for proposed structure **3**[69]
[d]Experiemntal δ_H in ppm from Wen-sen for proposed structures **4a** and **4b**[78]
[e]Omitting chemical shifts for protons 9 and 10

3.3.2.2 Carbon Chemical Shifts

Carbon chemical shifts were also calculated and compared to the experimental shifts from Hsieh *et al.,*[76] Wetzel *et al.,*[69] and Wen-sen[78] (Table 12). Hsieh and Wetzel give carbon chemical shifts for structure **3** and Wen-sen gives chemical shifts for structure **4a**.

Table 12. Computed and Experimental ^{13}C NMR Chemical Shifts for Structures **3-5**.

	3[a]	**3**[b]	**3**[c]	**4a**[a]	**4a**[d]	**4b**[a]	**5**[a]
1	115.0	144.9	118.4	114.1	116.8	110.5	114.5
2	143.3	116.8	146.5	142.4	144.9	143.6	143.4
3a	134.9	131.9	137.0	130.2	144.8	135.2	135.7
4	169.6	160.8	173.9	162.3	160.6	107.9	175.4
5	148.0	163.9	149.6	98.9	101.8	153.1	92.4
6	109.4	101.8	113.4	157.8	163.9	152.0	156.4
7a	137.4	139.2	139.5	137.4	139.1	137.2	136.5
8	108.0	116.9	110.6	114.7	116.6	115.3	113.2
9	128.3	130.9	130.9	128.5	122.4	128.0	128.3
10	120.8	125.0	124.1	122.0	130.8	123.0	121.7
11	121.3	122.5	123.9	120.2	124.9	120.2	120.8
11a	123.0	124.2	124.0	123.1	130.2	124.2	123.6
11b	131.2	130.5	133.0	128.5	124.2	127.4	131.0
11c	129.0	131.8	132.3	129.6	131.8	124.5	130.4
OMe	53.4	56.8	57.4	53.7	56.8	53.8	53.6

[a]Computed δ_C in ppm at the B3LYP/6-311+G(2d,p)//M06-2X/6-31+G(d,p) level of theory with a linear correction applied
[b]Experimental δ_C in ppm from Hsieh *et al.* for proposed structure **3**[76]
[c]Experiemental δ_C in ppm from Wetzel *et al*. for proposed structure **3**[69]
[d]Experiemntal δ_C in ppm from Wen-sen for proposed structures **4a** and **4b**[78]

Mean unsigned errors (MUE) were also computed between the experimental shifts and the calculated shifts (Table 13). Carbons 4, 5, and 6 were compared based on functional group. Hsieh's structure **3** shifts, once again, best line up with the computed shifts from structure **4a** (MUE of 5.7), while the MUE when compared to the computed **3** is higher (MUE of 7.9). As in the case of the proton chemical shifts, the other experimental data sets fit best with the computed data sets of the same structures.

Table 13. Mean Unsigned Errors Between Computed and Experimental ^{13}C NMR Chemical Shifts for Structures **3-5**.

	3[b]	**3**[c]	**4a**[d]
3[a]	7.9	2.8	6.0
4a[a]	5.7	5.6	4.7
4b[a]	7.6	5.0	5.6
5[a]	7.5	4.0	5.4

[a]Computed δ_C in ppm at the B3LYP/6-311+G(2d,p)//M06-2X/6-31+G(d,p) level of theory with a linear correction applied
[b]Experimental δ_C in ppm from Hsieh *et al.* for proposed structure **3**[76]
[c]Experiemental δ_C in ppm from Wetzel *et al*. for proposed structure **3**[69]
[d]Experiemntal δ_C in ppm from Wen-sen for proposed structures **4a** and **4b**[78]

3.3.3 Conclusions

Analysis of the calculated shifts of both the proton and carbon-13 indicate that the compound Hsieh *et al.*[76] isolated and assigned as structure **3** is actually structure **4a** as determined by Wetzel *et al*.[69] The calculated shifts for structures **3**, **4a**, and **4b** agreed correctly with the experimental shifts for Wetzel's **3** and Wen-sen's **4a** and **4b**. If calculations had been done on the possible isomers and compared to the shifts found for the originally isolated compound of Hsieh, the ambiguity in the experiments could have been addressed and led to the correct assignment of the compound originally.

3.4 Menthol

3.4.1 Background

The drymaritin family of molecules illustrated the ability of the computed chemical shifts to differentiate between structural (specifically, constitutional) isomers. However, being able to differentiate between stereoisomers is also an important goal. Menthol, a major component of peppermint oil, has three additional diastereomers; isomenthol, neomenthol, and neoisomenthol (Figure 6).

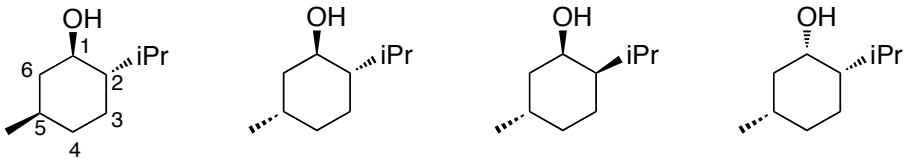

Figure 6. Structures of (**a)** (-)-menthol, (**b)** (-)-isomenthol, (**c)** (-)-neomenthol, and (**d)** (-)-neoisomenthol.

Three of the four isomers' chemical shifts were experimentally assigned by Aspaas.[79] This made the menthol family a satisfactory choice to examine. All four isomers where calculated for completeness.

3.4.2 Results

Proton shifts were calculated for each structure **6a** – **6d** and are shown in Table 14 along with the experimental chemical shits for structures **6a** – **6c**.

Table 14. Computed and Experimental ^{1}H NMR Chemical Shifts for Structures **6a-d**.

	6a[a]	**6b**[a]	**6c**[a]	**6d**[a]	**6a**[b]	**6b**[b]	**6c**[b]
1	3.42	3.78	4.05	4.00	3.41	3.80	4.11
2	1.14	1.16	0.91	1.11	1.11	1.15	0.87
3a	1.10	1.44	1.36	1.68	0.97	1.36	1.27
3e	1.63	1.52	1.75	1.48	1.61	1.54	1.84
4a	0.88	1.48	0.91	1.50	0.84	1.44	0.89
4e	1.66	1.42	1.72	1.45	1.66	1.30	1.71
5	1.43	1.95	1.73	1.71	1.43	1.97	1.67
6a	0.94	1.48	1.13	1.69	0.92	1.50	1.09
6e	1.88	1.67	1.80	1.61	1.96	1.61	1.73
CHC**H**$(CH_3)_2$	2.10	1.99	1.53	1.69	2.17	1.97	1.52

[a]Computed δ_H in ppm at the B3LYP/6-311+G(2d,p)//M06-2X/6-31+G(d,p) level of theory with a linear correction applied
[b]Experimental δ_H in ppm from Aspaas[79]

Mean unsigned errors were then calculated between the computed proton shifts and the experimental proton shifts (Table 15). In each case the computed shifts correspond best (smallest MUE) with the experimental shifts of the same structure.

Table 15. Mean Unsigned Errors Between Computed and Experimental ^{1}H NMR Chemical Shifts for **6a-d**.

	6a[b]	**6b**[b]	**6c**[b]
6a[a]	0.04	0.31	0.25
6b[a]	0.34	0.04	0.32
6c[a]	0.28	0.29	0.05
6d[a]	0.42	0.16	0.29

[a]Computed δ_H in ppm at the B3LYP/6-311+G(2d,p)//M06-2X/6-31+G(d,p) level of theory with a linear correction applied
[b]Experimental δ_H in ppm from Aspaas[79]

3.4.3 Conclusions

For a set of menthol stereoisomers, the computed proton shifts agree correctly based on the MUE with the assignments from the experimental work by Aspaas.[79] This is another example that indicates that the computational method can be sensitive enough to assign the structures of stereoisomers based on ^{1}H NMR shifts.

3.5 Conclusions

After testing the computational protocol for determining chemical shifts, it appears that the method can be useful in assigning both stereo- and structural isomers. In the case of the menthol stereoisomers, the calculated shifts agreed well with the shifts found experimentally. Comparatively, the MUE for the correct assignment is much smaller than the MUEs for incorrect assignments leaving no ambiguity in the assignments. For the structural isomers of drymaritin, once again the computational shifts agreed with the experimental shifts from Wetzel *et al.*[69] and Wen-sen.[78] In this case, the correct assignment MUEs are small enough to limit ambiguity in the assignments, although not as clear-cut as the menthol example. For drymaritin, the proton chemical shifts are more sensitive than the carbon-13 chemical shifts.

Menthol is a small molecule and all stereocenters examined include a hydrogen on the carbon. Drymaritin is a rigid molecule, only the methoxy group has free rotation. Future work could include examining larger, more flexible molecules and molecules where the stereocenters do not include hydrogens.

Chapter 4. NMR Chemical Shift Calculations for the Case of Patchouli Alcohol[3]

4.1 Introduction

Patchouli oil has long been a component in fragrances and perfumes and can be extracted from *Pogostemon patchouli* pellets.[80-82] The essential oil has a complex composition, but a major component is patchouli alcohol.[80,83] The scent of patchouli oil has been, at least partially, attributed to patchouli alcohol.[80,82,83] The alcohol was isolated in 1869 by Gal and Montgolfier who determined its formula as $C_{15}H_{26}O$.[80,82] Büchi *et al.* proposed the structure for patchouli alcohol shown in Figure 7.[80]

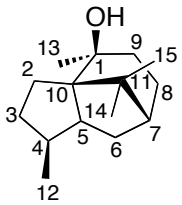

Figure 7. Structure of patchouli alcohol initially proposed by Büchi *et al.*[80]

The structure in Figure 7 was revised in 1963 by Dobler *et al.*[84] They performed an X-ray crystal structural analysis on a chromic acid diester derivative of patchouli alcohol and found that the X-ray structure could not be reconciled with structure 1.[84] They instead proposed a new structure for patchouli alcohol (Figure 8).[84]

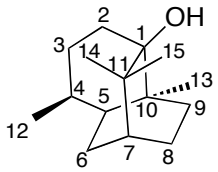

Figure 8. Structure of patchouli alcohol subsequently proposed by Dobler *et al.*[84]

[3] I'd like to acknowledge Matthew Jansma for the experimental work done in the Hoye Group of the University of Minnesota.

4.2 Computational Methods

The computational protocol previously described was used once again. Conformational searching was done using the MMFFs force field[60,61] in Schrodinger's Macromodel.[59] Structures were optimized at the M06-2x/6-31+G(d,p) level of theory[16,17] as implemented in Gaussian09[66] with IEF-PCM[23-27] chloroform solvation. GIAO[31,32] NMR calculations were done at the B3LYP/6-311+G(2d,p) level of theory[17,19,20] relative to TMS. Conformer chemical shifts were averaged using Boltzmann weighting[34,45] and then treated with a linear correction.[34]

4.3 Results

The original structure of patchouli alcohol by Büchi[80] (Figure 7) was found to have four conformers within the acceptable energy window and the revised structure (Figure 8) was found to have three such conformers.

4.3.1 Proton Chemical Shifts

Proton chemical shifts were computed for structures **7** and **8** and then compared to the experimental shifts recorded for patchouli alcohol by Barton *et al.*[85] The proton chemical shifts and MUEs are shown in **Table 16**. The MUE for **7** is more than three times larger than the MUE for **8**.

Table 16. Computed and Experimental ^{1}H NMR Chemical Shifts for Figures 7 and 8.

	7[a]	**8**[a]	Exp[b]
2	1.56	1.76	1.7
2	1.79	1.53	1.5
3	1.47	1.48	1.48
3	1.87	1.46	1.34
4	2.30	1.95	1.97
5	2.40	1.45	1.44
6	1.32	1.27	1.26
6	1.98	1.60	1.85
7	1.67	1.14	1.19
8	1.28	1.92	1.48
8	2.14	1.30	1.26
9	1.71	1.96	1.85
9	1.38	1.07	1.05
12	1.04	0.87	0.78
13	1.16	0.88	0.84
14	0.89	1.10	1.05[d]
15	1.30	1.11	1.07[d]
MUE[c]	0.28	0.08	

[a]Computed δ_H in ppm at the B3LYP/6-311+G(2d,p)//M06-2X/6-31+G(d,p) level of theory with a linear correction applied.
[b]Experimental δ_H in ppm from Barton *et al.*[85]
[c]Mean unsigned error between computed and experimental shifts.
[d]Experimental shifts may be interchanged to create better fit with computed shifts.

An experimental shift at 1.85 ppm was originally assigned to a hydrogen atom on carbon 6 while a shift of 1.48 ppm was originally assigned to a hydrogen on carbon 8. The calculated shifts for these hydrogens are 1.59 ppm and 1.91 ppm, respectively. By exchanging these experimental shifts, the MUE is improved by 0.03 (**Table 17**). This could indicate that the experimental shifts were assigned incorrectly. Matthew Jansma, a research student in the Hoye Group at the University of Minnesota, examined patchouli alcohol and performed 1-D and 2-D NMR. NOESY and COSY crosspeaks gave

evidence for interchanging the chemical shift assignments for the hydrogen atoms on carbon 6 and carbon 8.

Table 17. Unsigned Errors for **8**.

	8[a]	Exp[b]	UE[c]
2	1.76	1.7	0.06
2	1.53	1.5	0.03
3	1.48	1.48	0.00
3	1.46	1.34	0.12
4	1.95	1.97	0.02
5	1.45	1.44	0.01
6	1.27	1.26	0.01
6	1.60	1.85	0.25 (0.12)[d]
7	1.14	1.19	0.05
8	1.92	1.48	0.44 (0.07)[d]
8	1.30	1.26	0.04
9	1.96	1.85	0.11
9	1.07	1.05	0.02
12	0.87	0.78	0.09
13	0.88	0.84	0.04
14	1.10	1.05	0.05
15	1.11	1.07	0.04
MUE			0.08 (0.05)[d]

[a]Computed δ_H in ppm at the B3LYP/6-311+G(2d,p)//M06-2X/6-31+G(d,p) level of theory with a linear correction applied.
[b]Experimental δ_H in ppm from Barton *et al.*[85]
[c]Unsigned errors between the computed and experimental shift
[d]Value in parentheses is UE and MUE if the experimental values are reassigned to give a better fit.

4.3.2 Carbon Chemical Shifts

Carbon chemical shifts were also computed for **7** and **8** and compared to Barton *et al.*'s[85] carbon shifts (**Table 18**). The MUE for **7** is four times larger than the MUE for **8**.

Table 18. Computed and Experimental ^{13}C NMR Chemical Shifts for Figures 7 and 8.

	7[a]	**8**[a]	Exp[b]
1	76.88	75.0	57.29
2	25.02	32.8	32.63
3	38.57	29.45	28.58
4	36.86	30.04	28.03
5	51.34	45.04	43.68
6	29.14	25.32	24.28
7	48.82	41.09	39.09
8	26.80	25.05	24.54
9	35.75	29.15	28.79
10	65.81	39.24	37.53[d]
11	45.60	41.56	40.03[d]
12	14.45	17.32	18.48
13	26.58	19.29	20.53
14	28.34	22.45	26.80[e]
15	21.76	25.00	24.20[e]
MUE[c]	8.36	2.35	

[a]Computed δ_C in ppm at the B3LYP/6-311+G(2d,p)//M06-2X/6-31+G(d,p) level of theory with a linear correction applied.
[b]Experimental δ_C in ppm from Barton *et al.*[85]
[c]Mean unsigned error between computed and experimental shifts.
[d,e] Experimental shifts may be interchanged to create better fit with computed shifts.

4.4 Conclusions

The computed carbon-13 and proton chemical shifts for structure 8 best align with the experimental shifts from Barton *et al.*[85] agreeing with the presently accepted structure of patchouli alcohol. The MUE between the calculated chemical shifts for structure 7 and the experimental shifts are significantly larger than the MUE for structure 8, therefore the use of computed shifts could have greatly benefited the initial assignment of patchouli alcohol had this technology been available. In addition, the computed shifts seem to indicate that there was a misassignment of the experimental shifts and signals ascribed to protons on carbons 6 and 8 should be exchanged.

Chapter 5. Theoretical Prediction of Linear Free Energy Relationships Using Proton Nucleomers[4]

Giovanni La Macchia, Laura Gagliardi, Geoffrey S. Carlson, Ashley N. Jay, Erik Davis and Christopher J. Cramer

Values of σ and σ^+, for use in linear free energy relationships, are determined for *para* hydrogen atoms having nuclear charges other than 1 (nucleomers). Hammett ρ values for a variety of free energies of activation, reaction, and other extrathermodynamic properties (e.g., vibrational frequencies) are computed there from and compared to those computed using typical *para* functional groups. The nucleomer correlations show excellent qualitative agreement with standard correlations but the quantitative agreement is less good, typically underestimating the standard ρ-value by 10-60%.

5.1 Introduction

Linear free energy relationships have a long history in the study of mechanistic organic chemistry.[86-95] In early work, Hammett proposed that the effects of aryl substituents on benzoic acid ionization constants would correlate linearly with the effects of those same substituents on other reactions of substituted aromatics. That is, he suggested the prevalence of relationships of the form

$$\log\left(\frac{K_X^o}{K_H^o}\right) = \sigma_X \rho \tag{5}$$

where K_X is the equilibrium (or rate) constant for some reaction of an aromatic ring substituted with substituent *X*, and the specification of *X* includes whether it is *ortho*, *meta*, or *para* to the reacting functionality. The slope of the linear relationship, ρ, is characteristic for the reaction under study once substituent constants σ_X have been

[4] This work was supported by the US National Science Foundation (CHE-0610183) and the Swiss National Science Foundation (200021-111645/1).

chosen. Hammett chose these constants so as to make ρ=1 for the ionization constants of substituted benzoic acids in aqueous solution and as such this reaction defines the so-called σ scale.

Subsequent studies by Brown *et al*.[96,97] emphasized that the influence of substituents on aromatic reactions typically involves a balance between inductive effects and resonance effects, and these workers pointed out that the σ scale was more appropriate for reactions dominated by the former (because of the nature of its defining reaction, benzoic acid ionization). They proposed an equivalent relationship for cases where resonance effects were dominant,

$$\log\left(\frac{K_X^o}{K_H^o}\right) = \sigma_X^+ \rho \tag{6}$$

where the values of the σ^+ scale were defined for *para* substituents so as to construct a linear free energy relationship for substituted cumyl chloride ionizations in aqueous acetone.

Note that the ratios of logarithms of equilibrium or rate constants appearing in Eqs 5 and 6 can be related to free energy changes according to

$$\Delta G_X^o - \Delta G_H^o = -2.303RT\log\left(\frac{K_X^o}{K_H^o}\right) \tag{7}$$

and

$$\Delta G_X^{\ddagger,o} - \Delta G_H^{\ddagger,o} = -2.303RT\log\left(\frac{k_X^o}{k_H^o}\right) \tag{8}$$

where R is the universal gas constant, T is temperature, and the relationships in Eq 8 involving free energies of activation derives from transition-state (TS) theory.[86]

Operationally, determination of experimental ρ values is accomplished by (i) the synthesis of various substituted versions of some substrate of interest, (ii) the measurement of the relevant equilibrium or rate constants (or possibly other non-free-energy related properties, although any observed linear relationship is then extrathermodynamic in nature), and (iii) the regression of the experimental data on tabulated σ or σ^+ values. The same process can also be undertaken within the contest of a theoretical modeling study. That is, any process being studied computationally can be repeated with various substituents and a ρ-values determined for the level of theory being used.

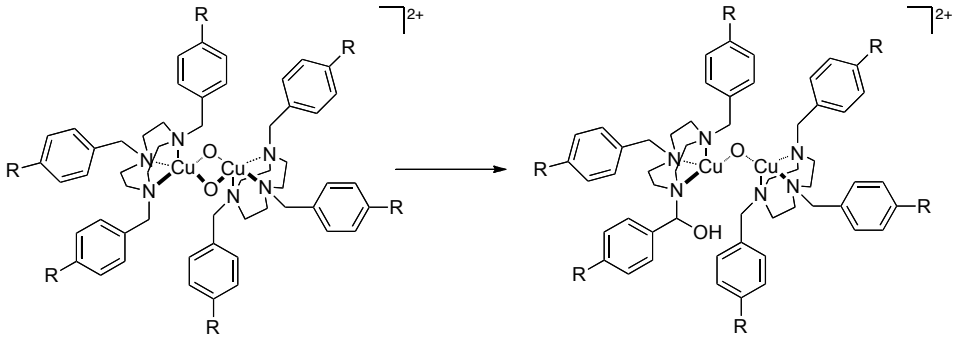

Scheme 1. Benzylic C–H bond activation by supported $Cu_2O_2^{2+}$ core.

Comparing computational and experimental ρ values can be useful for validating the theoretical model, particularly for cases where free energies of activation are being computed in order to gain insight into the nature of TS structures, the characterization of which is certainly one of the most powerful aspects of a modeling study. Thus, for example, one of us computed TS structures for the reaction shown in Scheme 1 using a mixed quantum-mechanical/molecular mechanical protocol;[98,99] the reaction in question involves a mechanistically interesting C–H bond activation by a $Cu_2O_2^{2+}$ core and had

been studied experimentally by Mahapatra *et al*.[100] Analysis of the computed rate-determining TS electronic structures suggested that the nature of the reaction was best described as a hydrogen-atom transfer from a benzylic carbon to a core oxygen atom (as opposed to, e.g., proton-coupled electron transfer or hydride transfer between these atoms). To further validate this interpretation, Cramer *et al.*[98,99] computed *r* by regression against σ values for R=H, CF_3, and OH and showed that there was indeed good agreement between the computed values and those measured experimentally by Mahapatra *et al*.[100] Given that the size and complexity of the molecules in Scheme 1 had imposed restrictions on the possible theoretical models that could be practically applied, this validation step was especially useful.

In sufficiently complex theoretical models, the computation of a large number of substituted systems can be quite tedious (we make this point with all due humility, noting that in most instances the computational tedium pales by comparison to its experimental counterpart). There is, however, a simplification that is only available to the alchemically minded theorist. When inductive effects are dominant, one may in principle introduce such effects without changing the atomic composition of the unsubstituted aromatic ring by adjusting the nuclear charge of the parent proton. Thus, increasing the proton charge to a value fractionally greater than one should inductively mimic the substitution of an electron-withdrawing group at that position, and reduction of the nuclear charge to a value fractionally less than one should mimic substitution by an electron-donating group. In this work, we address the utility of such an approach by examining its quantitative performance against full molecular calculations for the model reactions and properties

listed in Fig. 9. Thus, we establish σ values for H atoms having variable nuclear charge (which we call hydrogen nucleomers) and explore whether these values are as transferable to a wide variety of situations as are those already tabulated for synthetically accessible functional groups. We note that other theoretical approaches to replace standard σ values have been reported. For instance, Girones and Ponec[101] have suggested their replacement with fragment quantum self-similarity measures in quantitative structure-activity relationships.

5.2 Computational Methods

All molecular geometries were fully optimized at four different levels of theory. In three cases, the B3LYP functional[9-12] was employed with different basis sets, namely, MIDI!,[15] 6-31+G(d,p),[16] and aug-cc-pVDZ.[21,22] For the remaining case the PBE functional[5] was employed with the 6-31+G(d,p) basis set. Analytical vibrational frequencies were computed to verify the nature of all stationary points as either minima or TS structure; however, Hammett relationships involving energies were evaluated using the *electronic* energies in order to avoid possible complications associated with using the rigid rotator quantum-mechanical-harmonic-oscillator approximation for thermal contributions to free energies.[1]

For cases involving proton nucleomers, that is, molecules where the charge on an aryl proton was varied from its normal value of 1.0, we generally used the frozen geometry of the corresponding normal systems. In select instances, however, we reoptimized each nucleomer structure, for example to compute adiabatic ionization potentials or variations in carbonyl vibrational frequencies.

Calculations were performed using the Gaussian03,[102] MOLCAS v. 6.4,[103] and Turbomole[104] suites of electronic structure programs. In the cases of MOLCAS and Turbomole, the atomic charge can be varied as part of normal input. In the case of Gaussian03, a proton with a non-unit nuclear charge is most easily created by defining a ghost atom (not a hydrogen atom) to exist at the appropriate coordinates carrying the same basis functions as those defined for an H atom. In addition, a point charge is placed at the ghost atom's position with a value chosen so that the sum of the point charge and the molecular charge is the desired change in nucleomer charge. Thus, for example, the *para*-H nucleomer of benzaldehyde having additional charge +0.1 could be constructed as the 4-dehydrobenzaldehyde anion with a *para* ghost atom and point charge of magnitude +1.1 at the ghost atom's position. This procedure works for any nucleus.[105,106] However, to avoid convergence difficulties associated with very poor initial guess wave functions when highly charged molecules are combined with large point charges (to simulate a heavier atom) it is typically advisable to carry out a calculation on the 'normal' molecule first and use that wave function for the initial guess.

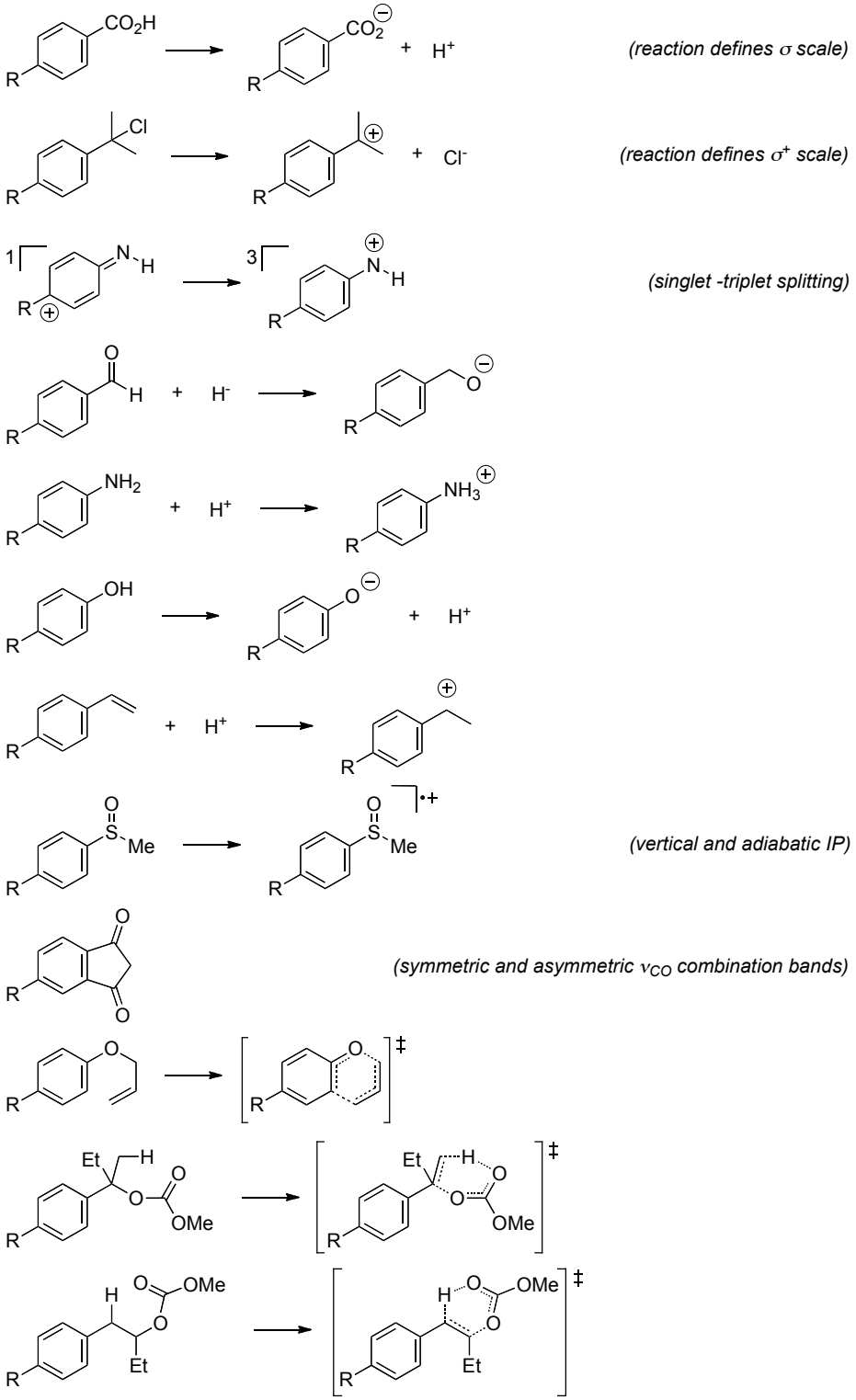

Figure 9. Reactions and molecules for which energy changes and other properties were computed for R=NH_2, OH, Me, Cl, CN, NO_2, and H atoms having nuclear charges of 0.80, 0.85, 0.90, 0.95. 1.00, 1.05, 1.10, 1.15, and 1.20 a.u.

Table 19. *R* and ρ' values versus σ and σ^+ for various reactions from different protocols

		σ		σ^+	
System/theory	ρ-substituent	ρ'	*R*	ρ'	*R*
Benzoic acid ionization[a]					
B3LYP/MIDI!	Actual	-12.2	-0.976	-7.9	-0.925
	H±ΔZ	-12.2	-1.000	-12.6	-1.000
/6-31+G(d,p)	Actual	-12.5	-0.976	-8.0	-0.917
	H±ΔZ	-12.5	-1.000	-11.8	-1.000
/aug-cc-pVDZ	Actual	-12.4	-0.978	-7.95	-0.918
	H±ΔZ	-12.4	-1.000	-11.8	-1.000
PBE/6-31+G(d,p)	Actual	-12.7	-0.980	-8.2	-0.925
	H±ΔZ	-12.7	-1.000	-11.8	-1.000
Cumyl chloride ionization[b]					
B3LYP/MIDI!	Actual	22.0	0.974	15.2	0.991
	H±ΔZ	14.8	1.000	15.3	1.000
/6-31+G(d,p)	Actual	22.1	0.986	15.0	0.984
	H±ΔZ	15.9	1.000	15.0	1.000
/aug-cc-pVDZ	Actual	21.7	0.986	14.8	0.985
	H±ΔZ	15.6	1.000	14.8	1.000
PBE/6-31+G(d,p)	Actual	21.6	0.981	14.8	0.985
	H±ΔZ	15.9	1.000	14.8	1.000
Arylnitrenium S– T splitting					
B3LYP/MIDI!	Actual	-6.7	-0.938	-4.8	-0.984
	H±ΔZ	-2.2	-1.000	-2.2	-1.000
/6-31+G(d,p)	Actual	-7.2	-0.937	-5.2	-0.979
	H±ΔZ	-2.4	-1.000	-2.3	-1.000
/aug-cc-pVDZ	Actual	-7.0	-0.930	-5.0	-0.975
	H±ΔZ	-2.4	-1.000	-2.2	-1.000
PBE/6-31+G(d,p)	Actual	-7.1	-0.922	-5.1	-0.970
	H±ΔZ	-2.3	-1.000	-2.2	-1.000
Benzaldehyde hydride affinity					
B3LYP/MIDI!	Actual	-14.9	-0.979	-9.65	-0.928
	H±ΔZ	-13.4	-1.000	-13.9	-1.000
/6-31+G(d,p)	Actual	-16.1	-0.976	-10.4	-0.918
	H±ΔZ	-14.1	-1.000	-13.3	-1.000
/aug-cc-pVDZ	Actual	-15.9	-0.979	-10.2	-0.922
	H±ΔZ	-13.9	-1.000	-13.2	-1.000
PBE/6-31+G(d,p)	Actual	-17.8	-0.973	-11.5	-0.917
	H±ΔZ	-14.7	-1.000	-13.6	-1.000
Aniline basicity					
B3LYP/MIDI!	Actual	15.1	0.993	10.0	0.962
	H±ΔZ	12.7	1.000	13.1	1.000
/6-31+G(d,p)	Actual	16.5	0.989	10.7	0.943
	H±ΔZ	14.8	1.000	14.1	1.000
/aug-cc-pVDZ	Actual	16.2	0.965	10.5	0.867
	H±ΔZ	15.0	1.000	14.3	1.000

Table 19. *(Continued)*

		σ		σ^+	
System/theory	ρ-substituent	ρ'	R	ρ'	R
PBE/6-31+G(d,p)	Actual	16.6	0.985	10.8	0.937
	H±ΔZ	15.1	1.000	14.0	1.000
Phenol acidity					
B3LYP/MIDI!	Actual	-20.7	-0.962	-13.2	-0.900
	H±ΔZ	-15.4	1.000	-15.9	-1.000
/6-31+G(d,p)	Actual	-21.0	-0.951	-13.3	-0.883
	H±ΔZ	-15.2	-1.000	-14.4	-1.000
/aug-cc-pVDZ	Actual	-21.6	-0.929	-13.8	-0.871
	H±ΔZ	-15.2	-1.000	-14.5	-1.000
PBE/6-31+G(d,p)	Actual	-20.8	-0.953	-13.2	-0.885
	H±ΔZ	-15.5	-1.000	-14.4	1.000
Stryrene proton affinity					
B3LYP/MIDI!	Actual	24.4	0.976	17.0	0.992
	H±ΔZ	16.0	1.000	16.6	1.000
/6-31+G(d,p)	Actual	24.5	0.986	16.7	0.984
	H±ΔZ	17.1	1.000	16.2	1.000
/aug-cc-pVDZ	Actual	25.8	0.949	17.6	0.949
	H±ΔZ	16.8	1.000	16.0	1.000
PBE/6-31+G(d,p)	Actual	23.6	0.982	16.2	0.985
	H±ΔZ	17.1	1.000	15.9	1.000
Methylphenylsulfoxide IP[c]					
B3LYP/MIDI!	Actual	17.9	0.979	12.4	0.991
		18.0	0.968	12.5	0.981
	H±ΔZ	13.3	1.000	13.7	1.000
		13.3	1.000	13.8	1.000
/6-31+G(d,p)	Actual	19.5	0.981	13.2	0.978
		19.4	0.978	13.2	0.977
	H±ΔZ	14.7	1.000	14.0	1.000
		14.7	1.000	14.0	1.000
/aug-cc-pVDZ	Actual	20.7	0.938	14.2	0.945
		18.8	0.979	12.8	0.978
	H±ΔZ	14.4	1.000	13.7	1.000
		14.4	1.000	13.7	1.000
PBE/6-31+G(d,p)	Actual	18.7	0.969	12.9	0.983
		19.0	0.970	13.1	0.980
	H±ΔZ	15.2	1.000	14.2	1.000
		15.3	1.000	14.2	1.000
5,7-Indanedione $\nu_{C=O}$[d]					
B3LYP/MIDI!	Actual	6.8	0.985	4.6	0.988
		7.2	0.985	4.9	0.984
	H±ΔZ	3.9	1.000	4.0	1.000
		3.8	0.999	3.9	0.999

Table 19. *(Continued)*

		σ		σ^+	
System/theory	ρ-substituent	ρ'	R	ρ'	R
/6-31+G(d,p)	Actual	13.7	0.994	9.3	0.986
		12.9	0.997	8.6	0.980
	H±ΔZ	7.1	0.998	6.7	0.998
		7.3	0.999	6.9	0.999
/aug-cc-pVDZ	Actual	13.1	0.992	8.9	0.990
		12.4	0.998	8.4	0.985
	H±ΔZ	7.0	0.993	6.7	0.993
		7.2	0.997	6.9	0.997
PBE/6-31+G(d,p)	Actual	12.7	0.987	8.7	0.988
		12.4	0.995	8.4	0.985
	H±ΔZ	7.1	0.998	6.6	0.998
		7.4	0.999	6.8	0.999
Claisen rearrangement					
B3LYP/MIDI!	Actual	1.9	0.956	1.3	0.990
	H±ΔZ	0.7	0.998	0.8	0.998
/6-31+G(d,p)	Actual	1.8	0.966	1.3	0.996
	H±ΔZ	0.8	0.997	0.8	0.997
/aug-cc-pVDZ	Actual	1.7	0.970	1.2	0.992
	H±ΔZ	0.8	0.997	0.8	0.997
PBE/6-31+G(d,p)	Actual	2.2	0.975	1.5	0.990
	H±ΔZ	0.9	0.998	0.9	0.998
Carbonate fragmentation I					
B3LYP/MIDI!	Actual	1.7	0.974	1.2	0.996
	H±ΔZ	0.7	1.000	0.7	1.000
/6-31+G(d,p)	Actual	3.8	0.976	2.6	0.989
	H±ΔZ	1.5	1.000	1.5	1.000
/aug-cc-pVDZ	Actual	3.7	0.974	2.6	0.991
	H±ΔZ	1.5	1.000	1.4	1.000
PBE/6-31+G(d,p)	Actual	3.1	0.961	2.2	0.986
	H±ΔZ	1.2	0.999	1.1	0.999
Carbonate fragmentation II					
B3LYP/MIDI!	Actual	-1.1	-0.978	-0.7	-0.946
	H±ΔZ	-0.3	-0.995	-0.3	-0.995
/6-31+G(d,p)	Actual	-0.7	-0.919	-0.5	-0.888
	H±ΔZ	0.0	0.582	0.0	0.582
/aug-cc-pVDZ	Actual	-0.7	-0.933	-0.5	-0.900
	H±ΔZ	0.0	-0.771	0.0	-0.771
PBE/6-31+G(d,p)	Actual	-1.0	-0.931	-0.6	-0.890
	H±ΔZ	-0.1	-0.960	-0.1	-0.960

[a]Reaction used to define σ scale.
[b]Reaction used to define σ^+ scale.
[c]Data above are for vertical ionization potential and below for adiabatic ionization potential.
[d]Data above for asymmetric combination stretch and below for symmetric combination stretch.

5.3 Results and Discussion

We consider first benzoic acid ionization. In order to compare theory directly to theory, thereby avoiding complications associated with, for example, solvation effects, we combine Eqs 5 and 7, absorb all other constants (-2.303*RT*) into the slope, and ignore thermal contributions to free energies to arrive at

$$\Delta E_X^o - \Delta E_H^o = \sigma_X \rho' \tag{9}$$

Where computed values of ρ' are not expected to be equal to measured values of ρ but may be used straightforwardly for defining σ_X values for hydrogen nucleomers. In the case of benzoic acid ionization, regression of computed energy changes for the first reaction shown in Fig. 9 on σ_X values[107] for the standard functional groups *X*=NH_2, OH, Me, H, Cl, CN, and NO_2 led to highly linear correlations at all four theoretical levels (absolute values of Pearson correlation coefficient *R* in excess of 0.976) with quite similar values of ρ', from -12.2 to -12.7 (Table 19, row labeled 'Actual' *para* substituent). The regression for PBE/6-31+G(d,p) is shown in Fig. 10. As expected, regression on σ_X^+ values led to reduced quality linear correlations and smaller corresponding values of ρ' (Table 19).

We next computed energy changes for the ionization of parent benzoic acid with the charge of the *para* hydrogen nucleus changed to values of 0.80, 0.85, 0.90, 0.95, 1.00 (i.e., a normal hydrogen nucleus), 1.05, 1.10, 1.15, and 1.20 a.u. At each level of theory, keeping the geometry of the parent benzoic acid frozen for maximum simplicity, the linear correlations between the ionization energy changes and the variations in nuclear charges were perfect (absolute values of *R*=1.000); σ_X values were assigned for each

level of theory so as to make the slopes of the respective correlations equal to those computed using actual *para* substituents (Table 19; row labeled H±ΔZ). The derived values, together with the normal functional group values used in this study, are listed in Table 20. The variation in the ionization energy was about 4.1 kcal mol^{-1} per 0.05 unit change in the proton nuclear charge.

For the σ^+ scale, an identical protocol was followed for the ionization of cumyl chloride. With actual functional group substituents and correlating against their respective σ_X^+ values,[107] very high correlation coefficients were found with computed energy changes; *R* values exceeded 0.984 for all levels of theory and similar ρ' values 14.8-15.2 were obtained (Table 1 and Fig. 3 for PBE/6-31+G(d,p) correlation). It is noteworthy that correlations of equally good quality were obtained when regressing on σ_X values instead of σ_X^+ values, indicating that the gas-phase calculations do not fully reflect differences in experimental conditions that distinguish one scale from the other. Again, nucleomer energy changes were computed and σ_X^+ values were assigned so as to match ρ' values computed from actual functional groups. The various σ_X^+ values are listed in Table 21. Once again, nucleomer energy-change correlations were perfectly linear with nuclear charge variation.

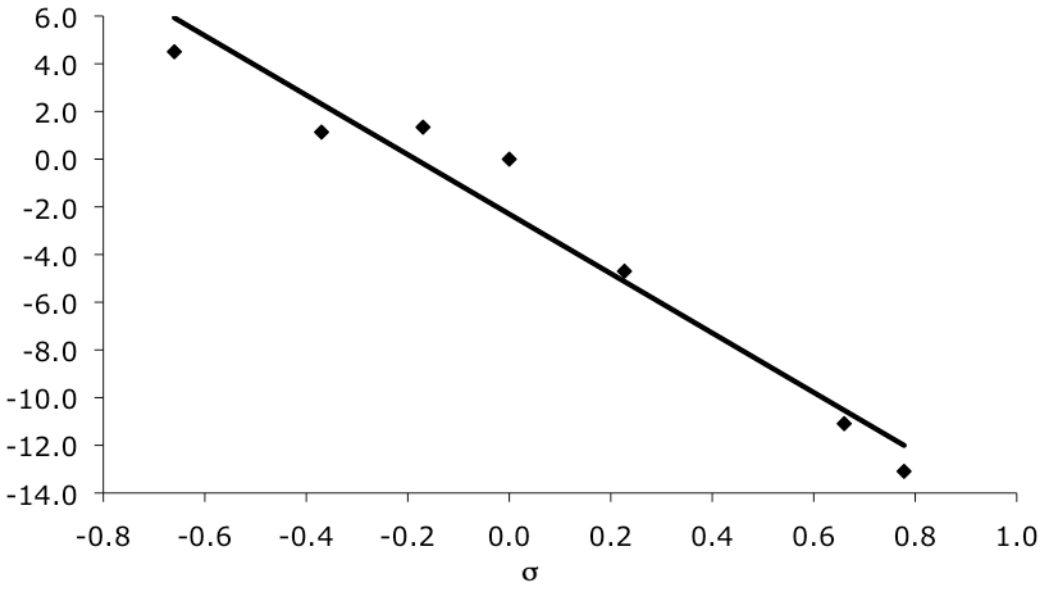

Figure 10. Computed energy changes for substituted benzoic acid ionization versus σ_X for various *para* substituents at the PBE/6-31+G(d,p) level

We note that DiLabio and Ingold,[108] using a similar computational protocol but with B3LYP/6-311+G(2d,2p) electronic energies and AM1 geometries and thermal contributions predicted a ρ'-values of 16.3, which is quite close to those reported here. DiLabio and Ingold[108] noted that including solvation effects with the SM5.42R/AM1 continuum solvation model[109] led to improved agreement with experiment, with a computed ρ'-value of 7.7 only slightly exceeding the experimentally determined value of 6.2.

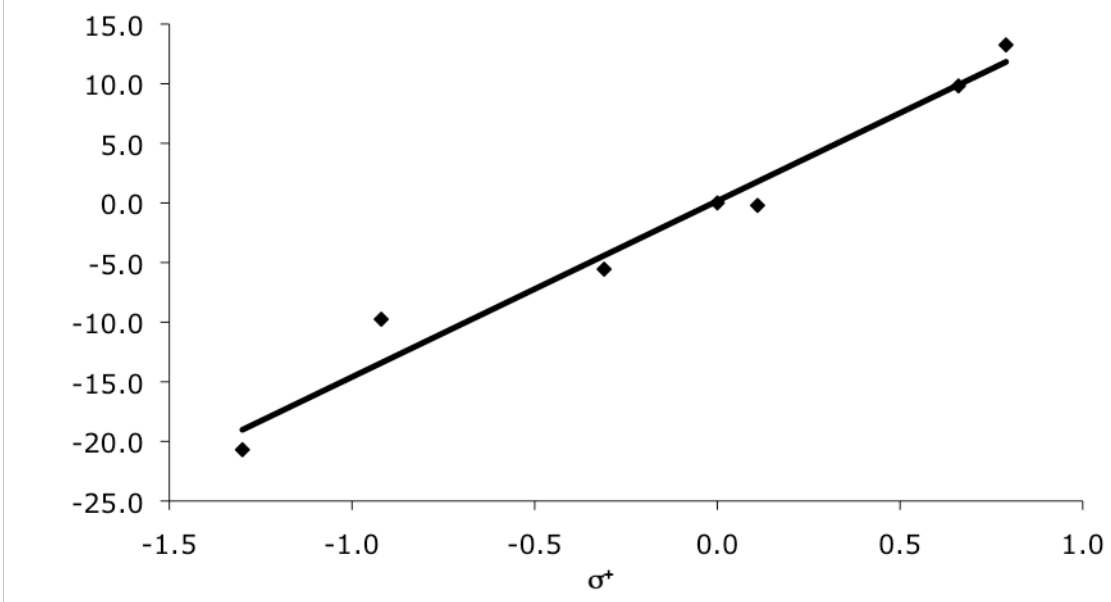

Figure 11. Computed energy changes for substituted cumyl chloride ionization versus σ_X^+ for various *para* substituents at the PBE/6-31+G(d,p) level

We next considered the influence of *para* substitution on singlet-triplet (S-T) splitting in substituted nitrenium ions. Because singlet arylnitrenium ions have been implicated in carcinogenesis,[110-115] the study of the influence of substituents on the relative energies of the singlet and triplet states of such systems has been a topic of considerable theoretical interest.[116-122] In this context, Sullivan *et al.*[120] have previously computed linear correlations against σ and σ^+ values for several actual functional groups and reported optimal linear correlation with the latter scale at the BPW91/cc-pVDZ level of theory (including thermal free-energy contributions and aqueous solvation effects with the SM5.42R continuum solvation model[123]). We observed similarly good correlations with σ^+ values for the levels of theory employed here, with gas-phase ρ' values of about -5.0. By contrast, correlation against the nucleomer σ^+ values listed in Table 21 was

somewhat disappointing. While the linear correlations were all essentially perfect, the computed ρ' vales were only about -2.2, which is less than half the value computed for actual substituents. This probably reflects the significant geometric differences between singlet and triplet species that can be enhanced by appropriate substituents other than H. Thus, as illustrated in Fig. 9 and confirmed by IR spectroscopy,[119] the singlet nitrenium is best represented as a substituted cyclohexadienium ion while the triplet nitrenium really has true nitrenium ion character. As a H nucleomer cannot hybridize with the cyclohexadienium cation the way a more complex functional group can, the computed group influence is strongly reduced when only nucleomers are considered.

Table 20. Values of σ_X for functional groups and H atom nucleomers having nuclear charge Z

			Theory level			
p-X	*Z*	Exp.[a]	B3LYP/ MIDI!	B3LYP/ 6-31+G(d,p)	B3LYP/ aug-cc-pVDZ	PBE/ 6-31+G(d,p)
NH_2		-0.660				
OH		-0.370				
Me		-0.170				
H	0.80		-1.456	-1.310	-1.337	-1.292
	0.85		-1.092	-0.983	-1.003	-0.969
	0.90		-0.728	-0.655	-0.668	-0.646
	0.95		-0.364	-0.328	-0.334	-0.323
	1.00	0.000				
	1.05		0.364	0.328	0.334	0.323
	1.10		0.728	0.655	0.668	0.646
	1.15		1.092	0.983	1.003	0.969
	1.20		1.456	1.310	1.337	1.292
Cl		0.227				
CN		0.660				
NO_2		0.778				

[a]From Reference [107].

Table 21. Values of σ_X^+ for functional groups and H atom nucleomers having nuclear charge Z

			Theory level			
p-X	*Z*	Exp.[a]	B3LYP /MIDI!	B3LYP/ 6-31+G(d,p)	B3LYP/ aug-cc-pVDZ	PBE/ 6-31+G(d,p)
NH_2		-1.300				
OH		-0.920				
Me		-0.310				
H	0.80		-1.456	-1.310	-1.337	-1.292
	0.85		-1.092	-0.983	-1.003	-0.969
	0.90		-0.728	-0.655	-0.668	-0.646
	0.95		-0.364	-0.328	-0.334	-0.323
	1.00	0.000				
	1.05		0.364	0.328	0.334	0.323
	1.10		0.728	0.655	0.668	0.646
	1.15		1.092	0.983	1.003	0.969
	1.20		1.456	1.310	1.337	1.292
Cl		0.110				
CN		0.660				
NO_2		0.790				

[a]From Reference [107].

More favorable results are obtained for the fourth reaction in Fig. 9, the hydride affinity of substituted benzaldehydes. Excellent correlations with σ are computed at all levels, with large negative ρ' values. Correlations with σ^+ are less linear, as expected for this reaction which should have no particular sensitivity to resonance stabilization. Correlation of reaction energies computed for H nucleomers against the σ values determined from benzoic acid ionization gives linear correlations with ρ' values about 10-15% smaller than those computed from actual substituted benzaldehydes at the various theoretical levels. Figure 12 shows the data from both sets of calculations on a common plot.

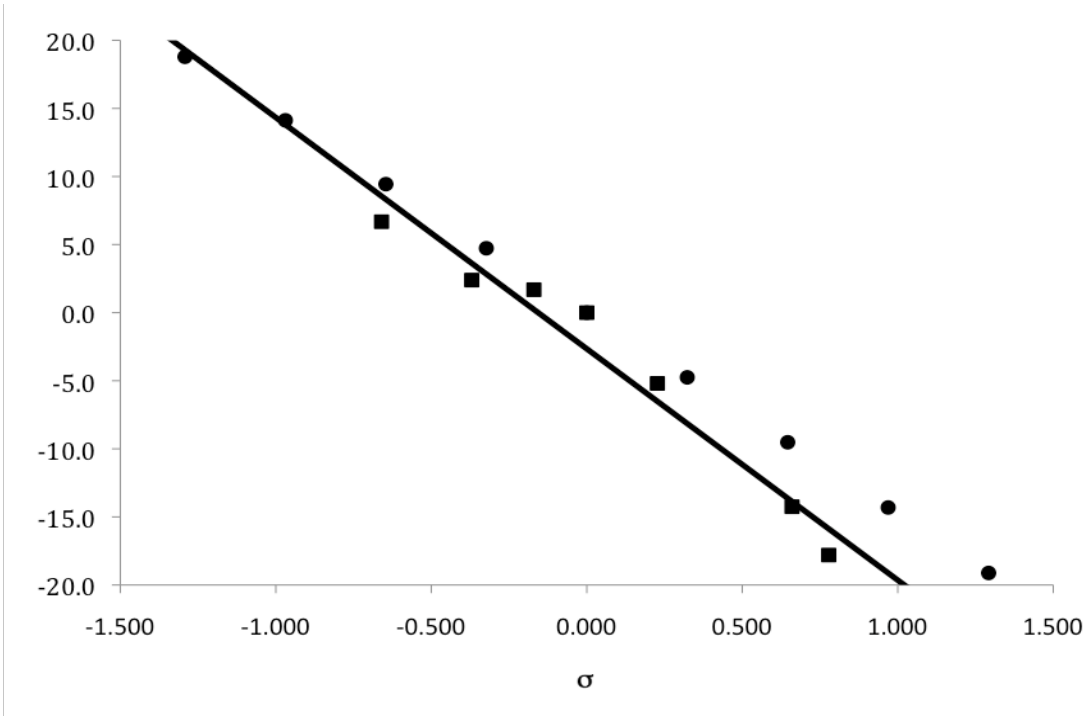

Figure 12. Computed energy changes for substituted benzaldehyde hydride affinities versus σ_X for various actual *para* substituents (squares) and H nucleomers (circles) at the PBE/6-31+G(d,p) level. The line is a linear fit to the data for actual substituents

Similarly good quality correlations for both actual substituents and H nucleomers are computed for the basicities of substituted anilines and acidities of substituted phenols (reactions 5 and 6 of Fig. 9, respectively). As with the benzaldehyde hydride affinities, in each case correlations of energy changes for actual substituents against σ values are more linear than those against σ^+ values – substantially so in the case of phenol acidities – although correlations against either set of nucleomer values are perfectly linear. Also similar to the benzaldehydes case, the ρ values computed for the H nucleomers using the σ scales are about 10-15% smaller than those computed from actual substituted anilines at the various theoretical levels. In the phenol case that disparity increases to about 30%, reflecting perhaps a deficiency in the use of nucleomers when a heteroatom directly attached to the aromatic ring carries a full charge and is otherwise unsubstituted.

Extremely good agreements – ρ' values within 2-3% – are obtained between actual substituent and nucleomer correlations against σ^+ values for substituted styrene proton affinities (Reaction 7 of Fig. 9). This is perhaps not surprising given that the product carbenium ion differs from the cumyl cation only by methyl substitution at the cationic center.

Another reaction that generates a positively charged functional group is the ionization of substituted methyl phenyl sulfoxides (Reaction 8 of Fig. 9), originally studied experimentally and computationally for a series of substituted examples by Baciocchi and Gerini.[124] In this case, we considered both the vertical ionization potential, that is, taking the radical cation geometry to be the same as that optimized for the neutral precursor, and also the adiabatic potential taking geometric relaxation of the radical cation into account. In the case of the nucleomers, the vertical IP then corresponds to using the neutral, unsubstituted geometry for nucleomer calculations, and the adiabatic IP is computed using the relaxed geometry of methyl phenyl sulfoxide radical cation (but *not* further relaxing when changing the nuclear charge). In this case, correlations against σ and σ^+ values are computed to be about equally linear at all theoretical levels. Moreover, ρ' values are about the same for the vertical and adiabatic processes, with the exception of the B3LYP/aug-cc-pVDZ level, where the adiabatic ρ'-values is computed to be about 10% smaller than the vertical one. Nucleomer correlations are perfectly linear in either scale. The predicted ρ' values against the σ scale are too low by 25-30% while those against the σ^+ scale are within about 10% of those computed for actual substituents, sometimes overestimating, sometimes underestimating. In the absence of

intuition, it is not obvious that one would be able to clearly determine whether correlation against σ and σ^+ values is more physical. Of course, the qualitative conclusions would be similar in either instance.

The situation is somewhat similar with respect to correlations of indanedione carbonyl stretching frequencies (one being a symmetric combination and the other asymmetric) against σ and σ^+ values. This correlation is extrathermodynamic, but a strong linear relationship is found nonetheless (the individual frequencies vary over a range of about 20 cm^{-1} across the actual substituents). Once again, there is no particular distinction between correlations against σ and σ^+. There *is* a surprisingly large basis set effect on the predicted ρ' values, with the MIDI! basis predicting much smaller variations in the stretching frequencies as a function of substitution. This effect is faithfully reproduced in the nucleomer correlations. Again, however, the nucleomer correlations against σ values lead to ρ' values too small by fairly substantial margins: 40-45%. Underestimation is also consistent on the σ^+ scale, but the magnitude is reduced to about 20%.

Returning to a correlation of free energy changes, but now free energies of activation, as opposed to reaction, we consider the Claisen rearrangement of *para* substituted allyl phenyl ethers (Reaction 10 of Fig. 9). Correlating the kinetics of this reaction against σ^+ values represented a very early example of linear free energy relationships.[125,126] White *et al*. measured a ρ'-value of about 1.4 correlating rearrangement rates against σ^+ values in carbitol as solvent. The theoretical gas phase values for actual substituents listed in Table 1 are in quite good agreement with this

result, and moreover have Pearson correlation coefficients in excess of 0.99, reflecting the weak solvent influence known for this reaction.[125] While nucleomer correlations are also very good, the predicted ρ' values are too small by a fairly substantial margin. We speculate that this may reflect the failure of nucleomers to properly represent the polarizability of actual substituents, as opposed to simply their polarity. As TS structures are usually more polarizable than equilibrium structures, this discrepancy should become more important when free energies of activation are considered compared to free energies of reaction.

Consistent with this analysis, nucleomer ρ' values are again about 50% too small compared to values computed with actual substituents for the first carbonate fragmentation shown as Reaction 11 in Fig. 9, although the proper qualitative trend is predicted. However, for the second carbonate fragmentation (Reaction 12 of Fig. 9), where the substituent influence is rather small, quite poor correlations are observed when nucleomer correlations are computed with the B3LYP functional and large basis sets. Curiously, with the smaller MIDI! basis set, a reasonable correlation is obtained with B3LYP even though the magnitude is again underestimated. At the PBE/6-31+G(d,p) level the activation free energy is predicted to be essentially independent of nucleomer.

While the nucleomer correlations at the B3LYP/MIDI! level underestimate the influences of substitution effects, they do correctly predict that rearrangement rates are (i) more sensitive to aryl substitution at the α position on the carbonate alkyl chain, as opposed to the β position and (ii) show contrasting sensitivity to electron-withdrawing versus electron-donating substituents. Van Speybroeck *et al.*,[127] who previously studied

these reactions at the B3LYP/6-311G(d,p) level, noted these same trends and used them reasonably to conclude that the TS structure has more C–O bond breaking, with development of carbocationic character at the α position, than any corresponding bond breaking. Owing to the complexity of the substituted carbonates, Van Speybroeck *et al*. developed initial geometries from PM3 calculations in order to be more efficient. This system, then, is a nice demonstration of when using nucleomers can be efficient, since only a single TS structure needs to be located for each reaction, and that only for the unsubstituted parent system.

5.4 Conclusions

Hammett ρ values computed from H nucleomer σ and σ^+ constants show good qualitative agreement with ρ values computed from typical *para* functional group substitution for a number of energetic and extrathermodynamic correlations, but quantitative agreement is sometimes disappointing. As H nucleomers cannot enjoy resonance interactions with the aromatic π system, there is typically little distinction between the nucleomer σ and σ^+ scales. In addition, in most instances the magnitudes of the ρ values computed from nucleomer correlations are some 10-60% smaller than those computed from actual *para* substituents. We speculate that some of this difference may be attributed to the lack of polarizability of the nucleomers compared to actual organic functional groups. Nevertheless, nucleomer correlations provide a very quick estimation of the ρ values and should prove useful for evaluation of the full range of linear free energy relationships.

Chapter 6. Experimental and Theoretical Investigations into the Unusual Regioselectivity of 4,5-, 5,6-, and 6,7-Indole Aryne Cycloadditions[5]

Ashley N. Garr, Diheng Luo, Neil Brown, Christopher J. Cramer, Keith R. Buszek, and David Vander Velde

The 6,7-indolyne shows remarkable regioselectivity in its cycloaddition with 2-substituted furans. Electron-donating groups give predominantly the more sterically crowded product, while electron-withdrawing groups display the opposite regioselectivity. By contrast, 4,5- and 5,6-indolynes show no regioselectivity. Optimized electronic structure calculations using the M06-2X density functional and 6-311+G(2df,p) basis set revealed that the 6,7-indolynes are highly polar structures and that their cycloadditions have substantial electrophilic substitution character that leads to the observed preference for contrasteric products.

6.1 Introduction

Benzynes and other common arynes (e.g., naphthalynes and pyridynes) have fascinated chemists for decades. Surprisingly, arynes occurring at all three benzenoid positions of the ubiquitous indole nucleus (indole arynes or indolynes **1-3**, Figure 13) were, until recently, unknown.

[5] We acknowledge support of this work by the National Institute of Health, NIGMS, Grant R01 GM069711 (KRB), and the National Science Foundation CHE06-10183 (CJC). Additional support of this work was provided by the NIH, NIGMS, Grant P50 GM069663 via the University of Kansas Chemical Methodologies and Library Development Center of Excellence (KU-CMLD). We that Dee Tanaka for synthetic technical assistance and Nalin Chandrasoma and Lincoln Maina for additional NMR acquisition.

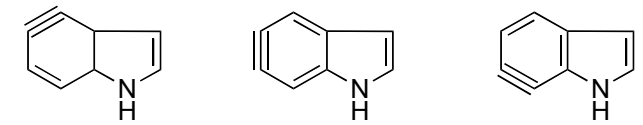

Figure 13. Benzenoid indole aryne (indolyne) sytems.

These newest members of the aryne family represent, inter alia, potentially attractive and powerful new tools for the total synthesis of complex natural products such as the nodulisporic acids,[128] trikentrins,[129] herbindoles,[129a,c] and the teleocidins.[130] (Figure 14). We recently discovered the first successful and general route to these reactive intermediates via metal-halogen exchange of *o*-dihalides[131] and later via fluoride-induced decomposition of *o*-silyltriflates.[132]

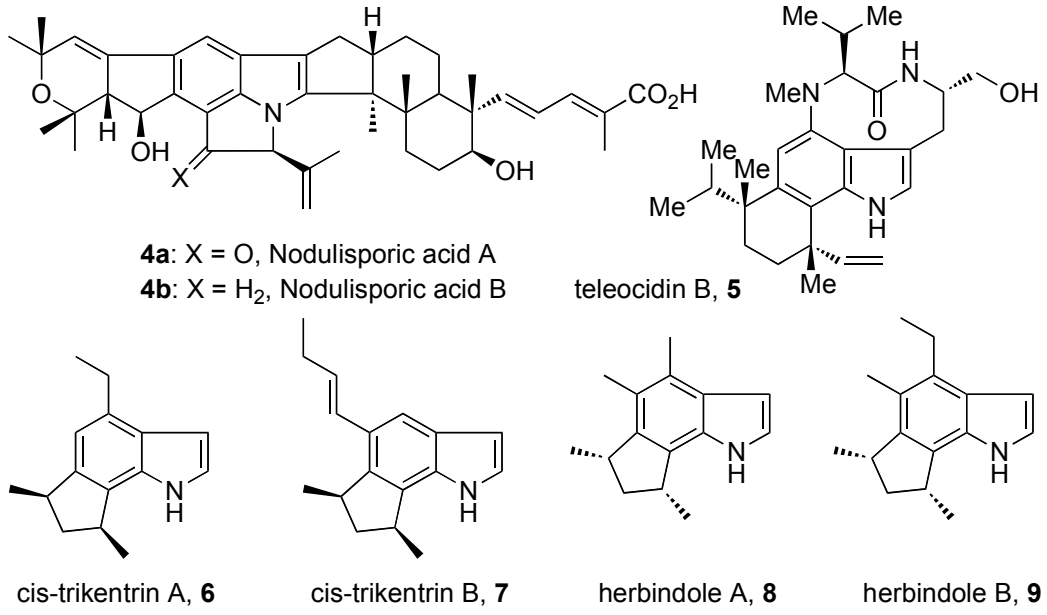

Figure 14. Examples of complex indole natural products.

We subsequently examined the regioselectivity of indolynes in Diels-Alder reactions with 2-substituted furans.[132a] These studies quickly led to the first application of indolynes in the construction of natural products and culminated in a concise and efficient total

synthesis of (±)-*cis*-trikentrin A and the (±)-herbindoles A and B.[133] This work and recently that of Garg clearly validated the utility of indolynes to gain quick access to architecturally challenging structures.[134]

During the course of these investigations, we were surprised to find that 2-substituted furans in particular displayed a striking regioselectivity when paired with the 6,7-indolynes (Scheme 2).[132a]

Scheme 2. Regioselective 6,7-Indolyne Cycloadditions with 2-Substituted Furans

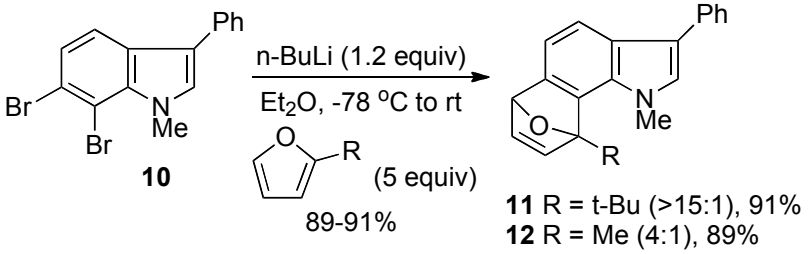

Using 2-*t*-butylfuran, for example, the contrasteric product **11** was formed in at least a 15:1 preference over the alternate regioisomer. Even with the less sterically demanding 2-methylfuran, there was a 4:1 preference for the indicated isomer. Analysis of the products by various 2D NMR methods (COSY, NOESY, HMBC, and HSQC) allowed for the unequivocal assignment of the structures.

By contrast, there was no preference for either regioisomer in the 4,5- and 5,6-indolyne cycloaddition examples involving 2-*t*-butylfuran. In each case, a nearly 1:1 ratio of cycloadducts was formed in excellent yield (Scheme 3).[132a]

Scheme 3. Furan and Azide Cycloadditions with 4,5-, and 5,6-Indolynes

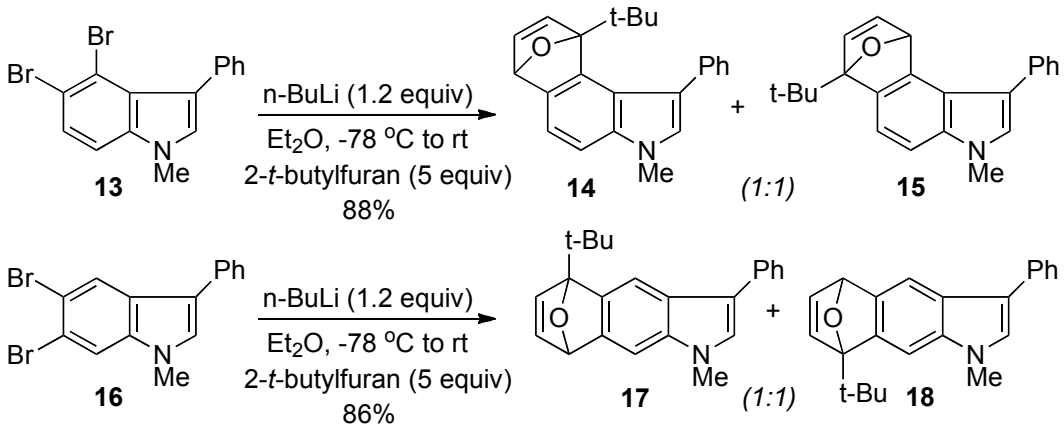

Intrigued by these observations, we wished to identify the fundamental electronic and steric parameters that account for these fascinating reaction profiles. The information obtained from this study will provide a better understanding of the structure and reactivity of the indole aryne system. This knowledge in turn should result in more versatile strategies and benefits for complex molecule total synthesis.

We began our investigation by examining a series of 2-substituted furans featuring electron-donating straight chain alkyl, branched alkyl, and aryl groups and electron-withdrawing groups (Table 22).[135] The electron-donating groups (entries 1-5) showed a remarkable preference for the more crowded cycloadduct **19**, while the opposite regiochemistry was found for an electron-withdrawing case (entry 6).

Table 22. Regioselective 6,7-Indolyne Cycloadditions with 2-Substituted Furans

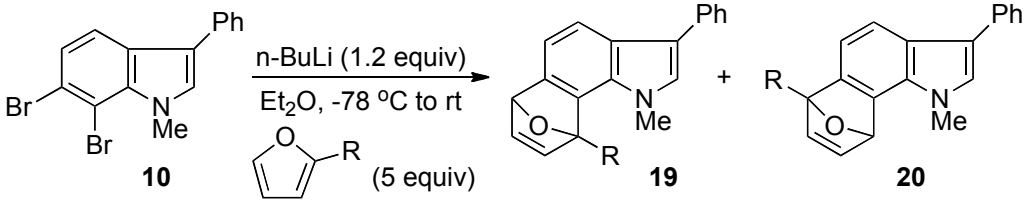

entry	furan, R	**19**	**20**	yield, %
1	Me	80	20	89
2	Et	84	16	90
3	*i*-Pr	94	6	88
4	*t*-Bu	98	2	91
5	Ph	>99	<1	92
6	SO_2Ph	<1	>99	83

In earlier studies involving the reaction of monosubstituted 3-benzynes with 2-substituted furans (Me, Et, *i*-Pr, *t*-Bu),[136] regioselectivity correlated well with the strength of inductively electron-withdrawing groups such as F and OMe on the benzyne to favor contrasteric products, while it was reversed with inductively electron-donating groups such as Me.

6.2 Computational Methods

To characterize this phenomenon in additional detail, electronic structure calculations were undertaken to predict the structure calculations were undertaken to predict the structures and reactivities of the *N*-methyl-4,5-, 5,6-, and 6,7-indolynes with furan and 2-alkylfurans. Similar calculations were also undertaken for the benzofuran and benzothiophene analogues of the indolynes as these heterocycles may prove useful for the construction of other interesting natural (or unnatural) products. With respect to methodology, all structures were optimized using the M06-2X density functional[13] and 6-311+G(2df,p) basis set[16] as implemented in MN-GFM,[137] a locally modified version of the Gaussian03 software package.[138] Analytical frequency calculations were employed to

characterize the nature of all gas-phase structures as minima or transition states. In select instances, the effects of diethyl ether solvation were taken into account using the SMD[28,29] implicit solvation model.

6.3 Results and Discussion

Table 23 lists the activation free energies computed for the reaction of the *N*-methylindolynes with the furans. With unsubstituted furan, $\Delta G^{\ddagger}$ is similar for the 4,5- and 5,6- indolyne isomers, and slightly smaller for the 6,7-isomer. Considering 2-*t*-butylfuran, the predicted free energies of activation are reduced by 3-4 kcal/mol compared to reaction with furan itself in the 4,5- and 5,6-indolyne cases. Regioselection becomes possible upon 2-substitution of the furan, and the differential free energies a activation in these two instances are predicted to be 1 kcal/mol or less. In the 6,7-indolyne case, by contrast, a free energy of activation similar to those for 4,5 and 5,6 is predicted for the formation of **26a** (which is equivalent to **19** but lacks the 3-phenyl sustituent), but no transition-state (TS) structure for the formation of **26b** (corresponding to desphenyl **20**) could be located–the approach of the furan to the indolyne led smoothly and without barrier to the final tetracyclic product in every instance.

To better understand this point, the reactions of other 2-alkylfurans with **23** were modeled. With R = Me, Et, or *i*-Pr, TS structures for formation of **26b** could be found in every instance. Interestingly, the differential free energies of activation for formation of **26a** vs **26b** favored formation of the latter in each case, with the margin being largest (2.1 kcal/mol) for R = *i*-Pr. Ethereal solvation effects on the free energies of activation are

predicted form the SMD continuum model to be 1 kcal/mol or smaller in every instance and to have no influence on regioselection.

Inspection of the TS structures for the formation of **26b** with the smaller alkyl groups provides insight into the failure to find such a TS structure for *t*-Bu. There are significant steric interactions between the *N*-Me group of the indolyne and the 2-alkyl group on the furan so that the bond forming to the 6 position is substantially shorter than that to the 7 position. The difference in the two formation bond lengths becomes increasingly long as the substituent is varied from Me to Et to *i*-Pr. This increase, however, is probably *not* associated with larger steric bulk since each of these furan 2-alkyl substituents orients a C–H bond toward the *N*-methyl group to minimize steric clash. Instead, it becomes clear from consideration of the preference for **26b** over **26a** and inspection of partial atomic charges that the 6,7-"cycloaddition" has substantial electrophilic substitution character.

Table 23. $\Delta G^{\ddagger}$ Values in kcal/mol for the Reaction of Indolynes with Substituted Furans

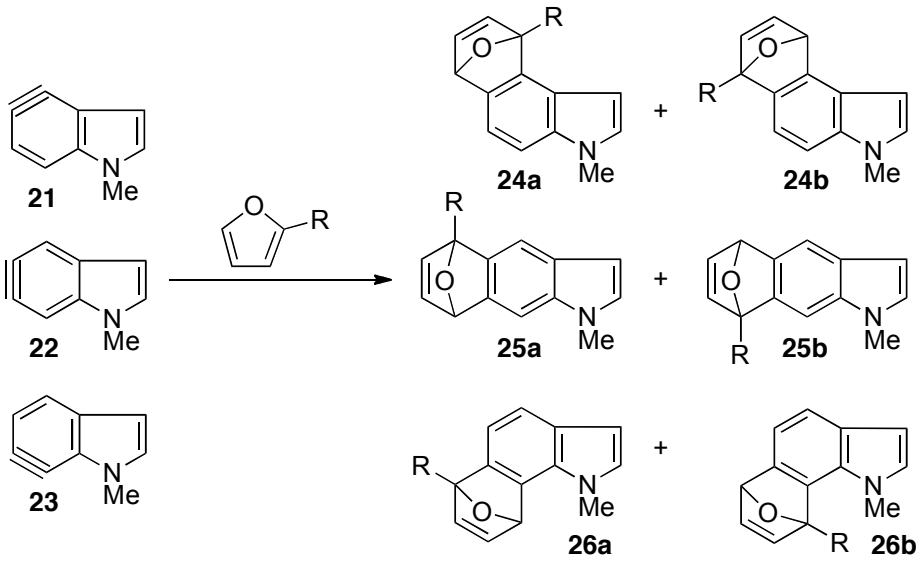

entry	aryne	furan, R	$\Delta G^{\ddagger}$ (**a**)	$\Delta G^{\ddagger}$ (**b**)
1	**21**	H	10.5	
2	**22**	H	10.0	
3	**23**	H	8.7 (8.4)[a]	
4	**21**	*t*-Bu	6.3	7.3
5	**22**	*t*-Bu	6.9	6.1
6	**23**	*t*-Bu	7.0 (8.0)	[b]
7	**23**	Me	9.2 (9.4)	7.5 (7.8)
8	**23**	Et	9.0 (9.4)	7.8 (8.2)
9	**23**	*i*-Pr	9.7 (10.3)	7.6 (8.2)

[a]Values in parentheses include continuum ethereal solvation effects.
[b]No barrier to reaction is predicted in the gas phase or continuum solution.

Thus, the electron-poor indolyne attacks the 2-substituted furan to generate the more stable 2-alkyldihydrofurylcarbenium ion. As the 2 substituent is varied from Me to Et to *i*-Pr, the increased stabilization provided by the larger alkyl groups increases this character and leads to increased regioselection and increased electrophilic substitution character so that bond formation becomes decreasingly synchronous. Thus, it appears that in the case of R = *t*-Bu the combination of unavoidably increased sterics (there is no longer a C–H bond that can be disposed toward the *N*-Me group) and enhanced carbenium ion stabilization switches the mechanisms for a highly asynchronous but still

concerted cycloaddition to a "stepwise" electrophilic substitution and subsequent ring closure. We place "stepwise" in quotes here because no TS structures nor intermediates can be located in either the gas phase or ethereal continuum solution for this process. To the extent that the reaction has an actual free energy of activation, it is likely associated with the displacement of discrete solvent molecules between the reacting partners that is not included in the present computational models, which otherwise are in reasonable quantitative agreement for predicted regioselection in **26a** and **26b** compared to **19** and **20**.

Support for the polarization of the 6,7-indolyne that makes the 6 position substantially more electrophilic than the 7 position may be obtained from inspection of atomic polar tensor partial charges[139] and the molecular geometry. Thus, C(6) is predicted to have a charge 0.26 au more positive than C(7), and the C(5)C(6)C(7) bond angle is predicted at the M06-2X level to be 135.3° while the C(6)C(7)C(7a) angle is predicted to be 117.2°. The former value is more consistent with carbocationic character, while the latter is more consistent with carbanionic character. For comparison, the corresponding bond angles in the analogous indyne (i.e., the hydrocarbon generated by replacing the *N*-methyl group with a methylene) are predicted at the DFT level to be 128.2 and 125.5°.[140] Thus, the C(6)—C(7) bond is strongly polarized in the expected direction by the nearby C(7a)—N bond dipole.

At the M06-2X level, the C(7a)—N bond dipole is predicted to lead to some polarization of the formal triple bonds in the 4,5- and 5,6-indolynes as well, although to a substantially smaller degree than in the 6,7 case (cf. entries 4 and 5 in Table 23). The

failure to observe any regioselection under experimental conditions (reactions of Scheme 3) may reflect reduced polarization associated with the 3-phenyl group in the experimental substrate, or some degree of solvent leveling of the gas-phase predictions, or simply solvent leveling of the gas-phase predictions, or simply overpolarization provided at the DFT level but the effect in any case is predicted to be about 1 kcal/mol.

Given the substantial synthetic utility of the indolyne cycloadditions, we modeled the analogous cycloadditions of furan and 2-*t*-butylfuran with benzofuran and benzothiophene; results are presented in Table 24. Very similar reactivity profiles are predicted for all three heterocyclic systems, with the benzofuran case being predicted to have the lowest free energies of activation by a small margin, as would be expected given the greater electrophilicity of this heterocycle. This suggests that synthetic efforts based on these other heterocycles should be equally fruitful.

Table 24. $\Delta G^{\ddagger}$ Values in kcal/mol for the Reaction of Benzofurans and –Thiophenes with Substituted Furans

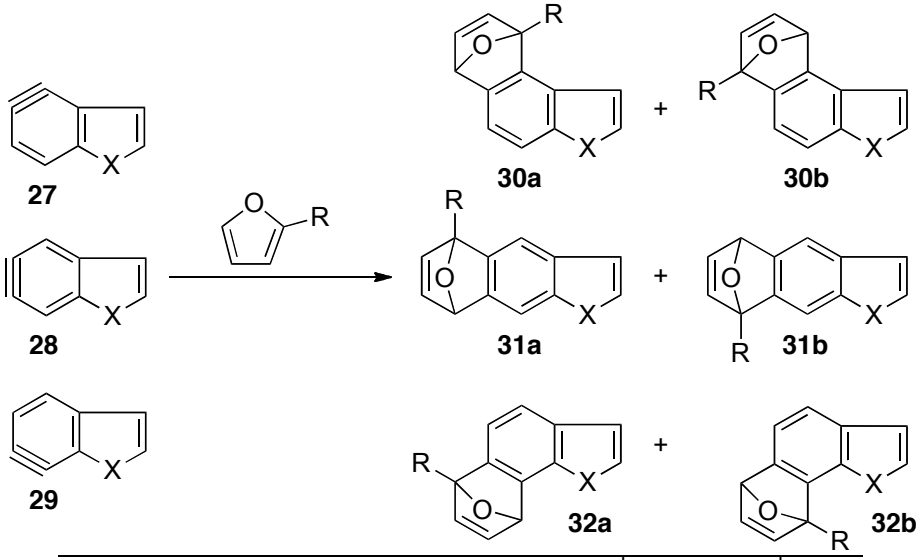

entry	aryne, X	furan, R	$\Delta G^{\ddagger}$ (**a**)	$\Delta G^{\ddagger}$ (**b**)
1	**27**, O	H	9.2	
2	**28**, O	H	9.1	
3	**29**, O	H	7.3	
4	**27**, O	*t*-Bu	4.9	6.4
5	**28**, O	*t*-Bu	5.8	4.9
6	**29**, O	*t*-Bu	6.2	[a]
7	**27**, S	H	9.6	
8	**28**, S	H	8.9	
9	**29**, S	H	8.4	
10	**27**, S	*t*-Bu	5.4	6.5
11	**28**, S	*t*-Bu	5.5	4.8
12	**29**, S	*t*-Bu	5.8	[a]

[a]No barrier to reaction is predicted in the gas phase or continuum solution.

6.4 Conclusions

Benzynes derived from benzannulated heterocycles are thus revealed to be powerful synthetic tools for the construction of highly functionalized tetracycles through [4 + 2] cycloaddition reactions. Dipolar effects can induce regioselection with asymmetrically substituted dienes when polarization of the benzyne triple bond imparts

substantial asynchronous electrophilic substitution character to the initial bond forming step.

Chapter 7. pH-Dependent Equilibrium Isotope Fractionation Associated with the Compound Specific Nitrogen and Carbon Isotope Analysis of Substituted Anilines by SPME-GC/IRMS[6]

Marita Skarpeli-Liati, Aurora Turgeon, Ashley N. Garr, William A. Arnold, Christopher J. Cramer, Thomas B. Hofstetter

Solid-phase microextraction (SPME) coupled to gas chromatography/isotope ratio mass spectrometry (GC/IRMS) was used to elucidate the effects of N-atom protonation on the analysis of N and C isotope signatures of selected aromatic amines. Precise and accurate isotope ratios were measured using polydimethylsiloxane/divinyl benzene (PDMS/DVB) as the SPME fiber material at solution pH-values that exceeded the pK_a of the substituted aniline's conjugate acid by two pH-units. Deviations of δ^{15}N and δ^{13}C-values from reference measurements by elemental analyzer IRMS were small (<0.9%) and within the typical uncertainties of isotope ratio measurements by SPME-GC/IRMS. Under these conditions, the detection limits for accurate isotope ratio measurements were between 0.64 and 2.1 mg L^{-1} for δ^{15}N and between 0.13 and 0.54 mg L^{-1} for δ^{13}C, respectively. Substantial inverse N isotope fractionation was observed by SPME-GC/IRMS as the fraction of protonated species increased with decreasing pH leading to deviations of –20% while the corresponding δ^{13}C-values were largely invariant. From isotope ratio analysis at different solution pHs and theoretical calculations by density functional theory, we derived equilibrium isotope effects, EIEs, pertinent to aromatic amine protonation of 0.980 and 1.001 for N and C, respectively, which were very similar

[6] This work was supported by the Swiss National Science Foundation (grant no. 200020-116447/1). We thank Jakov Bolotin for experimental support as well as Martin Elsner and C. Annette Johnson for valuable comments.

for all compounds investigated. Our work shows that N-atom protonation can compromise accurate compound-specific N isotope analysis of aromatic amines.

7.1 Introduction

Assessing transformation processes of organic micropollutants is crucial for addressing the risks of soil and water contamination. Compound-specific isotope analysis (CSIA) offers a complementary approach for identifying contaminant sources and degradation pathways, as well as for quantifying the extent of a transformation reaction even if several processes take place simultaneously. Because CSIA reveals the reactive position within an organic compound via detection of changes in isotopic composition, stable isotope ratio measurements also provide crucial information about the underlying reaction mechanism.[141] While CSIA is widely applied for the investigation of groundwater contaminants such as chlorinated solvents (polychlorinated alkenes[142-145]) and fuel components (methyl-tert butyl ether,[146-148] benzene,[149] toluene[150-152]), combined multielement isotope-fractionation analysis involving the elements C, H, and N is emerging for the transformation assessment of agrochemicals, explosives, and other priority pollutants.[153-155] In fact, micropollutants exhibiting N-containing functional groups are the most promising target molecules for CSIA, because the presence of N functional groups is key for many transformation processes including reductions, oxidations, substitutions, and eliminations.[156] Despite the importance of these reaction pathways, only few N-containing organic micropollutants are amenable to CSIA.

To date, nitrogen isotope fractionation has been successfully measured by GC/IRMS of amino acids,[157-159] selected N-containing herbicides,[153,160,161] and

nitroaromatic compounds.[151,154,162,163] To expand the applicability of CSIA, this study targets the N isotope analysis of substituted aromatic amines by GC/IRMS. Substituted anilines represent a class of toxic and mutagenic environmental pollutants[164] and they have also served as model compounds for studying the transformation of emerging contaminants such as sulfonamide antibiotics.[165] In contaminated environments, abiotic as well as microbial oxidation and addition reactions occur either directly at the nitrogen atom of the primary amino group[166-168] or via oxidation at the aromatic ring.[169] The availability of analytical methods for the precise and accurate measurement of N and C isotope ratios is therefore essential for assessing degradation pathways of substituted anilines in the environment.

Current approaches to isotope ratio measurements of substituted anilines in aqueous solutions b GC/IRMS coupled to solid phase microextraction (SPME), however, showed poor accuracy, that is, deviations from the correct N isotope signatures were above 2%.[154] Moreover, the consequences of aromatic amine protonation of the sensitivity and accuracy of CSIA is unexplored. Protonation of the anilines at pH values <7 deteriorates extraction efficiencies of the analytes from the aqueous solution to the SPME-fiber, because only neutral species can be expected to absorb to the nonpolar fiber coating and thus be measured by CSIA. Given that environmentally relevant pH-ranges coincide with the pK_a-values of many protonated aromatic amines (typical pK_a between 2.5 and 7,[156,170]) and that N atom protonation might be key for understanding the isotope fractionation of N-containing micropollutants,[171,172] the impact of equilibrium isotope fractionation of the isotope ratio analysis of aromatic amines requires closer examination.

It was the goal of this study to investigate how aromatic amino group protonation affects the sensitivity and accuracy of N and C isotope signatures, $\delta^{15}N$ and $\delta^{13}C$, of substituted primary aromatic amines while measured by SPME-GC/IRMS and whether significant N and C equilibrium isotope effects (EIE) are associated with proton exchange reactions. To this end, we examined the accuracy and precision of $\delta^{15}N$ and $\delta^{13}C$-values of a series of substituted anilines in aqueous samples in the pH-range 2.0—7.0 in the presence of various buffers. The compounds were chosen so that their pK_a-values (2.5—5.1) enabled us to study the effect of protonation on SPME-GC/IRMS under the chosen experimental conditions. Equilibrium isotope effects associated with aromatic amine protonation were determined experimentally and compared to independent estimates obtained from density functional theory calculations.

7.2 Experimental Section

7.2.1 Safety Considerations. Substituted anilines are toxic and potentially carcinogenic. When dealing with anilines, wear suitable clothing, gloves, and work in a well-ventilated fume hood.

7.2.2 Reagents and Materials. All chemicals in this study were used as received. The substituted anilines examined included aniline (≥99.5%, Fluka), 2-methylaniline (≥99.5%, Merck), 4-methylaniline (≥99%, Merck), 2-chloroaniline (≥99.5%, Aldrich), and 4-chloroaniline (≥99%, Fluka). Buffers used were sodium acetate trihydrate ($NaC_2H_3O_2 \cdot 3H_2O$, puriss, Riedel-de Haën), potassium phosphate dibasic (K_2HPO_4, puriss, Riedel-de Haën), sodium citrate tribasic dihydrate ($Na_3C_6H_5O_7 \cdot 2H_2O$, ≥99%, Fluka) and 2-morpholineoethanesulfonic acid monohydrate (MES, $C_6H_{13}NO_4S \cdot H_2O$, ≥

99%, Fluka). All buffer solutions were prepared in deionized water (18.2 MΩ·cm, NANOpute) and solution pH-values were adjusted with hydrochloric acid (Sigma Aldrich) and sodium hydroxide solution (Fluka). Solvents used were menthanol (>99.9%, Scharlau, Spain) and ethyl acetate (>99.8%, Riedel-de Haën). High purity Ar was used for deoxygenation of water and methanol and helium, nitrogen, and carbon dioxide were used for GC/MS and GC/IRMS measurements (all ≥99.999%, Carbagas).

7.2.3 Instrumentation. Prior to nitrogen and carbon isotope analysis, extraction efficiencies of the substituted anilines from the buffered aqueous solutions to the SPME-fibers were evaluated by means of GC/MS analysis. Instrumentation and procedures for chromatographic separation used for GC/MS analysis were similar to that of previous studies.[154] A GC (Trace GC Ultra, Thermo Electron Corp.) was combined with a quadrupole MS (Trace DSQESI 250, Thermo Electron Corp.) and a CombiPAL autosampler (CTC) and equipped with a cold on-column and a split/splitless injector with a Merlin Microseal (Merlin Instrument Co.). The isotope analysis was carried out using a Trace GC (Thermo Electron Corp.) coupled to an isotope ratio mass spectrometer (IRMS; Delta V PLUS, Thermo Electron Corp.) via a combustion interface (GC Combustion III).[173] Helium carrier gas was used at constant pressure of 100 kPa. For chromatographic separation, 1 m of a deactivated guard column (530 μm i.d.; BGB, Boeckten, Switzerland) and a 30 m x 0.32 mm fused-silica column (Zebron, ZB-5-ms, 0.25 μm, Phenomenex) were used. The applied temperature program was 1 min at 50 ^{o}C followed by a 10 ^{o}C/min ramp to 250 ^{o}C and 5 min at 250 ^{o}C.

For the $\delta^{13}C$ measurements the NiO/CuO/Pt wires of the combustion unit were oxidized with O_2 during 12 h prior to use at 940 ^oC. The N isotope signatures were measured with the same oxidation reactor but without preoxidation at 980 ^oC. The temperature of the reduction reactor was 650 ^oC. Additionally, liquid nitrogen was used to trap the CO_2 produced during combustion of the analytes to prevent isobaric interferences by CO^+-fragments.[174]

7.2.4 SPME of Aqueous Samples. The SPME fiber coating polyacrylate (PA, 85 μm, Supelco), used for the nitroaromatic compounds,[154] was compared to polydimethylsiloxane/divinylbenzene (PDMS/DVB, 65 μm, Supelco). Both materials led to reproducible measurements and enabled more than 100 injections per fiber according to the following procedure. 1.3 mL of buffered solution was transferred into 2 mL autosampler glass vials, which contained 0.30 g of NaCl (final ionic strength *I* of 4 M). The samples were shaken on a Vortex shaker to dissolve NaCl. The SPME fiber was immersed directly into the buffered aqueous solutions and the analytes were allowed to adsorb on the fiber for 45 min at 40 ^oC. Thermal desorption from the SPME fiber was performed in a split/splitless injector equipped with a deactivated liner at 270 ^oC for 3 min. All measurements were carried out in triplicates. The SPME fiber was conditioned for 30 min at 250 ^oC after 20 samples.

7.2.5 Extraction Efficiency. To determine the efficiency of substituted aniline extraction from buffered aqueous solutions by the SPME fibers, calibration curves of the analytes were measured on the GC/MS after cold on-column injection and compared to peak areas obtained after solid-phase microextraction. The ratio of the slopes of the calibration

curves for SPME- vs on-column-GC/MS (i.e., peak areas per amount of analyte in water vs ethyl acetate) was used as measure for the extraction efficiency of each compound (Table 25). Additionally, the preconcentration factors for both SPME-fibers were determined as ratios of the analyte concentrations in water or ethyl acetate, which are necessary for the detection of identical peak areas by SPME- vs on-column-GC/MS. Analyte solutions for cold on=column measurements (25 ^{o}C, 1 μL injection volume) were prepared in ethyl acetate and covered a concentration range of 5—50 μM. The SPME measurements were prepared in 10 mM MES buffer at pH 7 and the concentrations were typically between 1 and 10 μM to obtain peak areas similar to those measured by the cold on-column injection. Extraction efficiencies with the PDMS/DVB coated fiber were higher than with PA by a factor of 2 (4-Cl-aniline) to 13 (aniline, Table 25) for all substituted anilines used in this study. If not mentioned explicitly, the presented δ^{15}N and δ^{13}C values are measured with the PDMS/DVB-coated fiber.

Table 25. Names and Abbreviations of the Investigated Substituted Anilines as well as pK_a-Values of the Conjugate Acids. Extraction Efficiencies and Preconcentration Factors Obtained by SPME-GC/MS are Listed for Polyacrylate (PA) and Polydimethylsiloxane/Divinylbenzene (PDMS/DVB) as Fiber Material[a]

Compound name (abbreviation)	pK_a [156],[192]	extraction efficiency[b] PA-fiber (%)	preconcentration factor PA-fiber (%)	extraction efficiency PDMS/DVB -fiber (%)	preconcentration factor PDMS/DVB-fiber (-)
aniline (An)	4.63	0.96 ± 0.03	12.5 ± 0.4	12.7 ± 0.4	165 ± 5
2-methyl-aniline (2-CH_3-An)	4.45	3.51 ± 0.10	45.6 ± 1.3	-	-
4-methyl-aniline (4-CH_3-An)	5.10	5.10 ± 0.20	66.3 ± 2.7	38.3 ± 1.1	497 ± 15
2-chloro-aniline (2-Cl-An)	2.46	9.73 ± 0.22	127 ± 3	-	-
4-chloro-aniline (4-Cl-An)	3.98	9.56 ± 0.38	124 ± 5	19.2 ± 1.1	250 ± 14

[a]All extraction experiments were performed after addition of NaCl to 10 mM MES buffer solution at pH 7.0 (I = 4 M).
[b]See text for definition of extraction efficiencies and preconcentration factors.

7.2.6 Stable Isotope Measurements in Buffered Solutions with SPME-GC/IRMS. ^{15}N and ^{13}C signatures of the substituted anilines were measured after SPME and compared to isotope ratio measurements after on-column injection and to reference isotope ratios determined by elemental analyzer (EA, Carlo Erba) coupled to IRMS (Fisons Optima).[175] These comparisons were performed to evaluate whether isotopic fractionation occurred during SPME and/or combustion to analyte gases. Isotope signatures were measured as single compounds by SPME-GC/IRMS to avoid potential interferences from competitive adsorption of the analytes on the SPME fiber. The concentration range of the investigated anilines varied from 25 to 500 μM and 1—30 μM at pH 7 for δ^{15}N and δ^{13}C, respectively, depending on the SPME extraction efficiency of each compound. The sensitivity of the δ^{15}N-SPME analysis was 1.5 orders of magnitude lower compared to δ^{13}C-SPME analysis as noted previously.[154] All δ^{15}N- and $\delta^{13}C$-values are reported relative to air ($\delta^{15}N_{air}$) and Vienna PeeDee Belemnite ($\delta^{13}C_{VPDB}$), respectively, in per min (%).

$$\delta^{h}E = \left(R_{sample} / R_{standard} - 1\right) \times 1000 \qquad (10)$$

where $\delta^{h}E$ is the element's isotope signature, R_{sample} and $R_{standard}$ are the isotope ratio of sample and standard, respectively. To exclude nonlinearity effects, which may arise due to variations of the introduced mass into the IRMS and lead to inaccurate isotope signatures,[176] we determined the concentration range within which isotope signatures, both δ^{15}N and δ^{13}C, did not show any mass bias. The accuracy of the isotope measurements, $\Delta\delta^{h}E$, was expressed as deviation of the isotope signature measured by

SPME-GC/IRMS, $\delta^{h}E_{\text{SPME-GC/IRMS}}$, from the reference isotope signature determined by EA-IRMS,[177] $\delta^{h}E_{\text{ref}}$ (eq 11).

$$\Delta\delta^{h}E - \delta^{h}E_{SPME-GC/IRMS} - \delta^{h}E_{ref} \tag{11}$$

Isotope fractionation during the adsorption of aromatic amines to SPME fibers was ruled out from measurements of δ^{15}N and δ^{13}C-values measured with two different fiber materials (PA and PDMS/DVB) and comparison to isotope signatures determined after cold on-column injection of the analytes into the GC/IRMS system. No significant difference in accuracy between the two fiber coating materials was observed under optimized conditions (see discussion below), except for 4-Cl-aniline where extraction with the PDMS/DVB fiber decreased the $\Delta\delta^{15}$N value by approximately 4%.

pH-dependent isotope fractionation was investigated by SPME-GC/IRMS at several pH-values using 10 mM solutions of the following buffers (parentheses indicate pK_a-values) at ionic strength of 4 M (NaCl): MES (6.15) was used for the pH-range 5.0—7.0, acetate (4.76) for the pH 4.0—5.0, citrate (3.13 and 4.76) for pH 3.0—5.5, succinate (4.21 and 5.64) for pH 3.5—6.5, and phosphate (2.15) for pH 2.0. To avoid potential artifacts from acid-catalyzed modification of SPME-fibers, experiments were not run at pH-values below 2.0 thus limiting the extent to which the effect of protonation of N and C isotope analyses could be studied with some substituted anilines.

To verify whether the presence of dissolved oxygen causes aniline oxidation and thus biases isotope ratio measurements, we carried out SPME-GC/IRMS of samples that were prepared with anoxic stock and buffer solutions of the analytes at all relevant pH values in an anoxic glovebox (data not shown). Isotope signatures were identical

regardless of the dissolved oxygen content of the solution and thus no effort to deoxygenate solutions was made in this study.

7.2.7 Detection Limits for Accurate Isotope Ratio Measurements. The operational detection limits for accurate stable isotope analysis of the investigated substituted anilines were derived from repeated ^{15}N- and ^{13}C-SPME-GC/IRMS measurements using PDMS/DVB fibers, aqueous solutions buffered with 10 mM MES at pH 7 (I = 4 M), and different analyte concentrations corresponding to peak amplitudes between 300 and 2500 mV and 500 and 6000 mV for N and C isotope analysis, respectively. As specified in the discussion below, detection limits correspond to the lowest analyte concentration lying within a $\Delta\delta^{h}$E-interval defined by the precision and accuracy of δ^{15}N- and δ^{13}C-measurements.

7.2.8 DFT-Calculations. The geometries of all free base anilines and their protonates conjugate acids were fully optimized at the density functional (DFT) level using the gradient-corrected Perdew—Wang exchange and correlation functionals[6,7] as modified by Adamo and Barone[8] in conjunction with the 6-311+G(d) basis set.[16] Stationary equilibrium structures were confirmed by analytical calculation of vibrational frequencies, which were also used in the construction of ideal-gas, rigid-rotator, harmonic oscillator partition functions, from which thermal contributions to free energies G were computed.[1] Equilibrium isotope effects were computed as

$$\mathrm{EIE}^{N}_{B-BH^{+}} = \frac{^{14}N K_B}{^{15}N K_B} = \exp\left(\frac{-G_{^{14}BH^{+}} + G_{^{14}B} + G_{^{15}BH^{+}} - G_{^{15}B}}{RT}\right) \qquad (12)$$

where $EIE^{N}_{B-BH^+}$ is the N equilibrium isotope effect and K_B is the equilibrium constant associated with aromatic amine protonation. The isotopically sensitive free energy G was determined for the substituted anilines, that is the neutral ($G_{^{14}B}, G_{^{15}B}$) and protonated isotopologues ($G_{^{14}BH^+}, G_{^{15}BH^+}$). $EIE^{N}_{B-BH^+}$ was calculated for *para*- and *ortho*-substituted anilines including aromatic substituents with different electron donating and accepting properties (i.e., 4-$N(CH_3)_2$, 4-OCH_3, 4-CH_3, 4-F, 4-Cl, 4-NO_2 and 2-CH_3, 2-Cl). The corresponding $EIE^{C}_{B-BH^+}$ was calculated only for 4-CH_3-aniline and for each single carbon atom. All calculations made use of the Gaussian 03 electronic structure program suite.[102]

7.3 Results and Discussion

7.3.1 ^{15}N and ^{13}C Signatures Determined by SPME-GC/IRMS. The N and C isotope signatures ($\delta^{15}N$ and $\delta^{13}C$) of the substituted anilines measured by SPME-GC/IRMS at pH 7 correspond well with independent isotope signature measurements by elemental analyzer-IRMS (EA-IRMS). As shown in Table 26 accuracies were < ±0.3% for N and < ±0.5% for C isotope signatures, respectively, as revealed by the differences measured by the two methods ($\Delta\delta^{15}N_{SPME\text{-}EA}$ and $\Delta\delta^{13}C_{SPME\text{-}EA}$, eq 11). These deviations were within typical uncertainties (±0.5%,[178]) reported for $\delta^{15}N$ and $\delta^{13}C$-measurements (Table 26). Only $\Delta\delta^{15}N$-value of 4-Cl-aniline showed a significant offset by -4%. All isotope ratio measurements were highly linear within the amplitude range typically used for isotope analysis, that is, 300—5500 mV (see Experimental Section for details and example for 4-CH_3-aniline in Figure 15).

Table 26. Comparison of δ^{15}N- and δ^{13}C-Values of Substituted Anilines Measured by EA-IRMS and SPME-GC/IRMS[a]

Compound	δ^{15}N (%)		$\Delta\delta^{15}$N (%)	δ^{13}C (%)		$\Delta\delta^{13}$C (%)
	EA-IRMS	SPME-GC/IRMS		EA-IRMS	SPME-GC/IRMS	
An	7.6 ± 0.3	7.9 ± 0.3	0.3 ± 0.5	-30.0 ± 0.3	-29.1 ± 0.2	0.9 ± 0.4
2-CH_3-An	3.7 ± 0.3	3.9 ± 0.3	0.2 ± 0.4	-27.5 ± 0.3	-27.8 ± 0.6	-0.3 ± 0.7
4-CH_3-An	-5.1 ± 0.3	-4.8 ± 0.2	0.3 ± 0.4	-28.3 ± 0.3	-27.8 ± 0.3	0.5 ± 0.5
2-Cl-An	6.4 ± 0.3	6.5 ± 0.6	0.1 ± 0.7	-26.7 ± 0.3	-26.7 ± 0.2	0.0 ± 0.3
4-Cl-An	-3.1 ± 0.3	-7.1 ± 0.9	-4.0 ± 0.9	-27.3 ± 0.3	-26.8 ± 0.5	0.5 ± 0.6

[a]SPME was performed in 10 mM MES buffered solutions at pH 7.0. The accuracy of the SPME-GC/IRMS-measurements is expressed as deviation from reference measurements of the pure analytes by EA-IRMS ($\Delta\delta^{h}$E-values). All unvertainties correspond to ±1 standard deviation (n = 3).

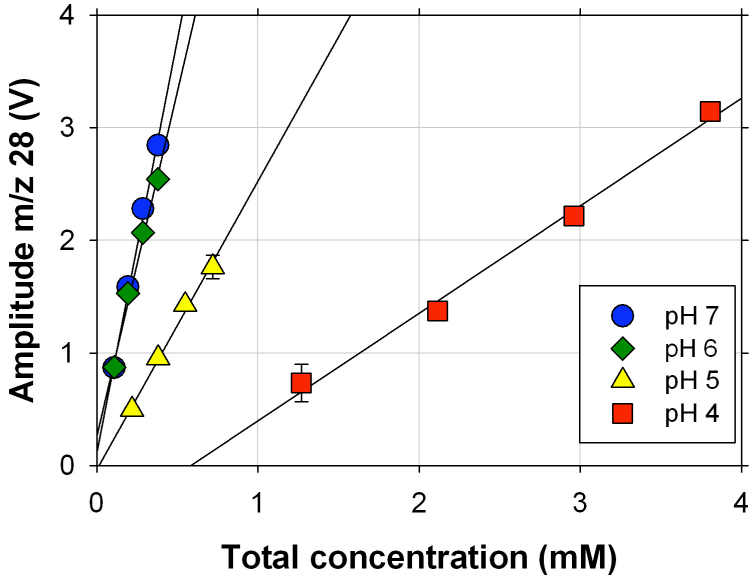

Figure 15. pH-dependence of 4-CH_3-aniline *m/z* 28 IRMS signal intensities for ^{15}N-SPME-GC/IRMS (fiber material PDMS/DVB) vs total aqueous 4-CH_3-aniline concentration in 10 mM MES (pH 6.0 and 7.0) and 10 mM acetate (pH 4.0 and 5.0) buffered solutions. Uncertainties of signal intensities are ± standard deviation (error bars mostly smaller than markers).

Despite good linearity, δ^{15}N-measurements of substituted anilines deviated substantially from the correct values if the solution pH approached or was below the pK_a of the substituted aniline's conjugate acid. We observed a decrease of δ^{15}N corresponding to a depletion of isotopically heavy nitrogen (^{15}N) in the measured analyte

with decreasing pH. The most substantial ^{15}N depletion was observed for 4-CH_3-aniline (-15%), 4-Cl-aniline (-22%), and aniline (-17%) at approximately 2 pH units below the pK_a of the conjugate acid. In contrast, no C isotope fractionation was found as the pH-value of solutions decreased under the identical conditions and $\delta^{13}C$-values remained constant within <0.9% (Figures 16 and 17). The observation of pH-dependent N isotope fractionation coincided with decreasing extraction efficiencies of the analytes from aqueous solution. Figure 15 illustrates the *m/z* 28 IRMS signal intensities of 4-CH_3-aniline between pH-values 4.0 and 7.0, which suggest that only neutral molecules are adsorbed to the SPME fiber while protonated species remain dissolved. The same observations was made for other substituted anilines (data not shown). The decreasing $\delta^{15}N$-values measured in adsorbed analytes at low pH (^{15}N depletion) imply that protonated compounds are enriched with ^{15}N, while the total analyte concentration in control solutions, which were not subject to SPME, remained unchanged. In contrast to earlier work,[154] our data suggest that accurate determination of $\delta^{15}N$ and $\delta^{13}C$ in substituted anilines measured by SPME-GC/IRMS is feasible if the pH of analyte solutions is controlled and maintained at least 2 pH-units above the pK_a of the conjugate acid.

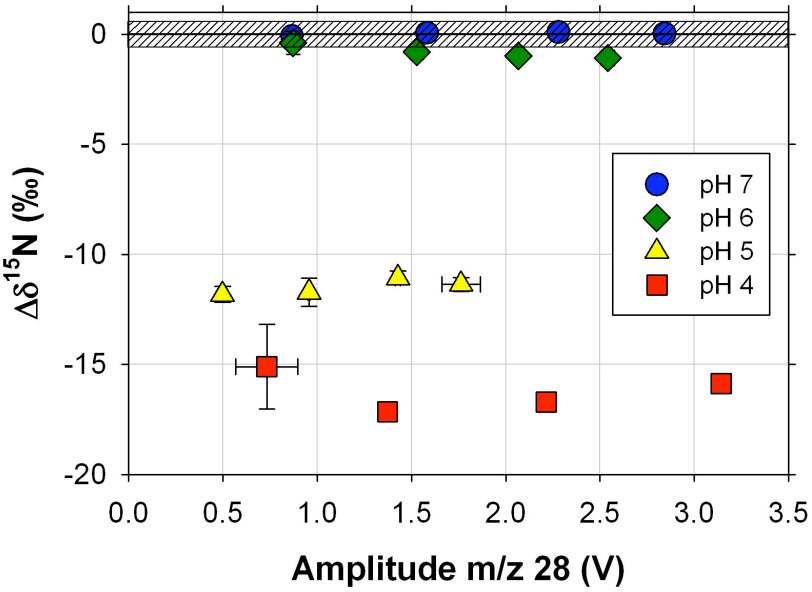

Figure 16. Accuracy of ^{15}N-SPME-GC/IRMS of 4-CH_3-aniline, $\Delta\delta^{15}$N, at solution pH-values between 4.0 and 7.0. Single δ^{15}N measurements at pH 6.0 and 7.0 were carried out in 10 mM MES buffer, those at pH 4.0 and 5.0 in 10 mM acetate buffer. The horizontal bar corresponds to the reference δ^{15}N (± standard deviation) of the pure 4-CH_3-aniline determined by EA-IRMS.

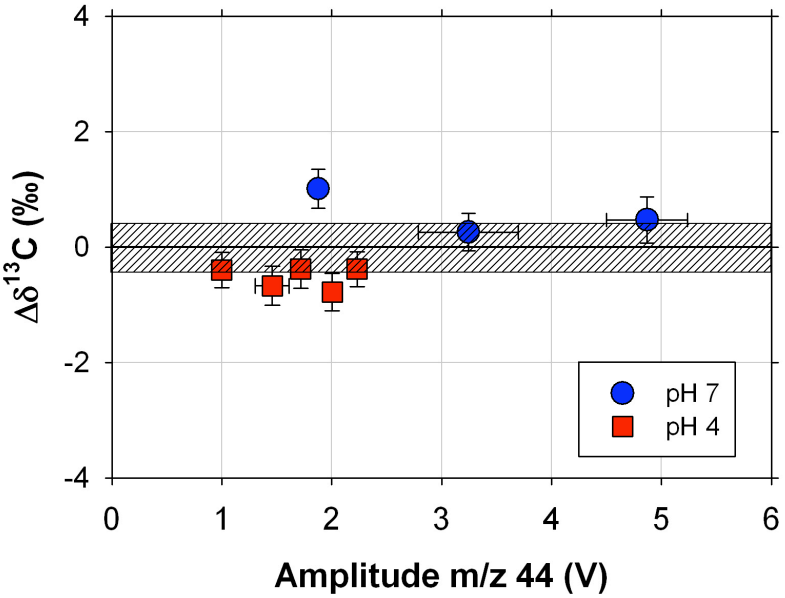

Figure 17. Accuracy of ^{13}C-SPME-GC/IRMS of 4-CH_3-aniline, $\Delta\delta^{13}C$, at solution pH-values 4.0 and 7.0. Single $\delta^{13}C$ measurements at pH 4.0 and 7.0 were carried out in 10 mM acetate and MES buffer, respectively. The horizontal bar corresponds to the reference $\delta^{13}C$ (± standard deviation) of the pure 4-CH_3-aniline determined by EA-IRMS.

7.3.2 Equilibrium Isotope Effect (EIE) Associated with the Protonation of Substituted Anilines. The observation of $\delta^{15}N$-decrease at lower solution pH values in combination with the preferential extraction of neutral substituted aniline species and the fact that a change of ambient pH did not affect C isotope composition implies a nitrogen equilibrium isotope effect originating from the protonation at the amino functional group. To obtain evidence for the magnitude of equilibrium isotope fractionation owing to N-atom protonation, we measured the $\delta^{15}N$ of the substituted anilines in solutions buffered with different organic buffers at pH-values between 3.5 and 7.0 and compared the outcome with reference isotope signature ($\delta^{15}N_{ref}$) obtained by EA-IRMS as follows. According to the isotopic mass balanced $\delta^{15}N_{ref}$ corresponds to the sum of neutral and the protonated aniline species (eq 13).

$$\delta^{15}N_{ref} = f_{BH^+} \times \delta^{15}N_{BH^+} + \left(1 - f_{BH^+}\right) \times \delta^{15}N_B \quad (13)$$

where f_{BH^+} is the fraction of the protonated species, and $\delta^{15}N_{BH^+}$ and $\delta^{15}N_B$ are the N isotope signatures of protonated and neutral species, respectively. The partitioning of N isotopes between protonated and neutral compounds is described by the isotopic fractionation factor α_{B-BH^+} and corresponds to the ratio of isotopic composition in each species[179]

$$\alpha^N_{B-BH^+} = \frac{R_{BH^+}}{R_B} \quad (14)$$

where R_{BH^+} and R_B are the measured $^{15}N/^{14}N$ ratios in the protonated and neutral species, respectively, typically reported in the per mil notation as in eq 10. Substitution of a modified eq 10 into eq 14 results in an expression, which can be inserted into eq 13 to yield the measured, neutral isotope signature $\delta^{15}N_B$ at any solution pH as function of the degree of protonation, f_{BH^+}, the reference isotope signature, $\delta^{15}N_{ref}$, and the fractionation factor α_{B-BH^+} (eq 15).

$$\delta^{15}N_B = \frac{\delta^{15}N_{ref} - f_{BH^+} \times 1000 \times \left(\alpha^N_{B-BH^+} - 1\right)}{f_{BH^+} \times \left(\alpha^N_{B-BH^+} - 1\right) + 1} \quad (15)$$

For typical isotope effects, the term $f_{BH^+} \times \left(\alpha^N_{B-BH^+} - 1\right)$ becomes negligible and eq 15 simplifies to

$$\delta^{15}N_B \approx \delta^{15}N_{ref} - f_{BH^+} \times 1000 \times \left(\alpha^N_{B-BH^+} - 1\right) \quad (16)$$

Using N isotope enrichment factors instead of fractionation factors (eq 17), the extent of equilibrium isotope fractionation is the slope of the correlation of measured δ^{15}N (ascribed to neutral species) vs f_{BH^+} (eq 18).

$$\varepsilon^{N}_{B-BH^+} = 1000 \times \left(\alpha^{N}_{B-BH^+} - 1\right) \tag{17}$$

$$\delta^{15}N_B = \delta^{15}N_{ref} - f_{BH^+} \times \varepsilon^{N}_{B-BH^+} = \delta^{15}N_{ref} + \left(1 - f_{BH^+}\right) \times \varepsilon^{N}_{B-BH^+} \tag{18}$$

Figure 18 shows the correlation of the measured δ^{15}N of aniline vs the fraction of neutral aniline species, (1- f_{BH^+}), in solution buffered with different organic buffers over a wide pH range. Notice that (1- f_{BH^+}) was calculated after pH measurements at high ionic strength owing to the addition of NaCl for extraction of the analytes. The slope of the regression line corresponds to an $\varepsilon^{N}_{B-BH^+}$-value of the 18.8 ± 1.1% or an inverse equilibrium isotope effect, $\mathrm{EIE}^{N}_{B-BH^+}$, of 0.9815 ± 0.0011 (eq 19, Table 27). The inverse $\mathrm{EIE}^{N}_{B-BH^+}$ reflects the formation of an additional bond to N in the protonated species[180]

$$\mathrm{EIE}^{N}_{B-BH^+} = \frac{^{14}N K_B}{^{15}N K_B} = \frac{1}{1 + \varepsilon^{N}_{B-BH^+}/1000} = \frac{1}{\left(\alpha^{N}_{B-BH^+} - 1\right)} \tag{19}$$

Some of the δ^{15}N of aniline measured in solutions containing citrate and succinate buffer deviated by up to 3% from the expected values. These deviations presumably originate from high ionic strength effects, which result in altered activities and ionization constants of dissolved ions, buffers, and substituted anilines due to ion pairing with the electrolyte (NaCl).[181,182] While ion pairing models allow for estimates of activity coefficients and ionization constants of typical ions in saline waters,[183,184] no data are available for assessing the buffers and substituted anilines used in this work. Ionic strength effects

might ultimately lead to different estimates of the fraction of neutral and protonated aniline concentrations and thus explain the lack of correlation for selected data points in Figure 18. However, this phenomenon does not alter the $\varepsilon^{N}_{B\text{-}BH^{+}}$ -value obtained from eq 18 beyond experimental uncertainty.

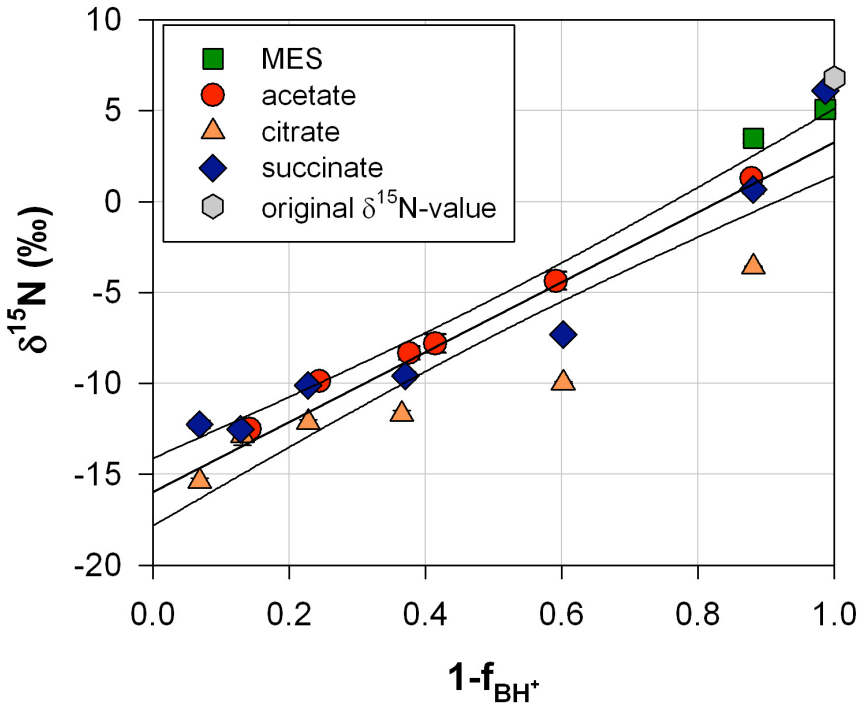

Figure 18. δ^{15}N-values of aniline determined by SPME-GC/IRMS vs the fraction of neutral aniline species in aqueous solution at different pH-values. Organic buffers used include: MES (pH-range 5.0—7.0), acetate (4.0—5.0), citrate (3.0—5.5), and succinate (3.5—6.5). The slope of the regression line corresponds to the enrichment factor $\varepsilon^{N}_{B-BH^{+}}$. Error bars of triplicate δ^{15}N measurements (± standard deviation) are smaller than the corresponding markers.

Table 27. Concentration Limits for Accurate N and C Isotope Analysis of Substituted Anilines by SPME-GC/IRMS Using PDMS/DVB Fibers

Compound	δ^{15}N (mg L^{-1})	δ^{13}C (mg L^{-1})
An	1.4	0.37
2-CH_3-An	1.3	0.21
4-CH_3-An	2.1	0.54
2-Cl-An	1.9	<0.13
4-Cl-An	<0.64	0.26

The $EIE^{N}_{B-BH^+}$ obtained from Figure 18 is in excellent agreement with data inferred from the chromatographic separation of ^{14}N and ^{15}N aniline isotopologues[185] and implies that the base dissociation constant of the ^{15}N-containing aniline species $^{15N}K_B$, exceeds that of the light isotopologues, $^{14N}K_B$. An $EIE^{N}_{B-BH^+}$ of 0.9815 in case of aniline (Table 28) implies that pK_B^{14N} exceeds pK_B^{15N} by 0.008 units. Thus, at any solution pH, the slightly higher basicity of the neutral ^{15}N-aniline causes the heavy (^{15}N) isotopologues to protonate to a larger extent compared to ^{14}N-aniline species because of stronger N—H bonds in the heavy isotope-containing conjugate acid. As only the deprotonated, that is, neutral compound is extracted by SPME, one therefore observes a depletion of ^{15}N and more negative δ^{15}N-values unless aromatic amine protonation is negligible at the solution pHs exceeding the pK_a of the conjugate acid by at least 2 units.

Table 28. Nitrogen Isotope Enrichment Factors, $\varepsilon^{N}_{B-BH^{+}}$, and N Equilibrium Isotope Effects, $EIE^{N}_{B-BH^{+}}$, Associated with the Protonation of the Substiuted Anilines: Comparison of Experimental (exp) and Theoretical Data (calc)

compound	experimental $\varepsilon^{N}_{B-BH^{+}}$ (‰)	$EIE^{N}_{B-BH^{+}}$, exp (-)	theoretical $EIE^{N}_{B-BH^{+}}$, calc (-)
An	18.8 ± 1.1	0.9815 ± 0.0011	0.9811
2-CH_3-An	17.2 ± 1.8	0.9831 ± 0.0018	0.9811
4-CH_3-An	19.9 ± 4.1	0.9804 ± 0.0041	0.9811
2-Cl-An	17.2 ± 1.2	0.9831 ± 0.0012	0.9811
4-Cl-An	18.6 ± 2.0	0.9817 ± 0.0020	0.9821
4-$N(CH_3)_2$-An	-	-	0.9718
4-OCH_3-An	-	-	0.9800
4-F-An	-	-	0.9894
4-NO_2-An	-	-	0.9842

We investigated the effects of aromatic substituents on the variability of $EIE^{N}_{B-BH^{+}}$ with additional experiments for 4-CH_3-aniline and 4-Cl-aniline and through density functional theory (DFT) calculations for a wide set of compounds. The results are reported in Table 28. The ^{13}C-EIE value reported in Table 28 corresponds to the average calculated for all carbon atoms 1 to 7. This accounts for the fact that the heavy carbon atom is more or less evenly distributed over all molecular positions so that the value measured by CSIA represents the average of all position-specific isotope effects. The data compiled in Table 28 show excellent agreement between experiment and theory confirming inverse $EIE^{N}_{B-BH^{+}}$-values for all substituted anilines. In addition, $EIE^{N}_{B-BH^{+}}$-values show little sensitivity to aromatic substitution albeit a slight trend to more inverse isotope effects with increasing electron-donating properties of the substituent (and vice versa) is observed. Note that our calculations also confirm the absence of significant C isotope fractionation (4-CH_3-aniline $EIE^{C}_{B-BH^{+}}$ of 1.0011, Figure 17).

7.3.3 Detection Limits for Accurate Isotope Analysis of Substituted Anilines. Current recommendations[178,186-189] regarding detection limits for isotope ratio measurements by GC/IRMS not only include the precision of repeated measurements but also account for accuracy and the rather narrow linear range continuous-flow isotope ratio measurements. To this end, we determined the lowest analyte concentrations, at which the δ^{15}N- and δ^{13}C-values did not deviate from the reference isotope signatures determined by EA-IRMS by more than the accuracy of the proposed method (i.e., between 0.3% and 0.9% in $\Delta\delta^{15}$N and $\Delta\delta^{13}$C (SPME vs EA, Table 26)). The results summarized in Tables 26 and 28 for five substituted anilines illustrate that the use of buffered solutions and PDMS/DVB fibers for SPME not only improved accuracy but also allowed for more sensitive quantification of isotope ratios in the μg to mg L^{-1}-range, which represents an improvement by a factor of 2 compared to earlier approaches.[154]

Note that previous contributions, which focus predominantly on δ^{13}C measurements, refer to typical intervals of ±0.5% as acceptable uncertainties, from which the lowest acceptable concentration is deduced.[186,187] Unfortunately, these limits are not as established for less common isotope systems such as N and O isotope ratios. Uncertainties of δ^{15}N-values for organic compounds determined by GC/IRMS lack widely accepted limits across different isotope laboratories because these measurements are carried out less frequently than C isotope analyses. Given these ambiguities, we feel that it is more appropriate in the present case to define the acceptable limit of uncertainty for every compound individually because factors such as SPME extraction efficiency and

the efficacy of combustion (and reduction) to analyte gases (N_2 and CO_2) cannot be assumed to be identical for all organic compounds analyzed for a specific isotope ratio.

7.4 Conclusion

Our study demonstrates the importance of adjusting the solution pH prior to compound-specific isotope ratio measurements of substituted anilies by SPME-GC/IRMS. Because the conjugate acids of many substituted anilines exhibit pK_a-values between 2.5 and 7,[156,170] the fraction of protonated species will be significant given the range of pH-values of natural waters (pH 5-8,[190]). Besides compromising the sensitivity of the analytical method, δ^{15}N-measurements by SPME-GC/IRMS might deviate by up to -20% depending on the contaminant's basicity and the pH of the aqueous sample.

Moreover, the equilibrium N isotope fractionation associated with protonation of aryl N atoms could potentially interfere with the quantification of N isotope fractionation during contaminant transformation if the latter involves reactions at N-containing functional groups. Even though the magnitude of C and N isotope fractionation for (bio)degradation processes of substituted anilines are currently unknown, recent work with structurally related organic contaminants supports this conclusion. Protonations of alkyl-, aryl-, and triazine-bound N atoms are important elementary reaction steps during hydrolysis of phenylurea and triazine herbicides.[153,171,172,191] For the hydrolysis of isoproturon, an inverse N equilibrium isotope effect of 0.992 was reported for the alkyl-N protonation during initial zwitterion formation,[171] which contributed partly to the overall, observable N isotope fractionation. The N-heteroatom protonation in the triazine ring of atrazine associated with its acid-catalyzed and biotic hydrolysis led to apparent kinetic N

isotope effects of similar inverse magnitude (0.974—0.995[172]). These inverse isotope effects were rationalized as a consequence of N atom hybridization changes or additional bonds to N in the transition state. Our interpretation of stronger N—H bonds in protonated heavy N isotopologues of substituted anilines due to inverse N equilibrium isotope effects in a similar range fully agrees with these findings.

Chapter 8. Using Nitrogen Isotope Fractionation to Assess the Oxidation of Substituted Anilines by Manganese Oxide[7]

Marita Skarpeli-Liati, Martin Jiskra, Aurora Turgeon, Ashley N. Garr, William A. Arnold, Christopher J. Cramer, René P. Schwarzenbach, and Thomas B. Hofstetter

We explored the N isotope fractionation associated with the oxidation of substituted primary aromatic amines, which are often the position of initial attack in transformation processes of environmental contaminants. Apparent ^{15}N-kinetic isotope effects, $AKIE_N$, were determined for the oxidation of various substituted anilines in suspensions of manganese oxide (MnO_2) and compared to reference experiments in homogeneous solutions and at electrode surfaces, as well as to density functional theory calculations of intrinsic KIE_N for electron and hydrogen atom transfer reactions. Owing to the partial aromatic imine formation after one-electron oxidation and corresponding increase in C—N bond strength, $AKIE_N$-values were *inverse*, substituent-dependent, and confined to the range between 0.992 and 0.999 in agreement with theory. However, $AKIE_N$-values become *normal* once the fraction of cationic species prevailed owing to ^{15}N-equilibrium isotope effects, EIE_N, of 1.02 associated with N atom deprotonation. The observable $AKIE_N$-values are substantially modulated by the acid/base pre-equilibria of the substituted anilines and isotope fractionation may even vanish under conditions where normal EIE_N and inverse $AKIE_N$ cancel each other out. The pH-dependent trends

[7] This work was supported by the Swiss National Science Foundation (Grant No. 200020-116447/1 to T.B.H.) and the U.S. National Science Foundation (CHE-0952054 to. C.J.C.). We thank Jakov Bolotin for experimental support, Michael Aeschbacher and Michael Sander for supporting the electrochemical experiments, Michael Plotze for assisting the BET- and XRD-measurements, Brian Sinnet for his help with ζ-potential measurements, Susanne Kern and Heinz Singer for assisting in the LC—MS/MS-measurements and Maarten Nachtefaal and Markus Janousch for conducting the XANES-measurements. We acknowledge XD10A SuperXAS beamline of the SLS-PSI for the provision of beam time.

of the $AKIE_N$-values provide a new line of evidence for the identification of contaminant degradation processes via oxidation of primary aromatic amino groups.

8.1 Introduction

Aromatic amino groups are often the position of initial attack in transformation processes of industrial chemicals, biocides, and pharmaceuticals in the environment.[165,166,193-196] A (quantitative assessment of these processes is therefore essential for evaluating the exposure and impact of these micropollutants on human and environmental health.[197] However, aryl amines can react along different, sometimes competing pathways, including the mineral- and enzyme-catalyzed oxidation of the N atom,[165,166,193] the microbial dioxygenation of the aromatic ring,[169] as well as through nucleophilic addition of the amino functional group to electrophilic sites of natural organic matter.[198] Identifying these transformation processes is also challenging because they give rise to products that are usually difficult to analyze quantitatively (e.g., radical coupling products, adducts to NOM etc.).

Compound specific isotope analysis (CSIA) has been shown to offer new avenues to track degradation processes of such N-containing contaminants, even if competing reaction pathways occur and reaction products are partially unknown.[141,199,200] This is because stable isotope compositions measured in the remaining fraction of the contaminant molecule over time or distance from the pollution source change systematically depending on the type of chemical bond(s) that are broken or formed as a consequence of kinetic or equilibrium isotope effects.[179] As shown for nitroaromatic explosives,[162,201,202] phenylurea[171,203] and triazine herbicides,[161,172,191] their enzymatic,

abiotic, and photochemical redox reactions lead to typical distinct trends of C, H, and N isotope signatures that are not only indicative for the active transformation processes but can also allow one to quantify the extent of their degradation. These observations are due to the fact that different (N-containing) functional groups are involved in reactions, which also exhibit distinct apparent ^{13}C-, ^{2}H-, and ^{15}N-kinetic isotope effects (AKIEs). Despite the importance of aromatic amine oxidation for contaminant transformations, their isotope effects are largely unknown.

The goal of the present study was to assess the isotope effects associated with the oxidation of aromatic amino groups under typical environmental conditions and to evaluate whether the isotope fractionation associated with contaminant transformation can be exploited by CSIA for tracking these processes in aquatic environments. As a first step we investigated the magnitude and variability of apparent ^{15}N-kinetic isotope effects ($AKIE_N$) during the abiotic oxidation of a series of substituted anilines in suspensions of manganese oxide (MnO_2), which represents an important heterogeneous oxidant in the environment. Oxidation of substituted anilines by MnO_2 was reported to proceed via initial electron transfer from the lone pair of the nitrogen leading to formation of arylamino radicals.[166,193] As shown recently for the reduction of nitroaromatic radical anions,[162,204] even such small bonding changes induced by electron transfer to and from N atoms are likely to generate N isotope fractionation that can be measured by ^{15}N-CSIA.

Here, we examine the N isotope fractionation of a series of *o*-, *m*-, and *p*-substituted anilines covering more than one order of relative reactivities.[193] Product analysis was performed to corroborate the proposed initial reaction mechanism involving

substituted aniline radicals. Because the investigated compounds exhibit pK_{BH^+} values between 4.0 and 5.3, we examined potential effects of contaminant speciation and contributions of ^{15}N-equilibrium isotope effects due to aromatic amine deprotonation[205] to the observable $AKIE_N$ through experiments conducted in MnO_2 suspension at pH-values between 4.0 and 7.0. Finally, independent evidence for the interpretation of N isotope fractionation was obtained (i) from homogeneous and electrochemical oxidation experiments and (ii) from computations of ^{15}N-kinetic isotope effects (KIE_N) pertinent to outer-sphere electron transfer and H atom transfer from substituted anilines using density functional theory.

8.2 Experimental Section

8.2.1 Experimental Systems for the Oxidation of Substituted Anilines.

8.2.1.1 MnO_2-suspensions. MnO_2 particles were synthesized through oxidation of Mn^{2+} by MnO_4^- according to the method of Murray.[206] The suspensions were prepared in 10 mM acetate buffer for experiments carried out at pH 4.0 and 5.1 and in 10 mM phosphate buffer for experiments at pH 7.0. XRD-measurements indicated that the synthesized MnO_2-mineral was highly amorphous with Mn oxidation state 3.9 ± 0.3 as determined by iodometric titration and the pH_{IEP} was 3.25 ± 0.09 as obtained from ζ-potential measurements.

Oxidation of substituted anilines by MnO_2 was carried out in batch reactors containing different concentrations of MnO_2 in buffer solutions, NaCl (final ionic strength to 0.02 M), and a PTFE-coated magnetic stirring bar. All batch experiments were conducted at room temperature under oxic conditions. Losses of the reactants due

to volatilization, oxidation by air and/or sorption to the Viton rubber stoppers were accounted for in reference experiments set up in the identical manner except for the addition of MnO_2. Note that lack of reactivity of some substituted anilines in MnO_2-suspensions as well as in reference experiments (oxidation by $ABTS^{\bullet-}$ (2,2'-azino-bis(3-ethylbenzthiazoline-6-sulfonic acid) radical anion) in aqueous solution and at electron surfaces) limited the selection of substituted anilines.

Experiments at pH 7.0 were conducted in duplicates. The reaction was initiated by the addition of variable amounts of substituted anilines from a methanolic stock solution to achieve initial concentrations of 400—600 μM. The MnO_2 concentrations were varied so that fast reactions did not exceed 50% conversion within the first minute of the experiment, while the oxidative turnover of slowly reacting compounds had to be >60% within 3 days. Samples were withdrawn at predefined time points with a gastight glass syringe and the oxidation reaction was stopped by filtering off MnO_2-particles with a 0.2 μm regenerated cellulose (RC) filter. Filtered solutions were stored in amber vials in the dark at 4 ^{o}C until concentration measurements and isotope analysis. Because the disappearance of substituted anilines from MnO_2-suspensions at pH 4.0 and 5.1 was too fast to be sampled as described for pH 7.0, variable amounts of MnO_2 were spiked to reactors containing the identical initial concentration of substituted aniline. This procedure was used to achieve different degrees of reactant conversion and was shown earlier for nitroaromatic compounds to enable the study of isotope fractionation of fast reactions.[162] Prior to concentration measurements and isotope analysis of substituted anilines, the pH of the filtered aqueous samples was adjusted to pH 7.0 with NaOH.

The loss of substrate due to adsorption and cation exchange to the mineral surface was assessed for aniline by experiments in which the compound's concentration was compared before and after reductive dissolution of the MnO_2-particles with ascorbic acid (0.3 M, pH 13) at different time points of the reaction. To this end, the aniline was extracted from the aqueous solution with ethyl acetate and the concentration in the extract was quantified by GC/MS. The extraction efficiency of aniline into ethyl acetate was 99.5 ± 2.5%.

For the identification of organic oxidation products by LC—MS/MS, samples of 1 mL MnO_2-suspension were reductively dissolved by ascorbic acid (0.3 M, pH 13) and diluted with 9 mL of nanopure water. Aqueous samples were processed following a modified procedure of Kern *et al*.[207] Inorganic salts were removed by solid phase extraction (SPE, HLB Extraction Cartridges, 100 μm, Oasis, Waters) of the dilute aqueous samples. Organic analytes were eluted from the cartridges with MeOH, dissolved in H_2O and filtered with a 0.45 μm RC filter prior to LC-MS/MS.

8.2.1.2 Homogeneous Oxidation. Oxidation of substituted anilines in homogeneous solution was performed in an anoxic glovebox using anoxic stock and buffer solutions identical to experiments with MnO_2-suspensions at pH 4.0 and 5.1 (see above), except for the addition of variable amounts of electrochemically produced oxidant instead of MnO_2 to achieve different degrees of contaminant conversion. The oxidant $ABTS^{\bullet-}$ was generated through direct electrochemical oxidation of the $ABTS^{2-}$ at an E_h of 0.667 V (SHE) in the electrochemical cell as described in Aeschbacher *et al.*[208] The ABTS dianion was added to buffer solutions (0.1 M phosphate at pH 7.0 and 0.1 M acetate at

pH 4.0 in 0.1 M KCl as supporting electrolyte) and the oxidative working current was monitored until it dropped below background values (30 μA). The $ABTS^{\bullet-}$ was used immediately after generation. All samples containing the residual substituted aniline were stored at 4 ^{o}C until concentration and isotope ratio analysis.

8.2.1.3 Direct Electrochemical Oxidation. All electrochemical experiments were conducted in an anoxic glovebox using anoxic stock and buffer solutions (0.1 M acetate and phosphate for pH 4.0 and 7.0, respectively) containing 01 M KCl as background electrolyte (see ref 208 for procedures). Direct electrochemical oxidation of the aromatic amines was performed in an electrolysis cell equipped with a glassy carbon (GC) working electrode, an Ag/AgCl reference electrode, and a coiled platinum wire auxiliary electrode.[208] Currents were measured with a CHI 630 instrument (CHInstruments, Austin, TX) and the potential was controlled by an Autolab PG 302 instrument (EcoChemieB.V., Utrecht, ML). The electrolysis cell was filled with the corresponding buffer solution and equilibrated at the desired reduction potential (E_h between 0.777 and 0.957 V vs SHE, Table 1) applied to the working electrode. The oxidation was initiated by the addition of defined amounts of substituted aniline stock solution. At given time intervals, 2 mL aqueous samples were withdrawn and stored outside the glovebox at 4 ^{o}C until further analysis.

8.2.2 Analytical Methods.

8.2.2.1 Chemical Analysis. Concentration measurements of substituted anilines were performed by reversed-phase HPLC (Supelcosil LC-18, 25 cm × 4.6 mm, 5 μm, Supelco) and UV—vis detection at wavelengths corresponding to the absorption maxima of the

substituted anilines. Different eluent mixtures KH_2PO_4/MeOH were used for each compound varying between 40/60% to 70/30% at a flow rate of 1 mL min^{-1} and sample injection volume of 10 μL. Quantification of substituted anilines extracted into ethyl acetate was conducted on a GC/MS (Ultra Trace GC and DSQII, Thermo Electron Corporation) upon on-column injection using the instrumental setup and settings described previously.[205]

The analytical procedure for identification of transformation products was adapted from Kern *et al.*[207] The measurements were performed by liquid chromatography coupled to an LTQ (Linear Trap Quadrupole) Orbitrap mass spectrometer (Thermo Electron Corporation) with electrospray ionization (LC-MS/MS). For liquid chromatographic separation a XBridge C-18 column was used (2.1 × 5.0 mm, 3.5 *m*m particle size, Waters) and a gradient was run from H_2O/MeOH 90/10% to 5/95% containing 0.1% formic acid. Identification of coupling products was performed only qualitatively due to lack of commercial standards. To this end exact masses of expected reaction products were extracted from the chromatograms in order to obtain MS/MS-fragment spectra. On the basis of the exact molecular mass and fragmentation pattern of each detected product, the most probable molecular structures were postulated.

The aqueous Mn^{2+}-concentration was measured by inductively coupled plasma mass spectrometry (ICP/MS 7500cx, Agilent Technologies). All samples were diluted with 0.1 M HNO_3 to final concentrations between 10 and 1000 μg Mn^{2+} L^{-1}.

8.2.2.2 Stable Isotope Ratio Measurements. Stable N and C isotope signatures (δ^{15}N and δ^{13}C) of the substituted anilines were determined by solid-phase microextraction (SPME)

coupled to a GC/IRMS (gas chromatography isotope-ratio mass spectrometry) with combustion interface.[205] SPME fiber material and extraction conditions were polydimethylsiloxane/divinylbenzene (PDMS/DVB, Supelco) and 45 min at 40 ^{o}C for all compounds except OCH_3-substituted anilines. The latter required DVB-Carboxen-PDMS coated fibers and 45 min extractions at 70 ^{o}C. All N and C isotope signatures are reported as arithmetic mean ($\pm 1\sigma$) of triplicate measurements relative to air ($\delta^{15}N_{air}$) and Vienna PeeDee Belemnite ($\delta^{13}C_{VPDB}$), respectively, in per mil (%). To account for uncertainty due to instrument nonlinearity,[187] all samples were diluted to concentrations yielding constant peak amplitudes (1—2 V for ^{15}N- and 4—5 V for ^{13}C-analysis). Accuracy of compound-specific isotope analysis was verified via standard bracketing procedures using a calibrated in-house standard (aniline) of known N and C isotope ratios.[205]

8.2.3 Data Evaluation. Bulk compound N and C isotope enrichment factors, ε_N and ε_C, were derived from linear regression analysis of δ^{15}N- and δ^{13}C-values, respectively, vs fractional amount of reactant conversion.[199] Data from replicate experiments were combined using the Pitman estimator[209] as shown previously.[152] While the extent of C isotope fractionation is reported as average ε_C for all C atoms present in the reactant molecules, interpretation of N isotope fractionation is based on position-specific apparent ^{15}N-kinetic isotope effects, $AKIE_N$, calculated from eq 20. Uncertainties associate with ε_N -, ε_C -, $AKIE_N$-values correspond to 95% confidence intervals.

$$AKIE_N = \frac{1}{1 + \varepsilon_N/1000} \tag{20}$$

To account for effects of substituted aniline protonation on the observed $AKIE_N$s, data obtained at pH-values below 7.0 were modeled as follows. N isotope fractionation of substituted aniline cations, BH^+, originates from the combination of an isotope-sensitive deprotonation step (eq 21)[205] and the subsequent oxidation reaction of the neutral species, B (eq 22).

$$BH^+ \underset{k_2}{\overset{k_1}{\rightleftharpoons}} B + H^+ \tag{21}$$

$$B \xrightarrow{k_3} P \tag{22}$$

where k_1, k_2, and k_3 are the reaction rate constants of the elementary reactions and P stands fro the radical products of the oxidation reaction. Using the steady-state treatment for the proton-exchange pre-equilibrium, the rate constant for the reaction of protonated substituted aniline species $k_{obs}^{BH^+}$ is given by eq 23.

$$k_{obs}^{BH^+} = \frac{k_1 \times k_3}{k_2\left[H^+\right] + k_3} \tag{23}$$

where $[H^+]$ is the proton concentration. Rewriting eq 23 for ^{14}N- and ^{15}N-isotopologues reveals that an apparent ^{15}N-kinetic isotope effect associated with species BH^+, $AKIE_N^{BH^+}$, is the product of the deprotonation ^{15}N-equilibrium isotope effect, $EIE_N^{BH^+}$, and the $AKIE_N$ of the neutral substituted aniline, $AKIE_N^B$ (eq 24).

$$AKIE_N^{BH^+} = EIE_N^{BH^+} \times AKIE_N^B \tag{24}$$

As a consequence of the simultaneous reactions of protonated and neutral substituted aniline species, the overall observable $AKIE_N$ is the weighted average of the

two fractions and their respective isotope effect. In eq 25, f_{BH^+} is the fraction of protonated compound, which equals $\left(1+10^{\left(\text{pH-p}K_{BH^+}\right)}\right)^{-1}$.

$$\text{AKIE}_N = f_{BH^+} \times \text{EIE}_N^{BH^+} \times \text{AKIE}_N^B + \left(1 - f_{BH^+}\right) \times \text{AKIE}_N^B \qquad (25)$$

8.2.4 Computational Methods. The gas-phase geometries of all molecular species were fully optimized at the density functional (DFT) level using the gradient-corrected Perdew—Wang exchange and correlation functionals[6,7] as modified by Adamo and Barone[8] using either the 6-311+G(d) or 6-311+G(2df,2p) basis sets.[16] Stationary points were confirmed as minima or transition-state (TS) structures by analytical calculation of vibrational frequencies, which were also used in the construction of ideal-gas, rigid rotator, harmonic oscillator partition functions, from which thermal contributions to free energies G were computed.[1] For outer-sphere electron-transfer rate constants, ^{15}N-kinetic isotope effects (KIE_Ns) were computed essentially according to the method of Kavner *et al*.[210] For hydrogen-atom transfer reactions involving active oxygen species, KIEs were computed from canonical transition-state theory.

8.3 Results and Discussion

8.3.1 Isotope Fractionation Associated with the Oxidation of Substituted Anilines in MnO_2-Suspensions. We observed measurable N isotope fractionation during the oxidation of neutral, substituted anilines in suspensions of MnO_2 at pH 7.0, while C isotope composition did not change significantly. Nitrogen isotope fractionation was always *inverse*, that is, ^{15}N-containing isotopologues reacted faster than molecules with ^{14}N leading to a decreasing δ^{15}N of the reactant with increasing conversion (Figure 19b).

The extent of N isotope fractionation observed in suspensions of MnO_2 did not exceed -12% compared to the initial $\delta^{15}N$ while the reactant turnover approached 55 to 88% (Table 29). Limited turnover was due to the biphasic disappearance kinetics of substitiuted aniline oxidation by MnO_2 (Figure 19a), which, as reported previously,[166,193,211] exhibited fast initial transformation followed by a decreasing rate of reaction. Increasing the concentration ratio of MnO_2 to substituted aniline slightly increased the oxidative turnover and thus the observable range of N isotope fractionation (Figure 19b) but did not influence the N isotope enrichment factors, ε_N, which quantify the extent of isotope fractionation per incremental amount of reacted substrate (Figure 19b and Figure 19c). As shown in Figure 19c, ε_N -values of aniline oxidation were identical within experimental error. This observation suggests that despite biphasic reaction kinetics, N isotope fractionation was associated with the identical elementary reaction step(s) of aromatic amine oxidation independent of the substituted anilines to oxidant ratio.

The occurrence of a single isotope fractionating elementary reaction step was confirmed with a series of complementary experiments, which showed that the biphasic reaction kinetics were due to a decrease in MnO_2 reactivity rather than a change in substituted aniline oxidation mechanism during the time course of the reaction. First, the decreasing rate of contaminant disappearance correlated with the decreasing average particulate Mn oxidation state monitored by X-ray absorption near edge structure (XANES) measurements, as illustrated in Figure 1d for the oxidation of *p*-OCH_3-aniline by MnO_2. The average Mn oxidation state decreased to 2.6 during the time course of the

reaction pointing to an increased share of reduced Mn species in the mineral including Mn(II) adsorbed on the mineral surface. The corresponding decrease of the average Mn oxidation state is indicative of the decreasing reactivity of the MnO_2-particles. The same process has been invoked previously for the reductive dissolution of MnO_2 (e.g., by arsenious acid, H_3AsO_3), where formation of intermediate Mn(III)oxyhydroxide layers at the mineral surface blocked the access to reactive oxidized Mn(IV) sites and led to the overall decrease of the MnO_2 reduction rate.[212,213] Measurements of dissolved Mn^{2+} at different time points of aniline oxidation by MnO_2 support the interpretation of XANES-data. After a conversion of >400 μM of the initial 600 μM of aniline, only 130 μM of Mn^{2+}_{aq} were recovered in solution. Therefore, only 65% of the oxidation equivalents of aniline could be detected as dissolved species, leaving Mn^{3+}- and Mn^{2+}-species bound to the mineral. Second, identical aniline disappearance kinetics were observed regardless whether aniline was measured in the supernatant or after dissolving the MnO_2-particles. Similarly, no inhibition of the reaction was found if Mn^{2+} and azobenzene had been added to the reactors in concentrations corresponding to the initial aniline oxidation-equivalents. These experiments indicate that under the experimental conditions, neither adsorption of aniline nor cosolutes to MnO_2 did influence the rate of aniline oxidation. Finally, identical ε_N-values for different MnO_2-loadings provide evidence that an electron transfer process is rate-limiting rather than any surface complex formation between the substituted aniline and the mineral. The assumption of an electron transfer as predominant rate-limiting step is also supported by the reported correlation of the half-

wave potentials and substituent Hammett constants of the aromatic amines with experimentally determined initial oxidation rates.[166,193]

8.3.2 Substituent Effects on AKIE$_N$s and Implications for the Reaction Mechanism. On the basis of the above discussion, the observable N isotope fractionation with ε_N-values between 1.3% and 8.3% can be attributed to the oxidation of the N atom in neutral substituted anilines resulting in apparent ^{15}N-kinetic isotope effects, AKIE$_N$ between 0.9987 and 0.9927 (Table 29, entries 1—8). The small C isotope fractionation represents an average secondary isotope effect for the C atoms that were not directly involved in the reaction (ε_C of -1.1 ± 0.1%).

We observed a marked influence of the position and type of the aromatic substituent on AKIE$_N$-values. *meta*-Substitution with –CH$_3$ or –OCH$_3$-groups did not cause the AKIE$_N$-value to deviate significantly from that of aniline (0.9960 ± 0.0009). Electron-donating substituents in *ortho* or *para* position, however, led to larger N isotope fractionation (lowest AKIE$_N$ of 0.9927 ± 0.0012 for *p*-OCH$_3$-aniline, entry 7, Table 29) compared to unsubstituted aniline, while electron-accepting substituents caused the opposite trend (AKIE$_N$ of 0.9987 ± 0.0004 for *p*-Cl-aniline, entry 8, Table 29). The identical AKIE$_N$-values within experimental error found for *o*-CH$_3$ and *p*-CH$_3$-aniline as well as *o*-OCH$_3$ and *p*-OCH$_3$-aniline, respectively, indicate that substituents in these positions exhibited the same effects on the bonds to N during its oxidation.

The observed inverse isotope effects can be rationalized by the formation of a radical intermediate after one-electron oxidation, which is delocalized over the aromatic ring causing the C—N bond to become stronger in the transition state, due to the formation of

a partial imine-type bonding of N in the subsequent intermediates (illustrated by the resonance structures in Scheme 4). Higher infrared stretching frequencies of C=N vs C—N bonds[214] imply stronger bonds to N in imines and support this interpretation. Similar findings of inverse N isotope fractionation have been reported for reactions in which additional bonds were formed to aromatic and heterocyclic N atoms and in amino acids.[172,205,215,216] In addition, the formation of radical intermediates gives rise to the sensitivity of the $AKIE_N$-values for aromatic substitution. The substituents' electron donating and accepting properties affect the radical stability, the preferential radical localization in *ortho* and *para*-position, and thus the C—N bond strength in the transition state, which explains the observed variations of the $AKIE_N$. While electron donating substituents like *o*-/*p*-$CH_3$and *o*-/*p*-OCH_3 cause the C—N bond to become stronger in the transition state, electron-withdrawing *p*-Cl substitution has only moderate impact on C—N bonding and thus the magnitude of the $AKIE_N$ compared to the unsubstituted aniline. Consequently, the lack of any radical stabilization and thus localization in *meta*-position is also responsible for the insensitivity of the $AKIE_N$ for *meta*-substituents. Analysis of reactor solutions for reaction products by LC-MS/MS confirmed these substituent effects indirectly. As proposed in previous studies,[165,166] head-to-head (N—N), head-to-tail (N—C) and tail-to-tail (C—C) products were found in the reduced as well as in the oxidized form, where radical coupling occurred at the *ortho*- and *para*-position.

Table 29. Bulk N Isotope Enrichment Factors, ε_N, Apparent ^{15}N-Kinetic Isotope Effects, $AKIE_N$, of Substituted Anilines in Various Experimental Systems

Entry	compound	pH (-)	E_h (V vs SHE)	conversion (%)[a]	ε_N[b] (%)	$AKIE_N$[b] (-)
MnO_2-suspensions						
1	aniline[c]	7.0		55	3.6 ± 0.6	0.9960 ± 0.0009
2	*o*-CH_3-aniline	7.0		65	6.0 ± 0.4	0.9948 ± 0.0009
3	*m*-CH_3-aniline	7.0		53	3.7 ± 0.9	0.9963 ± 0.0006
4	*p*-CH_3-aniline	7.0		63	6.0 ± 0.2	0.9941 ± 0.0003
5	*o*-OCH_3-aniline	7.0		65	7.6 ± 0.2	0.9925 ± 0.0004
6	*m*-OCH_3-aniline	7.0		52	4.9 ± 0.2	0.9952 ± 0.0001
7	*p*-OCH_3-aniline	7.0		54	8.3 ± 0.6	0.9927 ± 0.0012
8	*p*-Cl-aniline	7.0		88	1.3 ± 0.2	0.9987 ± 0.0004
9	*p*-CH_3-aniline	6.0		91	5.4 ± 1.1	0.9946 ± 0.0011
10	*p*-CH_3-aniline	5.1		35	1.1 ± 0.4	0.9986 ± 0.0007
11	*p*-CH_3-aniline	4.7		71	-4.3 ± 2.0	1.0043 ± 0.0020
12	*p*-CH_3-aniline	4.0		53	-6.6 ± 0.7	1.0064 ± 0.0015
13	*p*-OCH_3-aniline	4.0		45	-5.3 ± 0.9	1.0052 ± 0.0015
14	*p*-Cl-aniline	4.0		75	-1.9 ± 0.3	1.0019 ± 0.0006
ABTS in homogeneous solution						
15	aniline	7.0		75	2.3 ± 0.8	0.9977 ± 0.0021
16	*p*-CH_3-aniline	7.0		80	3.8 ± 0.1	0.9962 ± 0.0003
17	aniline	4.0		74	-1.0 ± 0.2	1.0010 ± 0.0006
18	*p*-CH_3-aniline	4.0		78	-4.5 ± 0.5	1.0045 ± 0.0014
Electrochemical oxidation						
19	*p*-CH_3-aniline	7.0	0.777	56	5.2 ± 0.5	0.9948 ± 0.0013
20	*p*-CH_3-aniline	7.0	0.837	58	6.2 ± 0.4	0.9938 ± 0.0012
21	*p*-CH_3-aniline	7.0	0.897	50	5.6 ± 0.7	0.9944 ± 0.0017
22	*p*-CH_3-aniline	7.0	0.957	52	3.7 ± 0.5	0.9963 ± 0.0013
23	*p*-CH_3-aniline	4.0	0.897	73	-2.2 ± 0.3	1.0022 ± 0.0008
24	*p*-CH_3-aniline	4.0	0.957	71	-2.5 ± 0.7	1.0025 ± 0.0019

[a]Decrease of reactant concentration/initial concentration × 100. [b]Uncertainties correspond to 95%-confidence intervals. [c]ε_N - and $AKIE_N$-values (Figure 19c) were derived using the Pitman estimator for combined data sets.

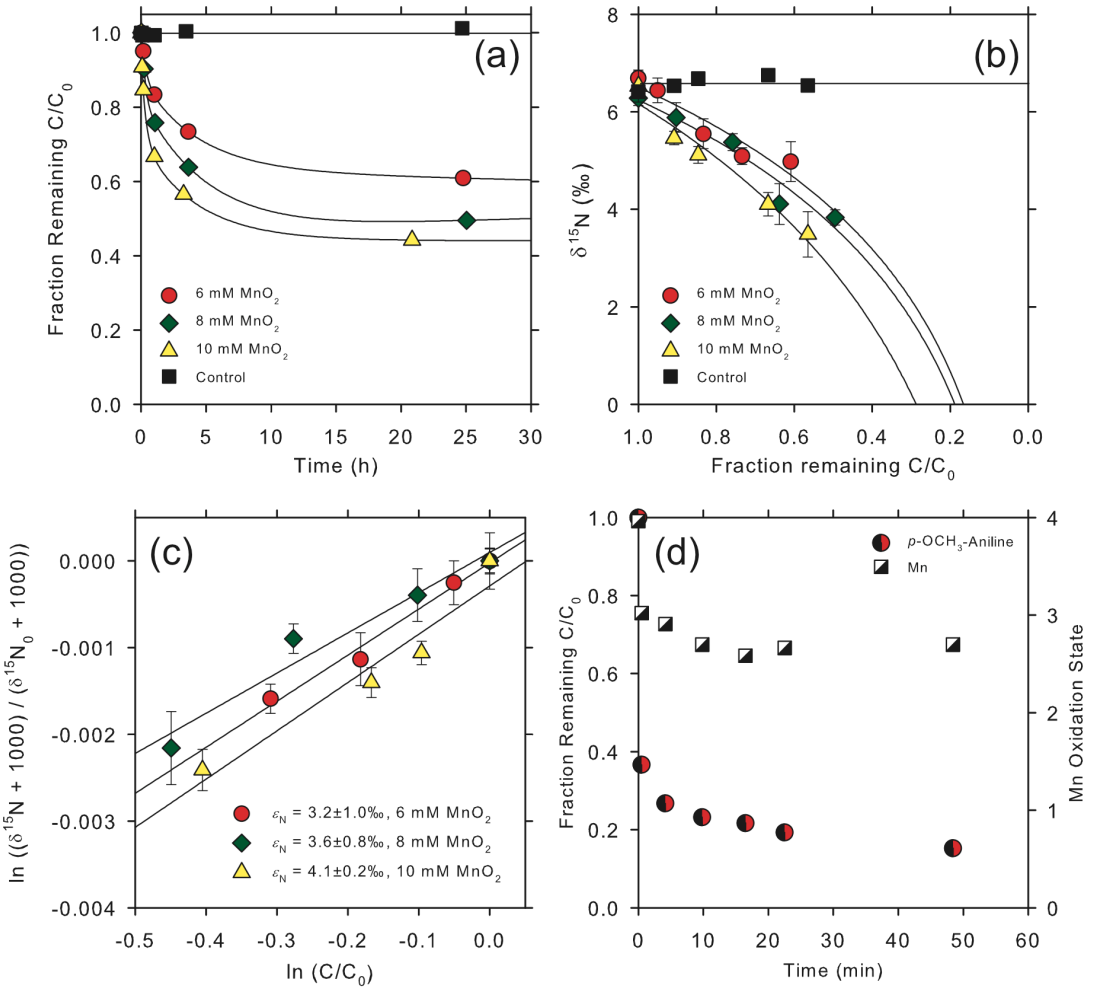

Figure 19. (a) Kinetics of aniline oxidation (C_0 = 0.6 mM) in suspensions containing 6,8, and 10 mM MnO_2 at pH 7.0. Uncertainty of the concentration measurements ($\pm\sigma$) is 2% (error bars are smaller than the markers); (b) N isotope fractionation during aniline oxidation in various MnO_2-suspensions: δ^{15}N-values vs fraction of remaining reactant (C/C_0); (c) linearized N isotope fractionation trends used for calculation of bulk N isotope enrichment factors: ε_N; (d) Oxidation of *p*-OCH_3-aniline (4.8 mM initial concentration) in 10 mM MnO_2-suspension at pH 7.0 and average Mn oxidation state.

Scheme 4. Resonance structures of anilinium radical cation formed by electron transfer from aniline.

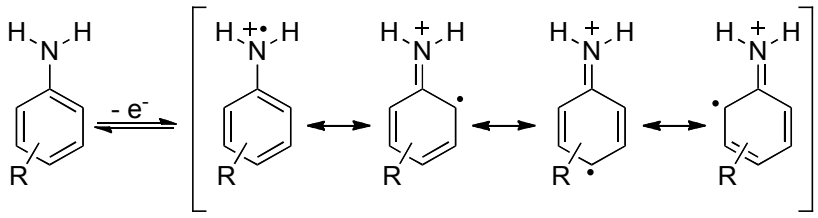

8.3.3 Reference Experiments and Density Functional Theory Calculations. Independent evidence for assigning the one-electron oxidation and subsequent partial imine-bond formation as isotope-sensitive and rate-limiting reaction step was obtained from measurements of N isotope fractionation of selected substituted anilines in homogeneous solution, in electrochemical experiments, and through calculation of KIE_N using density functional theory. Despite the different experimental conditions, oxidation of aniline and *p*-CH_3-aniline by $ABTS^{\bullet-}$ and at glassy carbon electrode surfaces at pH 7.0 also resulted in inverse $AKIE_N$s as observed in MnO_2-suspensions (Table 29). $AKIE_N$-values pertinent to electrochemical oxidation of *p*-CH_3-aniline at oxidation potentials differing by 180 mV, which corresponds to 3 orders of magnitude in electron transfer driving force, did vary by less than 2.5% (Figure 20a, Table 29, entries 19-22). The insensitivity of N isotope fractionation toward oxidation potential lends further support to the hypothesis that N isotope fractionation during substituted aniline oxidation is not caused exclusively by the electron transfer but also by hybridization changes at the N atom and change in C—N bond strength during formation of partial imine bonds. This interpretation is also supported by theoretical considerations.

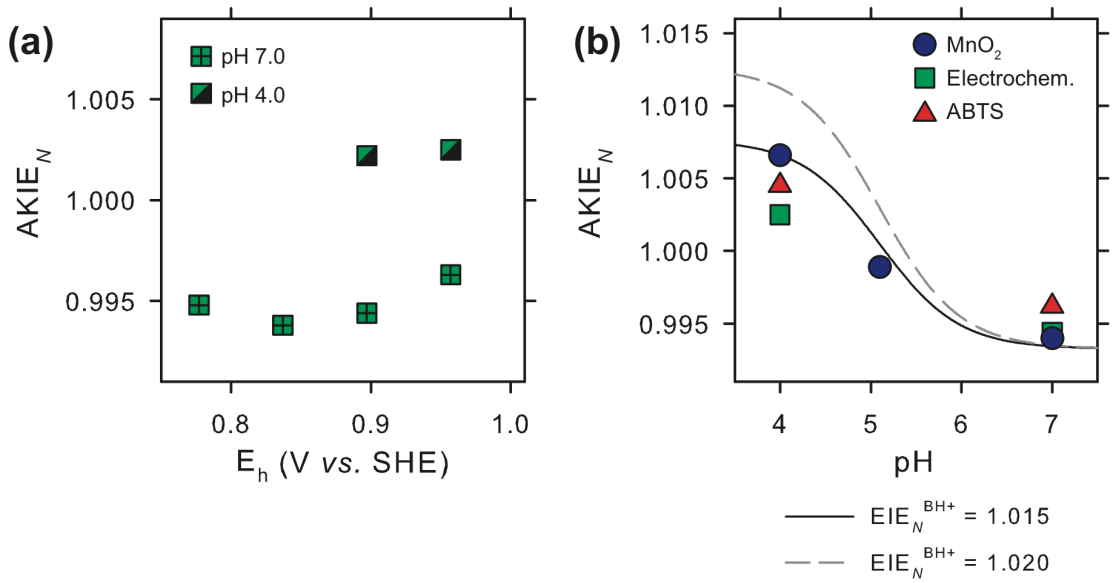

Figure 20. (a) Observed $AKIE_N$ associated with the electrochemical oxidation of *p*-CH_3-aniline at working electrode potential, E_h, between 0.78 and 0.96 V at pH 4.0 and 7.0 (see Table 29 for details); (b) Observed $AKIE_N$ of *p*-CH_3-aniline (pK_{HB^+} 5.10) for oxidation by MnO_2, $ABTS^{\bullet-}$ (2,2'-azino-bis(3-ethylbenzthiazoline-6-sulfonic acid), and at a glassy carbon electrode in the pH-range 4.0 to 7.0.

Density functional calculations were undertaken to predict KIE_Ns that would be expected under conditions of outer-sphere electron transfer (ET) and hydrogen-atom transfer (HAT) by an active oxygen species (Table 30). In the former case, isotopically sensitive rate constants were predicted by Marcus theory; in the latter case, such constants were predicted from canonical transition-state theory.

Table 30. Density functional theory (DFT) calculations ^{15}N-Kinetic Isotope Effects for electron transfer (ET-KIE$_N$) and hydrogen atom transfer (HAT-KIE$_N$) from neutral and cationic substituted anilines to ·OH and ·OOH, respectively.

Entry	Compound	E_h [a)] (V vs. SHE)	ET-KIE$_N$ (-)	HAT-KIE$_N$ $^{\cdot}OH$ (-)	HAT-KIE$_N$ $^{\cdot}OOH$ (-)
Neutral substituted anilines					
25	Aniline	0.850	0.9943	0.9959	0.9963
26	*o*-CH_3-Aniline	0.850	0.9945		
27	*m*-CH_3-Aniline	0.850	0.9948		
28	*p*-CH_3-Aniline	0.850	0.9948	0.9952	0.9972
29	*p*-CH_3-Aniline	0.750	0.9943		
30	*p*-CH_3-Aniline	0.950	0.9954		
31	*o*-OCH_3-Aniline	0.850	0.9951		
32	*m*-OCH_3-Aniline	0.850	0.9945		
33	*p*-OCH_3-Aniline	0.850	0.9959	0.9950	0.9992
34	*m*-Cl-Aniline	0.850	0.9938		
35	*p*-Cl-Aniline	0.850	0.9944	0.9955	0.9965
36	*p*-OH-Aniline			0.9950	0.9989
37	*p*-NO_2-Aniline			1.0008	0.9935
Cationic substituted anilines					
38	Aniline			0.9972	0.9910
39	*p*-OH-Aniline			0.9969	0.9929
40	*p*-OCH_3-Aniline			0.9944	0.9935
41	*p*-CH_3-Aniline			0.9991	0.9924
42	*p*-Cl-Aniline			1.0006	0.9920
43	*p*-NO_2-Aniline			0.9959	0.9824

[a]Working electrode potentials for ET-KIE$_N$ calculations only.

In general, there is good quantitative agreement between the predicted KIE$_N$s for ET and those determined experimentally (at pH 7.0, see electrochemical data below) with electrodes having reduction potentials similar to those employed in the calculations. The HAT-KIE$_N$s are also generally in good quantitative agreement with those determined experimentally at pH 7.0. All predicted KIE$_N$s are inverse (with the exception of HAT from *o*-NO_2-aniline by hydroxyl radical), reflecting that increased C_1—N bonding in the

anilinium radical cation of HAT transition state structure compared to the reactant aniline (Scheme 4). The quantitative similarity for the two processes is primarily attributable to the small change in this bonding character, which leads to predicted inverse KIE_Ns of substantially less than 10% in every instance consistent with experiments. Thus, theory indicates that the observed $AKIE_N$s cannot be considered to rule out HAT pathways in substituted aniline oxidation for cases where active oxygen species might be generated, but neither do they need to be invoked the good agreement between theory and electrochemical oxidation results where ET processes would be likely to be the only ones active. We note that neither the computational predictions for outer-sphere ET nor those for HAT show substituent effects consistent with those observed experimentally. This must be assigned to the simplifications inherent in the computational models, which make it challenging to reproduce the small substituent effects.

8.3.4 Influence of Substituted Aniline Speciation of $AKIE_N$. Because the deprotonation of substituted anilines is associated with a normal ^{15}N-equilibrium isotope effect, EIE_N, between 1.017 and 1.021,[205] we investigated the consequences of N-atom protonation on the observable N isotope fractionation trends during oxidation with selected *para*-substituted anilines in the pH-range 4.0—7.0. As shown in Table 29 (entries 4, 9—12) for *p*-CH_3-aniline, the $AKIE_N$ increased to almost unity at pH-values matching the pK_{HB^+} and isotope fractionation became normal once the protonated species (BH^+) prevailed. Our data imply that ^{14}N-isotopologues reacted faster at pH < pK_{HB^+} while they are outcompeted by ^{15}N-isotopologues at higher solution pH. The same trend was found for *p*-OCH_3-aniline (entries 7 and 13) and *p*-Cl-aniline (entries 8 and 14).

Assuming that N atom oxidation can only occur from the neutral species, we propose that pH-dependent N isotope fractionation is due to a combined *normal* ^{15}N-equilibrium isotope effect pertinent to the deprotonation of the substituted anilinium cation (BH^+, eq 21) and the *inverse* apparent ^{15}N-kinetic isotope effect associated with the oxidation of the neutral species (B, eq 22) as described in eq 25.

Fitting the data for *p*-CH_3-anilines in Table 29 to eq 25 adequately describes the trends of observable $AKIE_N$ at different pH-values of the MnO_2-suspensions (Figure 20b). The calculated $AKIE_N^B$ of 0.9933 agrees well with the observed $AKIE_N$ measured at pH 7.0 (entry 4, Table 29). Deviations at pH-values below the pK_{HB^+} imply that the $EIE_N^{BH^+}$ is smaller (1.015) than proposed previously but still within the experimental uncertainty of the $EIE_N^{BH^+}$ derived for *p*-CH_3-aniline (1.0199 ± 0.0040[23]) supporting agreement of eq 25 with experimental data. Our interpretation of the pH-dependent, observable $AKIE_N$ is supported by the results from reference experiments regarding the electrochemical and homogeneous oxidation of aniline and *p*-CH_3-anilin at pH 4.0 and 7.0. The trends of $AKIE_N$ vs pH for oxidation at glassy carbon electrode surfaces and by $ABTS^{\bullet-}$ were very similar to the ones observed in MnO_2-suspensions (Figure 20b, Table 29). These results confirm that at pH-values below the pK_{HB^+}, N isotope fractionation approaches the product of equilibrium and kinetic ^{15}N-isotope effects (eq 25), where the measured $AKIE_N$ values are dominated by the normal EIE. As a final check, we evaluated the predicted KIEs for HAT from protonated anilines by active oxygen species $^{\bullet}OH/^{\bullet}OOH$. In all cases, N isotope effects were predicted to be inverse,

providing further evidence that the observed normal N isotope effects reflect acid/base partitioning prior to oxidation of the conjugate base.

8.3.5 Environmental Significance. Our work illustrates that oxidation of primary aromatic amino groups inorganic contaminants is accompanied by a small and measurable N isotope fractionation thus enabling new avenues for the assessment of degradation reactions at N-containing functional groups. Because the pK_{HB^+} of many aromatic amines are in the range of pH-values encountered in many aquatic systems, the observable N isotope fractionation will be modulated substantially by the compound's acid/base equilibria. Isotope fractionation may even vanish under conditions where contributions from *normal* EIE_N associated with aromatic deprotonation and *inverse* $AKIE_N$ of N atom oxidation cancel each other out. This variability of N isotope fractionation slightly complicates the application of CSIA in that the contaminant's pK_{HB^+} and solution pH have to be taken into account. The systematic trends of $AKIE_N$-values, on the other hand, provide a new line of evidence for the identification of contaminant degradation processes via reactions of primary aromatic amino groups.

Nitrogen isotope enrichment factors below 10% at the reactive position, as reported in this study, imply that δ^{15}N-measurements should be carried out with small total uncertainties (< ± 0.5%) and require that N isotope fractionation is not diluted by many non-reactive N atoms in a contaminant. The impact of substituent properties on $AKIE_N$-values suggests that contaminant-specific ε_N-values will be required to assess their oxidation processes by CSIA. The compound-specific N isotope fractionation behavior contrasts earlier observations for the reduction of aromatic nitro groups,[162,163]

which found $AKIE_N$-values that were largely independent of the compound's molecular structure. The substituent-dependence might, together with the influence of acid/base equilibria, prove indicative for the identification of N aryl oxidation processes. Further studies targeting N isotope fractionation in alternative contaminant transformation processes such as oxidative N-dealkylations and nucleophilic additions are warranted to evaluate the proposed trends of N isotope effects.

References

1) Cramer, C. J. *Essentials of Computational Chemistry: Theories and Models*, 2nd ed. John Wiley & Sons, Chichester, **2004**.

2) Hohenberg, P.; Kohn, W. *Phys. Rev.* **1964**, *136*, B864-B871.

3) Kohn, W. Sham, L. J. *Phys. Rev.* **1965**, *140*, A1133-A1138.

4) Kohn, W. *Rev. Mod. Phys.* **1999**, *71*, 1253-1266.

5) Perdew, J. P.; Burke, K.; Enzerhof, M. *Phys. Rev. Lett.* **1996**, *77*, 3865-3868.

6) Perdew, J. P.; Yue, W. *Phys. Rev. B* **1986**, *33*, 8800-8802.

7) Perdew, J. P. In *Electronic Structure of Solids '91*; Ziesche, P.; Eschrig, H.; Eds.; Akademic Verlag: Berlin, 1991, pp 11-20.

8) Adamo, C.; Barone, V. *J. Chem. Phys.* **1998**, *108*, 664-675.

9) Becke, A. D. *Phys. Rev. A* **1988**, *38*, 3098-3100.

10) Lee, C.; Yang, W.; Parr, R. G. *Phys. Rev. B* **1988**, *37*, 785-789.

11) Becke, A. D. *J. Chem. Phys.* **1993**, *98*, 5648-5652.

12) Stephens, P. J.; Devlin, F. J.; Chabalowski, C. F.; Frisch, M. J. *J. Phys. Chem.* **1994**, *98*, 11623-11627.

13) Zhao, Y.; Truhlar, D. G. *Theor. Chem. Acc.* **2008**, *120*, 215-241.

14) Lynch, B. J.; Fast, P. L.; Harris, M.; Truhlar, D. G. *J. Phys. Chem. A* **2000**, *104*, 4811-4815.

15) Easton, R. E.; Giesen, D. J.; Welch, A.; Cramer, C. J.; Truhlar, D. G. *Theor. Chim. Acta* **1996**, *93*, 281-301.

16) Hehre, W. J.; Radom, L.; Schleyer, Pv.R.; Pople, J. A. *Ab Initio Molecular Orbital Theory*, Wiley, New York, **1986**.

17) Clark, T.; Chandrasekhar, J.; Spitznael, G. W.; Schleyer, Pv.R. *J. Comp. Chem.* **1983**, *4*, 294-301.

18) Hehre, W. J.; Ditchfield, R.; Pople, J. A. *J. Chem. Phys.* **1972**, *56*, 2257-2261.

19) Krishnan, R.; Binkley, J. S.; Seeger, R.; Pople, J. A. *J. Chem. Phys.* **1980**, *72*, 650-654.

20) Frisch, M. J.; Pople, J. A. *J. Chem. Phys.* **1984**, *80*, 3265-3269.

21) Dunning, T. H. *J. Chem. Phys.* **1989**, *90*, 1007-1023.

22) Woon, D. E.; Dunning, T. H. *J. Chem. Phys.* **1993**, *98*, 1358-1371.

23) Miertuš, S.; Scrocco, E.; Tomasi, J. *Chem. Phys.* **1981**, *55*, 117-129.

24) Miertuš, S.; Tomasi, J. *Chem. Phys.* **1982**, *65*, 239-245.

25) Cancès, E.; Mennucci, B.; Tomasi, J. *J. Chem. Phys.* **1997**, *107*, 3032-3041.

26) Mennucci, B.; Cancès, E.; Tomasi, J. *J. Phys. Chem. B* **1997**, *101*, 10506-10517.

27) Tomasi, J. Mennucci, B.; Cancès, E. *J. Molec. Struc.* **1999**, *464*, 211-226.

28) Marenich, A. V.; Cramer, C. J.; Truhlar, D. G. *J. Phys. Chem.* **2009**, *113*, 6378-6396.

29) Marenich, A. V.; Hawkins, G. D.; Liotard, D. A.; Cramer, C. J.; Truhlar, D. G. GESOL-version 2008, University of Minnesota, Minneapolis, 2008.

30) Keith, T. A.; Bader, R. F. W. *Chem. Phys. Lett.* **1993**, *210*, 223-231.

31) Ditchfield, R. *Mol. Phys.* **1974**, *27*, 789-807.

32) Wolinski, K.; Hinton, J. F.; Pulay, P. *J. Am. Chem. Soc.* **1990**, *112*, 8251-8260.

33) Cheeseman, J. R.; Trucks, G. W.; Keith, T. A.; Frisch, M. J. *J. Chem. Phys.* **1996**, *104*, 5497-5509.

34) Wiitala, K. W.; Hoye, T. R.; Cramer, C. J. *J. Chem. Theory Comput.* **2006**, *2*, 1085-1092.

35) Bagno, A.; Saielli, G. *Theor. Chem. Acc.* **2007**, *117*, 603-619.

36)Riccio, R.; Bifulco, G.; Cimino, P.; Bassarello, C.; Gomez-Paloma, L. *Pure Appl. Chem.* **2003**, *75*, 295-308.

37) Nicolaou, K. C.; Snyder, S. A. *Angew. Chem. Int. Ed.* **2005**, *44*, 1012-1044.

38) Hammett, L. P. *Chem. Rev.* **1935**, *17*, 125-136.

39) Maier, M. E. *Nat. Prod. Rep.* **2009**, *26*, 1105-1124.
40) Bifulco, G.; Dambruoso, P.; Gomez-Paloma, L.; Riccio, R. *Chem. Rev.* **2007**, *107*, 3744-3779.

41) Stahl, M.; Schopfer, U.; Frenking, G.; Hoffmann, R. W. *J. Org. Chem.* **1996**, *61* 8083-8088.

42) Rychnovsky, S. D. *Org. Lett.* **2006**, *8*, 2895-2898.

43) Forsyth, D. A.; Sebag, A. B. *J. Am. Chem. Soc.* **1997**, *119*, 9483-9494.

44) Barone, G.; Gomez-Paloma, L.; Duca, D.; Silvestri, A.; Riccio, R.; Bifulco, G. *Chem. Eur. J.* **2002**, *8*, 3233-3239.

45) Barone, G.; Duca, D.; Silvestri, A.; Gomez-Paloma, L.; Riccio, R.; Bifulco, G. *Chem. Eur. J.* **2002**, *8*, 3240-3245.

46) Cimino, P.; Gomez-Paloma, L.; Duca, D.; Riccio, R.; Bifulco, G. *Magn. Reson. Chem.* **2004**, *42*, S26-S33.

47) Smith, S. G.; Paton, R. S.; Burton, J. W.; Goodman, J. M. *J. Org. Chem.* **2008**, *73*, 4053-4062.

48) Hrobárik, P.; Horváth, B.; Sigmundová, I.; Zahrandník, P.; Malkina, O. L. *Magn. Reson. Chem.* **2007**, *45*, 942-953.

49) Roslund, M. U.; Tähtinen, P.; Niemitz, M.; Sjöholm, R. *Carb. Res.* **2008**, *343*, 101-112.

50) Infante-Caastillo, R.; Rivera-Montalvo, L. A.; Hernández-Rivera, S. P. *J. Molec. Struc.* **2008**, *877*, 10-19.

51) Benassi, R.; Ferrari, E.; Lazzari, S.; Spangnolo, F.; Saladini, M. *J. Molec. Struc.* **2008**, *892*, 168-176.

52) Kowalczyk, I. *J. Molec. Struc.* **2009**, *928*, 12-17.

53) Tähtinen, P.; Saielli, G.; Guella, G.; Mancini, I.; Bagno, A. *Chem. Eur. J.* **2008**, *14*, 10445-10452.

54) Mantel, C.; Chandor, A.; Gasparutto, D.; Douki, T.; Atta, M.; Fontecave, M.; Bayle, P.-A.; Mouesca, J.-M.; Bardet, M. *J. Am. Chem. Soc.* **2008**, *130*, 16978-16984.

55) Lodewyk, M. W.; Tantillo, D. J. *J. Nat. Prod.* **2011**, *74*, 1339-1343.

56) Smith, S. G.; Goodman, J. M. *J. Org. Chem.* **2009,** *74*, 4597-4607.

57) Smith, S. G.; Channon, J. A.; Paterson, I.; Goodman, J. M. *Tetrahedron* **2010**, *66*, 6437-6444.

58) Smith, S. G.; Goodman, J. M. *J. Am. Chem. Soc.* **2010**, *132*, 12946-12959.

59) MacroModel version 9.7, Schrodinger, LLC, New York, NY, 2009.

60) Halgren, T. A. *J. Comput. Chem.* **1996**, *17*, 490-519.

61) Halgren, T. A.; Nachbar, R. B. *J. Comput. Chem.* **1996**, *17*, 587-615.

62) Bondi, A. *J. Phys. Chem.* **1964**, *68*, 441-451.

63) Adamo, C.; Barone, V. *J. Chem. Phys.* **1999**, *110*, 6158-6170.

64) Perdew, J. P.; Chevary, J. A.; Vosko, S. H.; Jackson, K. A.; Pederson, M. R.; Singh, D. J.; Fiolhais, C. *Phys. Rev. B* **1992**, *46*, 6671-6687.

65) Perdew, J. P.; Burke, K.; Wang, Y. *Phys. Rev. B.* **1996**, *54*, 16533-16539.

66) Gaussian 09, Revision A.02, M. J. Frisch, G. W. Trucks, H. B. Schlegel, G. E. Scuseria, M. A. Robb, J. R. Cheeseman, G. Scalmani, V. Barone, B. Mennucci, G. A. Petersson, H. Nakatsuji, M. Caricato, X. Li, H. P. Hratchian, A. F. Izmaylov, J. Bloino, G. Zheng, J. L. Sonnenberg, M. Hada, M. Ehara, K. Toyota, R. Fukuda, J. Hasegawa, M. Ishida, T. Nakajima, Y. Honda, O. Kitao, H. Nakai, T. Vreven, J. A. Montgomery, Jr., J. E. Peralta, F. Ogliaro, M. Bearpark, J. J. Heyd, E. Brothers, K. N. Kudin, V. N. Staroverov, R. Kobayashi, J. Normand, K. Raghavachari, A. Rendell, J. C. Burant, S. S. Iyengar, J. Tomasi, M. Cossi, N. Rega, J. M. Millam, M. Klene, J. E. Knox, J. B. Cross, V. Bakken, C. Adamo, J. Jaramillo, R. Gomperts, R. E. Stratmann, O. Yazyev, A. J. Austin, R. Cammi, C. Pomelli, J. W. Ochterski, R. L. Martin, K. Morokuma, V. G. Zakrzewski, G. A. Voth, P. Salvador, J. J. Dannenberg, S. Dapprich, A. D. Daniels, O. Farkas, J. B. Foresman, J. V. Ortiz, J. Cioslowski, and D. J. Fox, Gaussian, Inc., Wallingford CT, 2009.

67) Wiitala, K. W.; Al-Rashid, Z. F.; Dvornikovs, V.; Hoye, T. R.; Cramer, C. *J. Phys. Org. Chem.* **2007**, *20*, 345-354.

68) Goodman Group, University of Cambridge. Assignment of stereochemistry and structure using NMR and CP3. www-jmg.ch.cam.ac.uk/tools/nmr/ (accessed July 11, 2012).

69) Wetzel, I.; Allmendinger, L.; Bracher, F. *J. Nat. Prod.* **2009***, 72*, 1908-1910.

70) Haynes, H. F.; Nelson, E. R.; Price, J. R. *Aus. J. Sci. Res.* **1952***, 5*, 387-400.

71) Anderson, L. A.; Harris, A.; Phillipson, J. D. *J. Nat. Prod.* **1983***, 46*, 374-378.

72) Kuo, P.-C.; Shi, L.-S.; Damu, A. G.; Su, C.-R.; Huang, C.-H.; Ke, C.-H.; Wu, J.-B.; Lin, A.-J.; Bastow, K. F.; Lee, K.-H.; Wu, T.-S. *J. Nat. Prod.* **2003***, 66*, 1324-1327.

73) Thouvenel, C.; Gantier, J.-C.; Duret, P.; Fourneau, C.; Hocquemiller, R.; Ferreira, M.-E.; Rojas de Arias, A.; Fournet, A. *Phytother. Res.* **2003***, 17*, 678-680.

74) Soriano-Agaton, F.; Lagoutte, D.; Poupon, E.; Roblot, F.; Fournet, A.; Gantier, J.-C.; Hocquemiller, R. *J. Nat. Prod.* **2005***, 68*, 1581-1587.

75) Xu, Z.; Chang, F.-R.; Wang, H.-K.; Kashiwada, Y.; McPhail, A. T.; Bastow, K. F.; Tachibana, Y.; Cosentino, M.; Lee, K.-H. *J. Nat. Prod.* **2000***, 63*, 1712-1715.

76) Hsieh, P.-W.; Chang, F.-R.; Lee, K.-H.; Hwang, T.-L.; Chang, S.-M.; Wu, Y.-C. *J. Nat. Prod.* **2004***, 67*, 1175-1177.

77) Puzik, A.; Bracher, F. *J. Heterocyclic Chem.* **2009***, 46*, 770-773.

78) Wen-sen, C. *Acta Bot. Sin.* **1986***, 28*, 450-452.

79) Aspaas, A. W. Part1: Statistical comparison of computed and experimental NMR coupling constants: a model study; Part 2: Reaction titration of hydride solutions by No-D NMR spectroscopy. Master's Thesis, University of Minnesota, Minneapolis, MN, 2005.

80) Büchi, G.; Erickson, R. E.; Wakabayashi, N. *J. Am. Chem. Soc.* **1961**, *83*, 927-938.

81) Naf, F.; Ohloff, G. *Helv. Chim. Acta* **1974**, *57* (6), 1868-1870.

82) Srikrishna, A.; Satyanarayana, G. *Tetrahedron* **2005**, *16*, 3992-3997.

83) Deguerry, F.; Pastore, L.; Wu, S.; Clark, A.; Chappell, J. Schalk, M. *Bichem. and Biophys.* **2006**, *454*, 123-136.

84) Dobler, M.; Dunitz, J. D.; Gubler, B.; Weber, H. P.; Buchi, G.; Padilla, J. O. *Proc. Chem. Soc.* **1963**, 383.

85) Barton, D. H. R.; Beleil, J.-C.; Billion, A.; Boivin, J.; Lallemand, J.-Y.; Mergui, S. *Hel. Chim. Acta.* **1987**, *70*, 273-280.

86) Hammett, L. P. *Chem. Rev.* **1935**, *17*, 125-136.

87) Jaffé, H. H. *Chem. Rev.* **1953**, *53*, 191-261.

88) Hammond, G. S. *J. Am. Chem. Soc.* **1955**, *77*, 334-338.

89) Stock, L. M.; Brown, H. C. *Adv. Phys. Org. Chem.* **1963**, *1*, 35-154.

90) Ritchie, C. D.; Sager, W. F. *Prog. Phys. Org. Chem.* **1964**, *2*, 323-400.

91) Koppel, I. A.; Palm, V. A. *Advances in Linear Free Energy Relationships*, Plenum Press, London, **1972**.

92) Kamlet, M. J.; Taft, R. W. *Prog. Org. Chem.* **1983**, *48*, 2877-2887.

93) Exner, O. *Prog. Phys. Org. Chem.* **1990**, *18*, 129-161.

94) Cramer, C. J.; Famini, G. R.; Lowrey, A. H. *Acc. Chem. Res.* **1993**, *26*, 599-605.

95) Famini, G. R.; Wilson, L. Y. *Rev. Comp. Chem.* **2002**, *18*, 211-255.

96) Brown, H. C.; Okamoto, Y. *J. Am. Chem. Soc.* **1957**, *79*, 1913-1917.

97) McDaniel, D. H.; Brown, H. C. *J. Org. Chem.* **1958**, *23*, 420-427.

98) Cramer, C. J.; Pak, Y. *Theor. Chem. Acc.* **2001**, *105*, 477.480.

99) Cramer, C. J.; Kinsinger, C. K.; Pak, Y. *J. Mol. Struct. (Theochem)* **2003**, *632*, 111-120.

100) Mahapatra, S.; Halfen, J. A.; Tolman, W. B. *J. Am. Chem. Soc.* **1996**, *118*, 11575-11586.

101) Girones, X.; Ponec, R. *J. Chem. Inf. Model.* **2006**, *46*, 1388-1393.

102) M. J. Frisch, G. W. Trucks, H. B. Schlegel, G. E. Scuseria, M. A. Robb, J. R. Cheeseman, J. A. Montgomery, T. Vreven, K. N. Kudin, J. C. Burant, J. M. Millam, S. S. Iyengar, J. Tomasi, V. Barone, B. Mennucci, M. Cossi, G. Scalmani, N. Rega, G. A. Petersson, H. Nakatsuji, M. Hada, M. Ehara, K. Toyota, R. Fukuda, J. Hasegawa, M. Ishida, T. Nakajima, Y. Honda, O. Kitao, H. Nakai, M. Klene, X. Li, J. E. Knox, H. P. Hratchian, J. B. Cross, C. Adamo, J. Jaramillo, R. Gomperts, R. E. Stratmann, O. Yazyev, A. J. Austin, R. Cammi, C. Pomelli, J. W. Ochterski, P. Y. Ayala, K. Morokuma, G. A. Voth, P. Salvador, J. J. Dannenberg, V. G. Zakrzewski, S. Dapprich,

A. D. Daniels, M. C. Strain, O. Farkas, D. K. Malick, A. D. Rabuck, K. Raghavachari, J. B. Foresman, J. V. Ortiz, Q. Cui, A. G. Baboul, S. Clifford, J. Cioslowski, B. B. Stefanov, G. Liu, A. Liashenko, P. Piskorz, I. Komaromi, R. L. Martin, D. J. Fox, T. Keith, M. A. Al-Laham, C. Y. Peng, A. Nanayakkara, M, Challacombe. P. M. W. Gill, B. Johnson, W. Chen, MW. Wong, C. Gonzalez, JA. Pople, *Gaussian 03*, Gaussian, Inc., Pittsburgh, PA **2003**.

103) Karlström, G.; Lindh, R.; Malmqvist, P.-Å.; Roos, B. O.; Ryde, U.; Veryazov, V.; Widmark, P. O.; Cossi, M.; Schimmelpfennig, B.; Neogrady, P.; Seijo, L. *Comput. Matl. Sci.* **2003**, *28*, 222-239.

104) Ahlrichs, R.; Bär, M.; Häser, M.; Horn, H.; Kölmel, C. *Chem. Phys. Lett.* **1989**, *162*, 165-169.

105) Cherman, B. F.; Cramer, C. J. *Inorg. Chem.* **2004**, *43* 7281-7283.

106) Gagliardi, L.; Cramer, C. J. *Inorg. Chem.* **2006**, *45*, 9442-9447.

107) March, J. *Advanced Organic Chemistry*, John Wiley & Sons, New York, **1992**, 198-202 and 866-873.

108) DiLabio, G. A.; Ingold, K. U. *J. Org. Chem.* **2004**, *69*, 1620-1624.

109) Li, J.; Zhu, T.; Hawkins, G. D.; Winget, P.; Liotard, D. A.; Cramer, C. J.; Truhlar, D. G. *Theor. Chem. Acc.* **1999**, *103*, 9-63.

110) Miller, J. A. *Cancer Res.* **1970**, *30*, 559-576.

111) Westra, J. G.; Kriek, E.; Hittenhausen, H. *Chem. Biol. Interact.* **1976**, *15*, 149-164.

112) Miller, E. C. *Cancer Res.* **1978**, *38*, 1479-1496.

113) Thorgairsson, S. S.; Wirth, P. J.; Staiano, N.; Smith, C. L. *Adv. Exp. Med. Biol.* **1982**, *136B*, 897-919.

114) Stadler, W. M. *Int. J. Oncol.* **1993**, *3*, 549-557.

115) Swaminathan, S.; Frederickson, S. M.; Hatcher, J. F. *Carcinogenesis* **1994**, *15* 611-617.

116) Ford, G. P.; Herman, P. S. *J. Am. Chem. Soc.* **1989**, *111*, 3987-3996.

117) Glover, S. A.; Scott, A. P. *Tetrahedron* **1989**, *45*, 1763-1776.

118) Falvey, D. E.; Cramer, C. J. *Tetrahedron Lett.* **1992**, *33*, 1705-1708.

119) Srivastave, S.; Toscano, J. P.; Moran, R. J.; Falvey, D. E. *J. Am. Chem. Soc.* **1997**, *119*, 11552-11553.

120) Sullivan, M. B.; Brown, K.; Cramer, C. J.; Truhlar, D. G. *J. Am. Chem. Soc.* **1998**, *120*, 11778-11783.

121) Sullivan, M. B.; Cramer, C. J. *J. Am. Chem. Soc.* **2000**, *122*, 5588-5596.

122) Thomas, S. I.; Falvey, D. E. *J. Org. Chem.* **2007**, *72*, 4626, 4634.

123) Zhu, T.; Li, J.; Hawkins, G. D.; Cramer, C. J.; Truhlar, D. G. *J. Chem. Phys.* **1998**, *109*, 9117-9133.

124) Baciocchi, E.; Gerini, M. F. *J. Phys. Chem. A* **2004**, *108*, 2332-2338.

125) White, W. N.; Gwynn, D.; Schlitt, R.; Girard, C.; Fife, W. *J. Am. Chem. Soc.* **1958**, *80*, 3271-3277.

126) Goering, H. L.; Jacobson, R. R. *J. Am. Chem. Soc.* **1958**, *80*, 3277-3282.

127) Van Speybroeck, V.; Martelé, Y.; Schacht, E.; Waroquier, M. *J. Phys. Chem. A* **2002**, *106*, 12370-12375.

128) Synthetic studies, see: a) Smith, A. B., III; Kuerti, L.; Davulcu, A. H.; Cho, Y. S.; Ohmoto, K. *J. Org. Chem.* **2007**, *72*, 4611-4620.

129) a) Jackson, S. K.; Kerr, M. A. *J. Org. Chem.* **2007**, *72*, 1405-1411. b) Huntley, R. J.; Funk, R. L. *Org. Lett.* **2006**, *8*, 3403-3406. c) Jackson, S. K.; Banfield, S. C.; Kerr, M. A. *Org. Lett.* **2005**, *7*, 1215-1218.

130) a) Dangel, B. D.; Godula, K.; Youn, S. W.; Sezen, B.; Sames, D. *J. Am. Chem. Soc.* **2002**, *124*, 11856-11857. b) Nakatsuka, S.; Marsuda, T.; Goto, T. *Tetrahedron Lett.* **1987**, *38*, 3671-3674.

131) Buszek, K. R.; Luo, D.; Kondrashov, M.; Brown, N.; VanderVelde, D. *Org. Lett.* **2007**, *9*, 4135-4137.

132) a) Brown, N.; Luo, D.; VanderVelde, D.; Yang, S.; Brassfield, A.; Buszek, K. R. *Tetrahedron Lett.* **2009**, *50*, 63-65. Another *o*-silyltriflate method for 4,5-indolyne formation and further cycloaddition reactions have subsequently been reported by Garg: b) Bronner, S. M.; Bahnck, K. B.; Garg, N. K. *Org. Lett.* **2009**, *11*, 1007-1010.

133) Buszek, K. R.; Brown, N.; Luo, D. *Org. Lett.* **2009**, *11*, 201-204.

134) Tian, X.; Huters, A. D.; Douglas, C. J.; Garg, N. K. *Org. Lett.* **2009**, *11*, 2349-2351.

135) 2-Methyl-, 2-ethyl-, and 2-*t*-butylfuran are readily available from commercial sources. The others were prepared as follows. a) 2-*i*-Propylfuran: see ref. 135c. b) 2-Phenylfuran: Negishi, E.; Takahashi, T.; King, A. O. *Org. Synth.* **1988**, *66*, 67-72. c) 2-Phenylsulfonylfuran: Malanga, C.; Aronica, L. A.; Lardicci, L. *Synth. Commun.* **1996**, *26*, 2317-2327.

136) a) Giles, R. G. F.; Sargent, M. V.; Sianipar, H. *J. Chem. Soc.*, *PT1* **1991**, 1571-1579. b) Newman, M. S.; Kannan, R. *J. Org. Chem.* **1976**, *41*, 3356-3359. c) Gribble, G. W.; Keavy, D. J.; Branz, S. E.; Kelly, W. J.; Pals, M. A. *Tetrahedron Lett.* **1988**, *29*, 6227-6230.

137) Zhao, Y.; Truhlar, D. G. *MN-GFM version 4.1*; University of Minnesota: Minneapolis, 2008.

138) Frisch, M. J.; Trucks, G. W.; Schlegel, H. B.; Scuseria, G. E.; Rogg, M. A.; Cheeseman, J. R.; Montgomery, J. A., Jr.; Vreven, T.; Kudin, K. N.; Burant, J. C.; Millam, J. M.; Iyengar, S. S.; Tomasi, J.; Barone, V.; Mennucci, B.; Cossi, M.; Scalmani, G.; Rega, M.; Petersson, G. A.; Nakatsuji, H.; Hada, M.; Ehara, M.; Toyota, K.; Fukuda, R.; Hasegawa, J.; Ishida, M.; Nakajima, T.; Honda, Y.; Kitao, O.; Nakai, H.; Klene, M.; Li, X.; Knox, J. E.; Hratchian, H. P.; Cross, J. B.; Bakken, V.; Adamo, C.; Jaramillo, J.; Gomperts, R.; Stratmann, R. E.; Yazyev, O.; Austin, A. J.; Cammi, R.; Pomelli, C.; Ochterski, J. W.; Ayala, P. Y.; Morokuma, K.; Voth, G. A.; Salvador, P.: Dannenberg, J. J.; Zakrzewski, V. G.; Dapprich, S.; Daniels, A. D.; Strain, M. C.; Garkas, O.; Malick, D. K.; Rabuck, A. D.; Raghavachari, K.; Foresman, J. B.; Ortiz, J. V.; Cui, Q.; Baboul, A. G.; Clifford, S.; Cioslowski, J.; Stefanov, B. B.; Lui, G.; Liashenko, A.; Piskorz, P.; Komaromi, I.; Martin, R. L.; Fox, D. J.; Keith, T.; Al-Laham, M. A.; Peng, C. Y.; Nanayakkara, A.; Challacombe, M.; Gill, P. M. W.; Johnson, B.; Chen, W.; Wong, M. W.; Gonzalez, C.; Pople, J. A. *Gaussian 03*, revision D.01; Gaussian, Inc.; Wallingford, CT, 2004.

139) Cioslowski, J. *J. Am. Chem. Soc.* **1989**, *111*, 8333.

140) Cramer, C. J.; Thompson, J. *J. Phys. Chem. A* **2001**, *105*, 2091-2098.

141) Hofstetter, T. B.; Berg, M. TrAC-*Trends Anal. Chem.* **2011**, *30*, 618-627.

142) Aeppli, C.; Hofstetter, T. B.; Amaral, H. I. F.; Kipfer, R.; Schwarzenbach, R. P.; Berg, M. *Environ. Sci. Technol.* **2010**, *44*, 3705-3711.

143) Dempster, H. S.; Lollar, B. S.; Feenstra, S. *Environ. Sci. Technol.* **1997**, *31*, 3193-3197.

144) Vieth, A.; Muller, J.; Strauch, G.; Kastner, M.; Gehre, M.; Meckenstock, R. U.; Richnow, H. H. *Isot. Environ. Health Stud.* **2003**, *39*, 113-124.

145) Hunkeler, D.; Aravena, R.; Berry-Spark, K.; Cox, E. *Environ. Sci. Technol.* **2005**, *39*, 5975-5981.

146) Zwank, L.; Berg, M.; Elsner, M.; Schmidt, T. C.; Schwarzenbach, R. P.; Haderlein, S. B. *Environ. Sci. Technol.* **2005**, *39*, 1018-1029.

147) Kuder, T.; Wilson, J. T.; Kaiser, P.; Kolhatkar, R.; Philp, P.; Allen, J. *Environ. Sci. Technol.* **2005**, *39*, 213-220.

148) Hunkeler, D.; Butler, B. J.; Aravena, R.; Barker, J. F. *Environ. Sci. Technol.* **2001**, *35*, 676-681.

149) Fischer, A.; Gehre, M.; Breitfeld, J.; Richnow, H. H.; Vogt, C. *Rapid Commun. Mass Spectrom.* **2009**, *23*, 2439-2447.

150) Vogt, C.; Cyrus, E.; Herklotz, I.; Schlosser, D.; Bahr, A.; Herrmann, S.; Richnow, H.-H.; Fischer, A. *Environ. Sci. Technol.* **2008**, *42*, 7793-7800.

151) Tobler, N. B.; Hofstetter, T. B.; Schwarzenbach, R. P. *Environ. Sci. Technol.* **2007**, *41*, 7773-7780.

152) Tobler, N. B.; Hofstetter, T. B.; Schwarzenbach, R. P. *Environ. Sci. Technol.* **2008**, *42*, 7786-7792.

153) Meyer, A. H.; Penning, H.; Lowag, H.; Elsner, M. *Environ. Sci. Technol.* **2008**, *42*, 7757-7763.

154) Berg, M.; Bolotin, J.; Hofstetter, T. B. *Anal. Chem.* **2007**, *79*, 2386-2393.

155) Bernstein, A.; Ronen, Z.; Adar, E.; Nativ, R.; Lowag, H.; Stichler, W.; Meckenstock, R. U. *Environ. Sci. Technol.* **2008**, *42*, 7772-7777.

156) Schwarzenbach, R. P.; Gschwend, P. M.; Imboden, D. M. *Environmental Organic Chemistry,* 2nd ed.; John Wiley & Sons: New York, 2003.

157)Hofmann, D.; Gehre, M.; Jung, K. *Isot. Environ. Health Stud* **2003**, *39*, 233-244.

158) Macko, S. A.; Uhle, M. E.; Engel, M. H.; Andrusevich, V. *Anal. Chem.* **1997**, *69*, 926-929.

159) Styring, A. K.; Sealy, J. C.; Evershed, R. P. *Geochim. Cosmochim. Acta* **2010**, *74*, 241-251.

160) Penning, H.; Elsner, M. *Anal. Chem.* **2007**, *79*, 8399-8405.

161) Hartenbach, A. E.; Hofstetter, T. B.; Tentscher, P. R.; Canonica, S.; Berg, M.; Schwarzenbach, R. P. *Environ. Sci. Technol.* **2008**, *42*, 7751-7756.

162) Hartenbach, A. E.; Hofstetter, T. B.; Aeschbacher, M.; Sander, M.; Kim, D.; Strathmann, T. J.; Arnold, W. A.; Cramer, C. J.; Schwarzenbach, R. P. *Environ. Sci. Technol.* **2008**, *42*, 8352-8359.

163) Hofstetter, T. B.; Neumann, A.; Arnold, W. A.; Hartenbach, A. E.; Bolotin, J.; Cramer, C. J.; Schwarzenbach, R. P. *Environ. Sci. Technol.* **2008**, *42*, 1997-2003.

164) Fishbein, L. *The Handbook of Environmental Chemistry—Antropogenic Compounds*; Springer: Berlin, Germany, 1984.

165) Zhang, H. C.; Huang, C. H. *Environ. Sci. Technol.* **2005**, *39*, 4474-4483.

166) Laha, S.; Luthy, R. G. *Environ. Sci. Technol.* **1990**, *24*, 363-373.

167) Simmons, K. E.; Minard, R. D.; Bollag, J. M. *Environ. Sci. Technol.* **1987**, *21*, 999-1003.

168) Parris, G. E. *Environ. Sci. Technol.* **1980**, *14*, 1099-1106.

169) Shin, K. A.; Spain, J. C. *Appl. Environ. Microbiol.* **2009**, *75*, 2694-2704.

170) Lu, H.; Chen, X.; Zhan, C. G. *J. Phys. Chem. C* **2007**, *111*, 10599-10605.

171) Penning, H.; Cramer, C. J.; Elsner, M. *Environ. Sci. Technol.* **2008**, *42*, 7764-7771.

172) Meyer, A. H.; Penning, H.; Elsner, M. *Environ. Sci. Technol.* **2009**, *43*, 8079-8085.

173) Zwank, L.; Berg, M.; Schmidt, T. C.; Haderlein, S. B. *Anal. Chem.* **2003**, *75*, 5575-5583.

174) Brand, W. A.; Tegtmeyer, A. R.; Hilkert, A. *Org. Geochem.* **1994**, *21*, 585-594.

175) Lehmann, M. F.; Bernasconi, S. M.; Barbieri, A.; McKenzie, J. A. *Geochim, Cosmochim. Acta* **2002**, *66*, 3573-3584.

176) Merritt, D. A.; Hayes, J. M. *Anal. Chem.* **1994**, *66*, 2336-2347.

177) Merritt, D. A.; Hayes, J. M. *J. Am. Soc. Mass Spectrom.* **1994**, *5*, 387-397.

178) *A Guide for Assessing Biodegradation and Source Identification of Organic Ground Water Contaminants Using Compound Specific Isotope Analysis (CSIA);* Hunkeler, D.; Meckenstock, R. U.; Sherwood Lollar, B.; Schmidt, T. C.; Wilson, J. T., Eds.; U.S. EPA: Waschington, DC, 2008.

179) Wolfsberg, M; Van Hook, W. A.; Paneth, P.; Rebelo, L. P. N. *Isotope Effects in the Chemical, Geological, and Bio Sciences*; Springer: New York, 2010.

180) Marlier, J. F. *Acc. Chem. Res.* **2001**, *34,* 283-290.

181) Millero, F. J. *Geochim. Cosmochim. Acta* **1981**, *45*, 2085-2089.
182) Pitzer, K. S. *J. Phys. Chem.* **1973**, *77*, 268-277.

183) Pitzer, K. S. In *Activity Coefficients in Electrolyte Solutions,*; Pytkovitz, R. M., Ed.; CRC Press: Boca Raton, **1991**; Vol. 2, pp75-153.

184) Millero, F. J.; Schreiber, D. R. *Am. J. Sci.* **1982**, *282*, 1508-1540.

185) Tanaka, N.; Yamaguchi, A.; Araki, M.; Kimata, K. *J. Am. Chem. Soc.* **1985**, *107*, 7781-7782.

186) Jochmann, M. A.; Blessing, M.; Haderlein, S. B.; Schmidt, T. C. *Rapid Commun. Mass Spectrom.* **2006**, *20*, 3639-3648.

187) Lollar, B. S.; Hirschorn, S. K.; Chartrand, M. M. G.; Lacrampe-Couloume, G. *Anal. Chem.* **2007**, *79*, 3469-3475.

188) Hunkeler, D.; Bernasconi, S. M. In *Environmental Isotopes in Biodegradation and Bioremediation*, ed.; Aelion, M. C., Höhener, P., Hunkeler, D., Aravena, R., Eds.; CRC Press: Boca Raton, 2010; pp 23-42.

189) Blessing, M.; Jochmann, M. A.; Schmidt, T. C. *Anal. Bioanal. Chem.* **2008**, *390*, 591-603.

190) Stumm, W.; Morgan, J. J. *Aquatic Chemistry*, 3rd ed.; John Wiley & Sons: New York, 1996.

191) Dybala-Defratyka, A.; Szatkowski, L.; Kaminski, R.; Wujec, M.; Siwek, A.; Paneth, P. *Environ. Sci. Technol.* **2008**, *42*, 7744-7750.

192) Colon, D.; Weber, E. J.; Baughman, G. L. *Environ. Sci. Technol.* **2002**, *36*, 2443-2450.

193) Klausen, J.; Haderlein, S. B.; Schwarzenbach, R. P. *Environ. Sci. Technol.* **1997**, *31*, 2642-2649.

194) Bialk, H. M.; Pedersen, J. A. *Environ. Sci Technol.* **2008**, *42*, 106-112.

195) Dodd, M.; Buffle, M.; Gunten, U. V. *Environ. Sci. Technol.* **2006**, *40*, 1969-1977.

196) Paul, T.; Dodd, M. C.; Strathmann, T. J. *Water Res.* **2010**, *44*, 3121-3132.

197) Schwarzenbach, R. P.; Egli, T.; Hofstetter, T. B.; von Gunten, U.; Wehrli, B. *Annu. Rev. Environ. Resour.* **2010**, *35*, 109-136.

198) Thorn, K. A.; Pettigrew, P. J.; Goldenberg, W. S.; Weber, E. J. *Environ. Sci. Technol.* **1996**, *30*, 2764-2775.

199) Elsner, M. *J. Environ. Monit.* **2010**, *12*, 2005-2031.

200) Hofstetter, T. B.; Schwarzenbach, R. P.; Bernasconi, S. M. *Environ. Sci. Technol.* **2008**, *42*, 7737-7743.

201) Hartenbach, A.; Hofstetter, T. B.; Berg, M.; Bolotin, J.; Schwarzenbach, R. P. *Environ. Sci. Technol.* **2006**, *40*, 7710-7716.

202) Hofstetter, T. B.; Spain, J. C.; Nishino, S. F.; Bolotin, J.; Schwarzenbach, R. P. *Environ. Sci. Technol.* **2008**, *42*, 4764-4770.

203) Penning, H.; Sorensen, S. R.; Meyer, A. H.; Aamand, J.; Elsner, M. *Environ. Sci. Technol.* **2010**, *44*, 2372-2378.

204) Gorski, C. A.; Nurmi, J. T.; Tratnyek, P. G.; Hofstetter, T. B.; Scherer, M. M. *Environ. Sci. Technol.* **2010**, *44*, 55-60.

205) Skarpeli-Liati, M.; Turgeon, A.; Garr, A. N.; Arnold, W. A.; Cramer, C. J.; Hofstetter, T. B. *Anal. Chem.* **2011**, *83*, 1641-1648.

206) Murray, J. W. *Colloid Interface Sci.* **1974**, *46*, 357-371.

207) Kern, S.; Fenner, K.; Singer, H. P.; Schwarzenbach, R. P.; Hollender, J. *Environ. Sci. Technol.* **2009**, *43*, 7039-7046.

208) Aeschbacher, M.; Sander, M.; Schwarzenbach, R. P. *Environ. Sci. Technol.* **2010**, *44*, 87-93.

209) Scott, K. M.; Lu, X.; Cavanaugh, C. M.; Liu, J. S. *Geochim. Cosmochim. Acta* **2004**, *68*, 433-442.
210) Kavner, A.; Bonet, F.; Shahar, A.; Simon, J.; Young, E. *Geochim. Cosmochim. Acta* **2005**, *69*, 2971-2979.

211) Zhang, H. C.; Chen, W. R.; Huang, C. H. *Environ. Sci. Technol.* **2008**, *42*, 5548-5554.

212) Zhu, M. Q.; Paul, K. W.; Kubicki, J. D.; Sparks, D. L. *Environ. Sci. Technol.* **2009**, *43*, 6655-6661.

213) Nesbitt, H. W.; Canning, G. W.; Bancroft, G. M. *Geochim. Cosmochim. Acta* **1998**, *62*, 2097-2110.

214) Pretsch, E. A. C.; Bühlmann, P. M. B. *Spektroskopische Daten zur Strukturaufklärung Organischer Verbindungen*, 4th ed.; Springer Verlag: New York, 2001.

215) Fitzpatrick, P. F. *Arch. Biochem. Biophys.* **2010**, *493*, 13-25.

216) Ralph, E. C.; Hirschi, J. S.; Anderson, M. A.; Cleland, W. W.; Singleton, D. A.; Fitzpatrick, P. F. *Biochemistry* **2007**, *46* 7655-7664.